Discovery of an Allosteric Site on Furin, contributing to Potent Inhibition: A Promising Therapeutic for the Anemia of Chronic Inflammation

Andrew Jacob Gross
Brigham Young University

Discovery of an Allosteric Site on Furin, Contributing to Potent Inhibition:

A Promising Therapeutic for the Anemia of Chronic Inflammation

Andrew J. Gross

A dissertation submitted to the faculty of
Brigham Young University
in partial fulfillment of the requirements for the degree of

Doctor of Philosophy

Richard K. Watt, Chair
Dixon J. Woodbury
Roger G. Harrison
Chad R. Hancock
John T. Prince

Department of Chemistry and Biochemistry

Brigham Young University

July 2014

ABSTRACT

Discovery of an Allosteric site on Furin, Contributing to potent Inhibition:
A promising Therapeutic for the Anemia of Chronic Inflammation

Andrew J. Gross
Department of Chemistry and Biochemistry, BYU
Doctor of Philosophy

Anemia of chronic inflammation (ACI) is a condition that develops in a setting of chronic immune activation. ACI is characterized and triggered by inflammatory cytokines and the disruption of iron homeostasis. Hepcidin, a small peptide hormone, is the master regulator of iron homeostasis, and rapidly responds to iron supply and demand.

Under conditions of chronic inflammation, hepcidin is elevated, and alters the way that iron is absorbed and disrupted throughout the body, resulting in disrupted iron homeostasis through inhibition of the iron exporter protein ferroportin. Anemia arises when insufficient erythropoietic activity combined with inadequate iron supply abrogates the healthy development of mature red blood cells (RBCs).

The proprotein convertase (PC) known as furin is a serine protease capable of cleaving peptide precursors into their active state. Furin is critical for normal activation of proteins and enzymes but recently, furin has been implicated in critical roles within cancers, viral and pathogenic infections, and arthritis through activating precursors novel to the disease type. Furin has previously been identified as being the sole PC responsible for generating active hepcidin. Hepcidin is initially synthesized as a larger precursor protein, before undergoing furin cleavage. Furin is known to form mature, bioactive hepcidin, with the removal of this pro-region.

Our discovery of a novel regulatory site on Furin has led to potent inhibition using small molecules. This inhibition is shown with the use of *in vitro* fluorogenic assays, *in vivo* cell tissue cultures, and within an animal model of ACI. Our results demonstrate that in using these small molecules we can decrease hepcidin levels even in the presence of potent inflammatory cytokines.

The inhibition of hepcidin by these small molecules causes an increase in stably expressed ferroportin on cell surfaces and the restoration of the ability to mobilize iron from storage tissues and absorption from the diet. The ability to "fine-tune" inhibition of furin in targeting its allosteric site along with its catalytic domain designates these small-molecule inhibitors as promising therapeutics for treatment of diseases ranging from Alzheimer's and cancer to anthrax and Ebola fever.

Keywords: furin, anemia of chronic inflammation, hepcidin, protease inhibitors, ferroportin

ACKNOWLEDGEMENTS

The test of a man is the fight he makes,

The grit that he daily shows;

The way he stands on his feet and takes

Fate's numerous bumps and blows.

A coward can smile when there's naught to fear,

When nothing his progress bars;

But it takes a man to stand up and cheer

While some other fellow stars.

It isn't the victory, after all,

But the fight that a brother makes;

The man who, driven against the wall,

Still stands up erect and takes

The blows of fate with his head held high;

Bleeding, and bruised, and pale,

Is the man who'll win in the by and by,

For he isn't afraid to fail.

It's the bumps you get, and the jolts you get,

And the shocks that your courage stands,

The hours of sorrow and vain regret,

The prize that escapes your hands,

That test your mettle and prove your worth;

It isn't the blows you deal,

But the blows you take on the good old earth,

That show if your stuff is real

Table of Contents

List of Tables

List of Figures

Abbreviations

α1-PDX – alpha-1 antitrypsin portland variant

aa – amino acid

Abz – ortho-aminobenzoic acid

ACI – anemia of chronic inflammation

AMC – 7-amino-4-methyl coumarin

BMP – bone morphogenic protein

BSA – body surface area

CBC – complete blood count

CHARMM – chemistry at harvard molecular mechanics

CKD – chronic kidney disease

DMT1– divalent metal transporter 1

Dnp – 2,4-dinitrophenyl

ECM – extracellular matrix

EDDnp – N-(2, 4-dinitrophenyl) ethylenediamine

EPO – erythropoietin

ER – endoplasmic reticulum

ESA – erythropoiesis stimulating agents

ESI – electrospray ionization

FACTS – fast analytical continuum treatment software

FDA – food and drug administration

Fl - femtoliter

Hb – hemoglobin

HCT – hematocrit

HCV – hepatitis C virus

HIF-1α – hypoxia inducible factor-1α

HIV – human immunodeficiency virus

IDA – iron deficiency anemia

IGF-1 – insulin-like growth factor

IL-6 – interleukin-6

IRE – iron response element

JAK – janus kinase

LDL – low density lipoprotein

LGA – lamarckian genetic algorithm

LigPlot – ligand plot

MCA – 4-methyl-7-amino coumarinamide

MCV – mean corpuscular volume

MT-SP1 – membrane-type serine protease-1

NCBI – national center for biotechnology information

ND – nelfinavir darunavir

NMR – nuclear magnetic resonance

PC – proprotein convertase

PC1/3 – proprotein convertase 1/3

PDB – protein database

PG-LPS – streptococcal peptidoglycan-polysaccharide

PI – protease inhibitor

pStat3 – phosphorylates signal transducer and activator of transcription-3

RBC – red blood cell

RDW – red blood cell distribution width

RES – reticuloendothelial system

RNAi – ribonucleic acid interference

SDF – standard data file

Smad – small mothers against decapentaplegic homolog

SMILES – simplified molecular input line entry system

STAT – signal transducer and activator of transcription

sTfR – soluble transferrin receptor

Succ – succinoyl group

TfR – transferrin receptor

TGF- β – transforming growth factor β

TGN – trans golgi network

TIBC – total iron-binding capacity

TNF – tumor necrosis factor

TTSP – type II transmembrane serine protease

Tyx – 3-nitro tyrosine

VLDL – very low density lipoprotein receptor

WB – western blot

CHAPTER 1: Introduction to Anemia of Chronic Inflammation

Anemia

The word anemia comes from the Greek word ('Αναιμία)(an-haîma) meaning "without blood". Anemia is a medical condition where a decrease in number of red blood cells (RBCs) is usually accompanied with a lower than normal quantity of hemoglobin in the blood. The primary function of the red blood cell is to deliver oxygen to the tissues. Anemia impairs the ability of the blood to efficiently transport oxygen to body tissue, usually leading to hypoxic (low oxygen) conditions in vital organs.

Patients with severe or prolonged anemia are easily fatigued, appear pale, portray dyspnea (shortness of breath), and have a tendency to develop irregular heartbeats known as palpitations[1]. These symptoms involve physiologic compensation, including decreased hemoglobin oxygen affinity, increased cardiac output, and redistribution of blood flow.

Characterizing anemia is often sub-classified into three differing categories. Pathogenesis, red blood cell morphology, and clinical presentation[2]. Pathogenic mechanisms involve inappropriate over-production of erythrocytes, or loss of erythrocytes due to hemolysis or bleeding. Further classified as being regenerative versus hypo-regenerative. Polycythemia is a disease state in which the proportion of blood volume occupied by the red blood cells increases. Red blood cell morphology

relates to morphologic characteristics within the complete blood count (CBC), identifying the anemia as being microcytic, macrocytic, or normocytic (Table 1.1). These are analytical parameters provided by automated hematology analyzers, including such values as mean corpuscular volume (MCV) and red blood cell distribution width (RDW). MCV is measured as the average volume of a red blood cell (normal range: 82-98 fL) reported in femtoliters (10^{-15}L). RDW is a measure of the variation of red blood cell size. RBCs are usually 6-8μm in diameter. In humans, the normal RDW range is 11.5-14.5%[1]. Levels of reticulocytes (immature RBCs) compose about 1% of the total RBC in a healthy individual. Higher percentages of reticulocytes are attributable to anemia.

Clinical presentation involves other analysis useful in anemia diagnosis. Serum levels of iron, urea, creatinine, vitamin B12, folate, and bilirubin are used as important indicators. The levels of protein involved in iron metabolism within serum can also be indicative of iron status and anemia, including transferrin, soluble transferrin receptor (sTfR), and ferritin.

Treatment of anemia is usually aimed at correcting the underlying issue, by identifying the source of blood loss, providing transfusions, or supplementing mineral deficiency. In cases of chronic inflammation, chronic disease, or genetic abnormalities, successful treatment of the underlying problem is not always an option.

Table 1.1. Morphological MCV and RDW of red blood cells used in anemia diagnosis.

Type of Anemia	MCV (fl)*	RDW (%)	Common factors
Microcytic	Low (< 80 fl)	High: (low iron) Normal: thalassemia (high iron)	ACI, Reduced heme synthesis
Macrocytic	Very high(> 100 fl)	High (> 15%)	B12 or folate deficiency, alcoholism, hypothyroidism,
Normocytic	Normal(82-98 fl)	Normal (11.5-14.5%)	Increased destruction of RBC, blood loss

* fl refers to femtoliter (10^{-15}L).

Anemia of Chronic Inflammation

Anemia of chronic inflammation (ACI) is a type of anemia that commonly occurs in patients with chronic, or long term, immune activation[3–5]. It is the most frequent anemia in hospitalized patients, and is associated with increased morbidity and mortality[6]. In 2012 alone, more than 117 million Americans live with at least one chronic illness. Over 40% of these cases have resulted in significant debilitating anemia[7]. One study has suggested that the relationship between Hb values and levels of mortality is U-shaped[8], for as Hb levels fall, mortality percentages correspondingly increase.

Chronic diseases that lead to abnormal activation of the immune response and eventually ACI, include infectious and inflammatory diseases, heart disease, kidney disease, and cancer (Table 1.2). The severity of ACI is most commonly related to the severity of the underlying disorder. Certain treatments for chronic diseases may also impair red blood cell production and further contribute to ACI (Table 1.3).

Healthy levels of hematocrit (HCT) are about 45% for men, and 40% for women. Healthy hemoglobin values range from 15-18 g/dL[9]. ACI is a mild to moderate anemia where hematocrits can range between 30% and 40%, while Hb levels range between 9-13 g/dL. It is common, however, that hematocrit will drop below 25%[5]. Marginal normocytic anemia is initially observed, and will later progress into microcytic anemia, as severity of the underlying disease progresses.

Table 1.2. Foremost underlying causes of Anemia of Chronic Inflammation (ACI)[3].

Associated Diseases	Estimated Prevalence*
Infections (acute and chronic)	20-95%
Viral, including HIV	
Bacterial	
Parasitic	
Fungal	
Cancer	30-77%
Hematologic	
Solid tumor	
Autoimmune	10-70%
Rheumatoid arthritis	
Vasculitis	
Sarcoid	
Inflammatory bowel disease	
Chronic rejection of transplant	10-70%
Chronic kidney disease	23-50%
Inflammation	23-50%

*Data is not available for all conditions associated with ACI. The prevalence is the percent of people with the disease. Occurrence and severity of anemia are correlated with the stage of the underlying condition[10].

Anemia Statistics for Patient Populations

Table 1.3. Major patient population statistics for Anemia of Chronic Inflammation (ACI).

Patient Population	Anemia Statistics*
Cancer Patients	80% of chemotherapy patients have severe anemia 8 million people die from cancer each year worldwide[11]
Chronic Kidney Disease (CKD)	26 million Americans have CKD[12] 28% of mild CKD patients are anemic 87% of severe CKD patients are anemic[13,14]
Critically Ill Patients	50% of patients in intensive care unit are anemic[15] 75% of long-stay critically ill patients are anemic
Diabetes	25.8 million Americans have diabetes[16] 33% of type 1 diabetic develop CKD after 15 years[17]
Elderly	50% of persons in nursing homes have anemia Anemic elderly are twice as likely to be hospitalized for falls[18]
Heart Disease	17-48% of anemic patients experience heart failure 43% of hospitalized heart attack patients have anemia[19]
Hepatitis C Virus (HCV) Patients	3.2 million Americans have chronic HCV infection 67% of hepatitis C patients have treatment-related anemia[20,21]
HIV/AIDS	75-80% of people with AIDS have anemia[22,23]
Inflammatory Bowel Disease (IBD) Patients	More than 1 million people in US have IBD 17-41% of all types of IBD patients have anemia[24]
Rheumatoid Arthritis	2.1 million Americans have rheumatoid arthritis[25] 30-60% of rheumatoid arthritis patients have anemia[26]

*All values are representative of passing World Health Organization (WHO) criteria for the diagnosis of anemia[27].

Despite a patient having adequate iron stores, ACI elicits low serum iron concentrations and a high erythrocyte sedimentation rate. ACI has similarities with other types of anemia, where the red blood cells show hypochromic microcytic characteristics similar to iron deficient anemia (Table 1.4).

ACI is easily confused with iron deficiency anemia (IDA). In both forms of anemia, levels of iron circulating in the blood are low. Circulating iron is necessary for supplying iron for red blood cell production in the bone marrow. Low blood iron levels occur in IDA because levels of the iron stored in the tissues are depleted (Figure 1.1). In ACI, however, iron stores are normal or high. Low blood iron levels occur in ACI, despite normal iron stores. Microcytic cells are usually present in both disorders, despite being more prominent in true iron deficiency.

Transferrin is another biomarker used in diagnosing anemia. Transferrin is a serum protein known for its ability to transport iron throughout the body. During iron-deficiency anemia, transferrin levels in serum are elevated. With ACI, transferrin levels drop[28].

A soluble transferrin receptor test can be used to help differentiate between iron-deficiency anemia and anemia of chronic disease. The soluble transferrin receptor is much less affected by inflammation than serum ferritin, and so results will be high in iron-deficiency anemia and usually low to normal in anemia of chronic disease. Medical practitioners or researchers can take the ratio of the soluble transferrin receptor to the

logarithm of the serum ferritin concentration, to more clearly distinguish between ACI and IDA. A study reported median values for patient groups of ACI as 0.5-0.8, where IDA patients range 5.0-6.2, and ACD/IDA 2.8-3.4[29].

Serum ferritin is also a biomarker used to distinguish between ACI and IDA. Early studies with serum ferritin correlated the serum ferritin levels with the iron content of bone marrow aspirates. Ferritin tracked with iron content in the bone marrow and allowed serum ferritin concentrations to predict iron status in an individual. This method works well for healthy individuals. But circumstantial consideration should be taken when considering ferritin levels. Ferritin is known to be an acute-phase reactant, meaning it can be elevated at onset of inflammation[30,31]. Therefore, elevated serum ferritin levels do not accurately correlate with bone marrow iron content if the patient has inflammation. Often C-reactive protein is measured along with serum ferritin content to determine if the serum ferritin content accurately predicts iron status.

Table 1.4. Anemia of Chronic Inflammation (ACI) versus Iron Deficiency Anemia (IDA)[1,3].

Investigation	ACI	IDA	Both ACI and IDA*
Iron	reduced	reduced	reduced
Transferrin	reduced to normal	increased	reduced
Transferrin saturation	reduced	reduced	reduced
Ferritin	normal to increased	reduced	reduced to normal
TIBC	reduced	increased	variable
Cytokine levels	increased	normal	increased

*Patients with both conditions include those with anemia of chronic disease and true iron deficiency.

Total iron-binding capacity (TIBC) is a medical laboratory test that measures the blood's capacity to bind iron with transferrin.   TIBC values are used as an indirect measurement to determine the iron content in the blood. These values are reported as being significantly low with ACI. This is due to iron not being as easily accessible, as the body stores the iron intracellularly. As iron stores deplete, TIBC values will increase. When iron stores are elevated, the TIBC will decrease. Normal values for TIBC range from 240-400 mcg/dL. In IDA, the TIBC is higher than 400-450 mcg/dL because stores are low. In ACI, the TIBC is usually below normal because iron stores are elevated[32].

As ACI develops in inflammatory diseases, increased levels of cytokines are found in such patients. Direct correlations have been previously shown between cytokine concentrations and the degree of anemia[33−36].

Pathophysiology of Anemia of Chronic Inflammation

Several processes are involved in the pathogenesis of ACI. Stunted erythropoiesis and inflammatory cytokines are implicated in all of them. These include impaired RBC survival, impaired proliferation of erythroid progenitor cells, blunted erythropoietin response, iron-restricted erythropoiesis and most importantly, impaired mobilization of reticuloendothelial system (RES) iron stores due to the regulation of the peptide hormone hepcidin.

Anemic patients with rheumatoid arthritis (a common model for ACI) show an inverse relationship between cytokine levels and RBC survival[37]. Similar results have

been reported in mice following exposure to the cytokine tumor necrosis factor (TNF) *in vivo*[38]. Human studies have also indicated that transfused ACI erythrocytes have a normal lifespan in normal recipients but transfused normal erythrocytes have a decreased lifespan in ACI recipients[39]. These findings suggest that increased erythrocyte destruction is due to the activated immune response. Finally, increased erythrophagocytosis during inflammation leads to a decreased erythrocyte half-life[40,41]

Impaired proliferation of erythroid precursors is clearly evident in ACI. Cytokines of inflammation inhibit the proliferation and differentiation of erythroid burst-forming units, which are the precursors to mature RBCs[42−44]. Interferon-α, -β, and -γ along with the interleukin and TNF families of cytokines all appear particularly potent[43,45,46]. Cytokine-mediated apoptosis, formation of ceramide, and down-regulation of erythropoietin have all been claimed as mechanisms. Cytokines can also form labile free radicals such as nitric acid or superoxide[47]. Inhibition is reflected by lowered Hb and reticulocytes concentrations.

Erythrocyte proliferation is regulated to a large extent by erythropoietin (EPO), which is produced in the kidney. Expression of EPO can be inversely related to tissue oxygenation and Hb levels. During ACI, EPO tends to stay at normal to low levels. This is in contrast to IDA, where EPO levels will dramatically increase[48−52]. The responsiveness of erythroid precursors to EPO seems to almost always be related to the severity of the disease involved.

Restricted iron availability can be illustrated during the intermediate step of heme production, where iron is incorporated into protoporphyrin IX. Protoporphyrin IX is a precursor to heme. Zinc is a known alternative to iron, and in circumstances where iron

9

is unavailable, zinc protoporphyrin is readily increased. In ACI, zinc protoporphyrin levels are increased, indicating insufficient iron. The presence of zinc in hemoglobin produces hypochromic RBCs, a true marker of IDA.
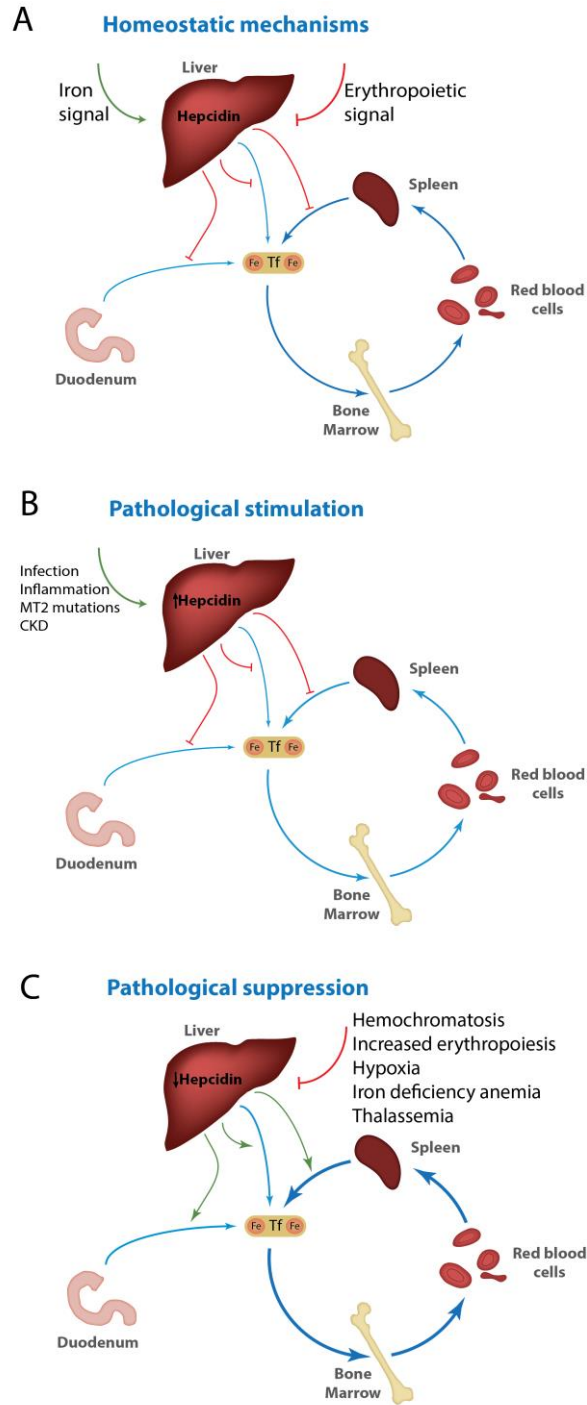
Figure 1.1. Hepcidin is a master regulator of the iron cycle. A) Homeostatic mechanisms involved in iron transport. **B)** Pathological stimulation and consequent suppression of iron transport.

Iron homeostasis

One of the more prominent underlying mechanisms behind restricted iron availability in ACI, is the disruption of iron absorption, iron mobilization from storage tissue and the transport of iron from the site of absorption and storage to the bone marrow. Inflammatory cytokines and cells of the RES system interfere with the body's ability to use stored iron and absorb iron from the diet[53]. This iron then becomes unavailable for efficient erythropoiesis, as it is sequestered in macrophages and other cells.

An average person stores 1-2 g of iron within the blood and tissue. Normally 1-2 mg of iron is lost daily (through shedding of intestinal enterocytes). This is replenished daily, as 1-2 mg is again absorbed through the gut from the diet[54].

Senescent erythrocytes are recycled daily by macrophages, recycling 20 mg of iron daily. Iron absorbed from the diet is absorbed through the intestines into duodenal enterocytes. This process is aided with the help of the protein divalent metal transporter-1 (DMT1). DMT1 is highly expressed at the apical pole of enterocytes, and is best characterized for its ability to transport ferrous iron (Fe^{2+}) into enterocytes[55].

Ferroportin-1 is an intermembrane protein iron exporter also known as Slc40a1. It is found on the surface of cells that store or transport iron including enterocytes in the duodenum, hepatocytes in the liver, and macrophages. Iron is absorbed into the duodenal enterocytes through DMT1, before being exported into the circulation via ferroportin.

Iron is then transported by transferrin to the bone marrow. Each individual transferrin protein is capable of carrying two ferric iron (Fe^{3+}) atoms. When iron arrives at the bone marrow, it is delivered to erythrocyte precursors to be incorporated into Hb. Circulating macrophages phagocytize senescent erythrocytes, recycling iron, and storing it in ferritin. Ferritin is capable of storing about 4,500 iron atoms during times of iron excess[56].

When iron is needed for cellular metabolic functions including erythropoiesis, macrophages are able to release the iron in ferritin into the cytosol where it is exported through ferroportin into the serum where it is bound to transferrin. This allows for restoration of serum and cellular iron levels when needed[57,58].

Hepcidin

Hepcidin is a cysteine rich 25 amino acid peptide that plays a major role in iron metabolism[59]. Hepcidin is synthesized in liver tissue cells known as hepatocytes. Initially it is formed intracellularly from the HAMP gene as an 84 amino acid (aa) precursor named preprohepcidin. Enzymatic cleavage converts this aa chain into a 64 aa long prohormone known as prohepcidin, and is then cleaved again into the mature biologically active 25 aa form known as hepcidin[60]. Hepcidin can then be excreted into the blood serum and circulated to various tissues, before being filtered by the glomerulus and excreted in the urine.

Hepcidin is most commonly found as hepcidin-25, but shorter forms have also been characterized. These include hepcidin-22 and hepcidin-20. The 22 aa isoform has

currently only been detected in urine, suggesting that it may be a degradation product of hepcidin-25.

Although liver is the main source of hepcidin, hepcidin mRNA and protein have been found in other cells and tissues. Heart, kidney, retina, monocytes and macrophages, splenocytes, pancreatic β cells, and adipocytes have also been observed to express mature hepcidin[61−68]. However, basal expression of hepcidin in these tissues is much lower than the basal expression rate of hepcidin in the liver. Basal levels of hepcidin in the serum normally range form 20-30ng/ml in healthy individuals, whereas in circumstances of chronic inflammation can reach 200-250ng/ml[69].

Production of hepcidin is regulated by the need of iron and erythropoiesis, as is critical regarding anemia (Figure 1.1). During active erythropoiesis hepcidin production is suppressed, making more iron available for the synthesis of heme for hemoglobin. The idea that a suppressive signal exists is not fully understood, but there is evidence that an erythroid factor produced by erythroid precursors in the bone marrow could be responsible[44,70].

The molecular target of hepcidin is the cellular iron exporter ferroportin. Ferroportin is a 571 aa intermembrane protein, whose leading purpose is to control iron efflux. Ferroportin exports iron, from the enterocytes into the plasma. It also supplies iron from macrophages of the spleen and liver that recycle senescent blood cells, and from hepatocytes involved in iron storage. When the concentration of hepcidin is low, ferroportin levels are uninhibited. When hepcidin is highly concentrated, ferroportin is internalized and iron is trapped within the enterocytes, hepatocytes, and macrophages[71].

14

Hepcidin acts as a ligand for ferroportin. When hepcidin binds to ferroportin, a conformational change occurs, leading to induced endocytosis and degradation of the hepcidin-ferroportin complex[72] (Figure 1.2). Binding to ferroportin is dependent on an extracellular loop containing a cysteine (C326)[73]. When this residue is mutated, iron efflux will continue despite the presence of hepcidin. People who suffer from the heterozygous mutation of this residue (C326S) quickly develop severe iron overload[74]. This is because iron absorption through the enterocytes will continue to occur without regulation or inhibition.
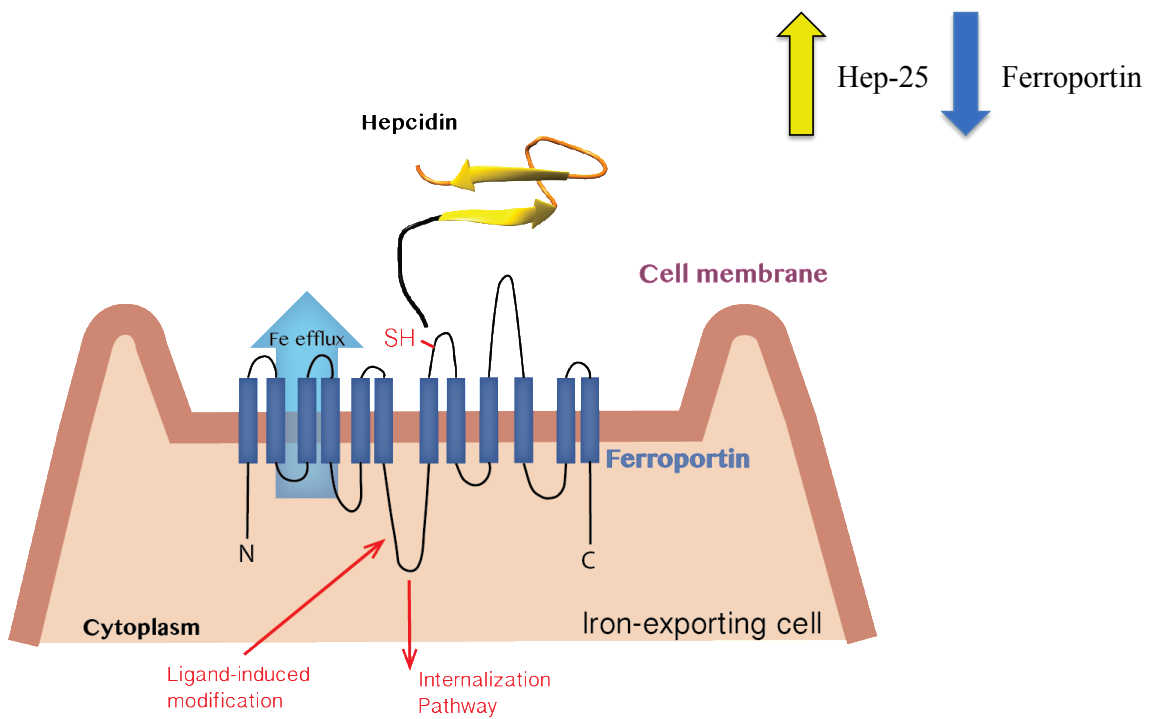
Figure 1.2. Hepcidin binding to ferroportin. Hepcidin binding region is located within the first five amino acids (DTHFPI). Hepcidin binds to an outer loop of ferroportin (C326) to induce endocytosis and degradation of the hepcidin-ferroportin complex. When hep-25 increases, ferroportin is lowered, and vice versa.
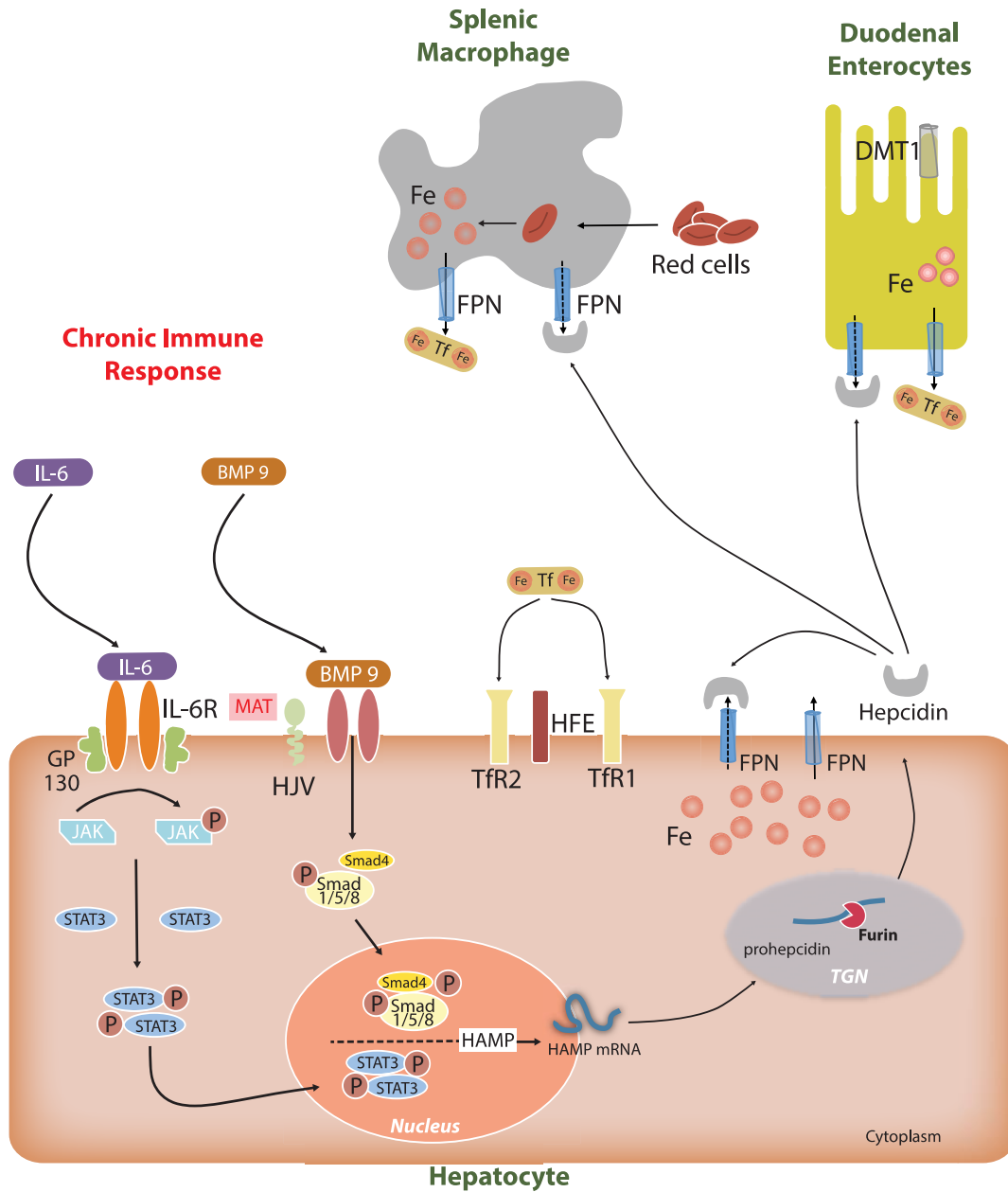
Figure 1.3. Overview of proteins involved stimulating Hepcidin production. During chronic immune activation, release of cytokines IL-6 and BMP9 activate HAMP gene expression, increasing the concentration of hepcidin. Hepcidin is exported out of the cell inducing endocytosis of ferroportin in different cells, perpetuating anemia.

Hepcidin-induced loss of ferroportin decreases iron transfer and availability to serum. This occurrence is known as hypoferremia, as hepcidin is able to regulate the concentration of ferroportin on the cell surface. Cell experiments where ferroportin has been expressed or over-expressed, have shown that small changes in hepcidin concentration drastically inhibit iron efflux[75,76].

To coordinate iron absorption from the apical membrane of enterocytes with ferroportin on the basolateral surface, several key factors are involved.

First, the stimulatory effect for DMT1 can be removed. Cellular iron is a cofactor of oxygen sensing prolyl hyroxylases. These induce the hydroxylation of hypoxia-inducible factor (HIF-1α), leading to degradation. HIF1α is no longer able to stimulate transcription of DMT1[77].

Second, as hepcidin binds to ferroportin, cellular iron increases because of diminished export. Increased cellular iron inactivates iron regulatory proteins (IRP1 and IRP2) that normally bind to the 3' iron regulatory element (IRE) of DMT1 mRNA[78]. This destabilizes the DMT-1 mRNA, leading to less transcription, and less expression of DMT1. In contrast, the IRPs are released from the mRNA encoding ferritin and ferritin synthesis increases. This leads to sequestration of iron in ferritin so that free cytosolic iron is not available for export into the bloodstream by ferroportin. Eventually the enterocytes are sloughed off the intestinal wall and excreted with the iron sequestered inside ferritin.

Third, DMT1 is down regulated by hepcidin through activation of ubiquitin ligases. As hepcidin binds to ferroportin, ubiquitin ligases distribute throughout the cytoplasm and consequently stimulate degradation of DMT1[79]. Other apical proteins

may be affected as well. Ubiquitination of other enterocyte transporters are currently being investigated.

Activation of hepcidin by Bone Morphogenic protein

BMPs represent a superfamily of transforming growth factor β (TGF- β) ligands, which share common 'cross-talk' or tranduction[80].

Liver and serum iron stores regulate hepcidin transcription and secretion through many different pathways. One of the major pathways to which hepcidin transcription is upregulated, occurs with inflammation. Cytokines known as bone morphogenic proteins (BMPs) are elevated in serum by inflammation and bind to hepatocytes and activate the BMP receptor and its corresponding pathway[51].

BMP receptors facilitate the activation of Small mothers against decapentalegic homolog (Smads) proteins (Figure 1.3). Smads are intracellular cascade proteins able to activate downstream transcription. Upon phosphorylation, Smads can act as transcription regulators for the HAMP gene, which encodes hepcidin (Figure 1.3). Signaling begins when ligands bind to complexes of two type I and two type II receptors. Type II phosphorylate type I receptors, which then phosphorylate Smads (Smad1, Smad5, Smad8)[81].

Although serum and liver iron accumulation alone can activate the BMP receptor and its Smad 1/5/8 pathway to increase hepcidin transcription[82], chronic inflammatory situations cause high concentrations of BMPs to circulate in the serum. During these

situations, the HAMP gene is activated above and beyond physiologically healthy constitutive levels[83].

A co-receptor protein known as hemojuvelin (HJV) also acts to regulate BMP signaling. HJV is essential for dietary iron sensing, and its mutation leads to severe iron overload[84]. Although the exact function of HJV is still unclear, HJV mutations cause severe hepcidin deficiency resulting in juvenile hemochromatosis[85].

Matriptase (MT-SP1) is an intergral membrane trypsin-like serine protease that is a member of the type II transmembrane serine proteases (TTSP). Matriptase-2, has been shown to cleave and activate HJV in liver tissue, and have an inhibitory effect on hepcidin promotion[86]. Expression of matriptase-2 mutants in zebrafish results in anemia, confirming its role in iron metabolism and its interaction with HJV[87].

Activation of hepcidin through IL-6 and other mediators

Inflammation has been shown to increase hepcidin synthesis through interleukin-6 (IL-6). IL-6 is an interleukin (cytokine protein family) secreted by T cells and macrophages to stimulate an immune response. IL-6 activates hepcidin production through the Jak/STAT signaling pathway. IL-6 acts as the ligand, and when bound to the glycoprotein 130 (gp130) receptor, activates janus kinases (JAKs). JAKs are then able to phosphorylate and activate Signal Transducers and Activators of Transcription (STATs), particularly STAT3. Activated STAT3s form dimers, translocate to the nucleus, bind to specific response elements in promoters of target genes, and transcriptionally activate

these genes[88]. When the IL-6 inflammatory stimulus is upregulated, HAMP gene transcription responds significantly (Figure 1.3)

HAMP reporter constructs (as shown by RT-qPCR) respond to both IL-6 and the BMPs in a manner consistent with endogenous hepcidin[89].

Studies show that hepcidin concentrations are significantly increased with patients having chronic inflammatory disorders. Inflammatory secretion of IL-6 and BMPs, as well as other cytokines are well documented and are expected to contribute to anemia of chronic inflammation[31,48,90−92].

Some diseases result from inadequate hepcidin production. The classic example of this would include the iron overload disease hemochromatosis. Hyper-absorption of dietary iron leads to accumulation of iron in the tissues, iron mediated injury, and organ dysfunction[93]. Hereditary hemochromatosis (HH) usually results from an autosomal recessive mutation in the hemochromatosis protein (HFE) gene. The end result is insufficient production of hepcidin by the liver. This leads to improper iron absorption through enterocytes, and excessive iron transport into the serum.

Similar symptoms occur in β thalassemia hereditary diseases. β thalassemia patients have inherited a mutation where the beta chain synthesis of hemoglobin has been negatively affected. Affected individuals require lifelong blood transfusions, and are essentially receiving repeated doses of recycled iron without being able to properly stop absorbing it. Iron chelation and even phlebotomy treatments have been used as therapeutics.

Pharmacological approaches of hepcidin-targeting

Hepcidin excess or deficiency clearly plays a role in the pathophysiology of various iron disorders. Hepcidin agonists include agents that mimic the function of hepcidin, or promote its synthesis. Whereas hepcidin antagonists are factors that inhibit function or reduce hepcidin production. Therefore, the use of hepcidin agonists, or antagonists, could potentially be used as therapeutics in treating disease (Table 1.5). For example, over expression of hepcidin in a model for HH prevented liver iron overload[94]. And with ACI, hepcidin knockout mice are shown to produce a milder anemia with quick recovery[95].

Table 1.5. Hepcidin targeting pharmacological approaches[96].

Therapeutic Approach	Targeted Disease	Mode of Action	Agents
Hepcidin Agonists	Iron overload (HH/ β thalassemia)	Hepcidin mimics or Stimulators of hepcidin production	Minihepcidins[97] BMP pathway agonists[98]
Hepcidin Antagonists	Iron restricted anemia (IDA/ACI)	Suppressors of hepcidin production	BMP pathway inhibitors[99]
			Anti-inflammatory agents[100,101]
			Erythropoiesis stimulating agents[102,103]
			Gene silencing of hepcidin and its regulators*
		Hepcidin peptide neutralizing binders	Anti-hepcidin antibodies[104]
		Agents interfering with hepcidin-ferroportin interaction	Anti-ferroportin antibodies[105]

*Information available at clinicaltrials.gov, a service of the U.S. National Institutes of Health.

The very nature of using gene-silencing techniques successfully avoids the potentially dangerous side effects of drugs. However, these techniques are difficult to deliver throughout a tissue or system, and can have undesired over-lapping long-term effects[106]. Erythropoiesis stimulating agents promote RBC production, but do not address issues with iron homeostasis.

Antibody therapies have had marginal success, most likely because of the small size and tightly folded structure of hepcidin. BMP pathway agonists have for the most part also pursued inhibition through the use of antibodies. Antibodies have high specificity and low toxicity. Despite these advantages there are drawbacks, including high production costs, eventual resistance, poor pharmacokinetics and tissue penetration, as well as limited efficacy requiring highly sustained doses[107].

Hepcidin is the master negative regulator of iron homeostasis and rapidly responds to iron supply and demand, as well as to inflammation and erythropoietic activity. Its synthesis is inhibited by iron deficiency, and yet stimulated by inflammation. The hepcidin-ferroportin iron disorders including iron over-load and iron restricted anemia's, are significantly affected by even minute changes at the hepcidin-ferroportin axis[108]. These minute changes provide a potentially promising environment to which minor pharmacological changes have greater therapeutic results.

Although hepcidin synthesis in hepatocytes is regulated by iron, erythropoietic activity and inflammation, the processing of hepcidin is specifically dependent on furin processing. As such, furin is considered an attractive target with new therapeutics[109]. The success of the strategies used depends heavily on the safety and efficacy of the

23

compounds involved, being non-toxic, biocompatible, and able to avoid recognition by the host's defense mechanisms.

Furin Activates Hepcidin

The proprotein convertase (PC) known as Furin (PC1/3), has been specifically identified as being the sole PC responsible for generating active hepcidin[110−112]. Hepcidin is initially synthesized as a larger precursor protein, undergoing two cleavages (the signal sequence then the pro-region). Furin is known to form mature, active hepcidin, with the removal of this pro-region. Furin activates hormones and other substrates by cleavage of the inactive protein precursor at multi-basic consensus amino-acid sequence. In the case of hepcidin, furin readily hydrolyzes the preprohepcidin at its arginine rich consensus site, producing active hepcidin-25 (Figure 1.4)[111,112].

Pre-Pro-Hepcidin:

Target signal for Endoplasmic reticulum

MALSSQICLLLLLLLLASLTSGSVFPQQTGQLAELQPQDRAGARASWMPMFGRRRRRDTHFPICIFCCGCCHRSKCGMCCKT

Full Length 84-amino acid expression of hepcidin

Pro-Hepcidin:

Cleaved to activate hepcidin

SVFPQQTGQLAELQPQDRAGARASWMPMFGRRRRRDTHFPICIFCCGCCHRSKCGMCCKT

Prohepcidin - 35-amino acid precursor

Hepcidin:

DTHFPICIFCCGCCHRSKCGMCCKT

Hepcidin-25 - active form of hepcidin

Figure 1.4. Processing of Preprohepcidin to hepcidin. Cleavage of prohepcidin occurs just after the multibasic poly-arginine motif, by the protease furin. Preprohepcidin has a molecular weight of 9.5 kDa, while prohepcidin and hepcidin have the molecular weights of 6.9 kDa, and 2.8 kDa respectively.

Serine Proteases

Serine proteases make up at least one third of all known protease enzymes. Serine proteases are known for their use of the catalytic triad in hydrolyzing peptide bonds (Figure 1.5). The –OH group serine residue is responsible for the nucleophilic attack, attacking the carbonyl carbon on the peptide bond of the substrate. The –OH group acts as the nucleophile, and the nitrogen on the histidine has the ability to accept the hydrogen from the serine –OH group. The aspartic acid residue's carboxyl group then hydrogen bonds with the histidine, making the nitrogen on the histidine more electronegative[113]. A nearby pocket of positively charged residues also stabilizes the transition state of the deprotonated oxygen. This pocket is usually referred to as an oxyanion hole. Oxyanion holes also aid with substrate insertion, preventing steric hindrance by substrates that otherwise would not fit.
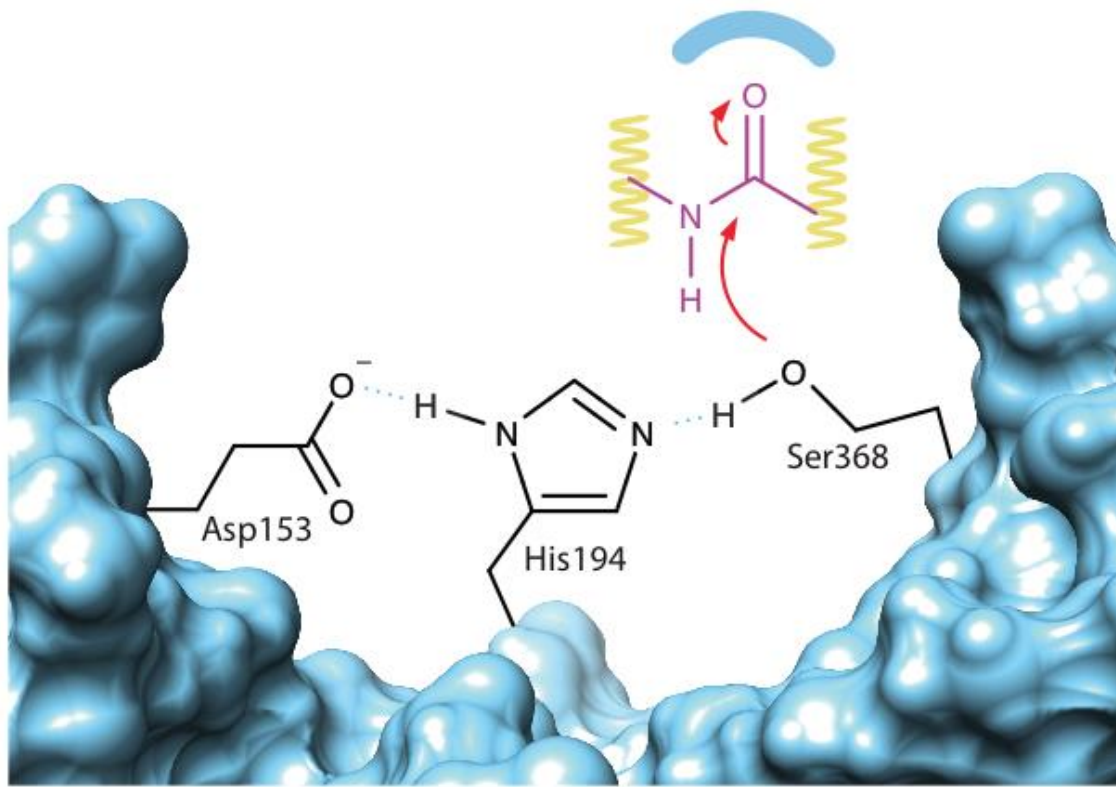
Figure 1.5. The catalytic triad of furin. Shown, is the mechanism to which peptide cleavage is activated by a serine (368) residue, and stabilized by histidine (194) and aspartate (153). Serine's hydroxyl group acts as a nucleophile to attack the peptide's carbonyl carbon. Consequent tetrahedral intermediates are stabilized by a water molecule within the oxyanion hole, designated by the curved blue bar.

The most abundant sub-group of the serine proteases is the chymotrypsin-trypsin like protease family. These are involved in a multitude of physiological processes, including digestion, tissue repair, apoptosis, embryogenesis, and cell activation[114].

There is however another, smaller, family of proteases known as the proprotein convertases. These perform a variety of activation functions within critical cellular pathways.

The Proprotein Convertases

Proprotein convertases are a family of Ca^{2+} dependent proteins known to activate other proteins. These proteolytic enzymes cleave larger inactive protein precursors into smaller active forms. So far, nine PCs have been identified and characterized (Table 1.6). PCs are initially formed as zymogens. Zymogens are the inactive precursors that are chaperoned by their prodomains[115]. The prodomains are essential in orchestrating folding and eventual departure from the endoplasmic reticulum (ER). Following exit from the ER, a pH and calcium dependent cleavage event in the trans-Golgi network activates the enzyme[116].

PC activity occurs through the kinetic contribution of the highly conserved catalytic domain (C domain) and protein-protein domain (P domain). Clustering of negatively charged amino acids within the C domain are common throughout all known PCs[117]. This organization is likely responsible for the selectivity of pro-basic substrates[118−120].

While seven PCs cleave after single or paired basic residues, two (SKI-1, PC9) cleave at non-basic residues[121].

Fluorogenic Assays for Proprotein Convertases

Novel approaches in studying PC kinetics and substrate specificity have been developed, including the use of fluorogenic assays. Although there is some cross talk between substrate specificity, each PC has been reported to perform unique proteolytic tasks specific to that enzyme. Fluorogenic assays are particularly ideal for studying the kinetics of an enzyme. In this method, a fluorogenic peptide contains a fluorescent portion located at the C-terminus just after the known cleavage site. The most commonly used fluorescent groups are the 4-methyl-7-amino coumarinamide (MCA)[122,123] and 7-amino-4-methyl coumarin (AMC)[124] groups (Table 1.6).

Table 1.6. Characteristics of the Proprotein Convertases.

Protein Name	Gene Name	Known peptidyl-MCA activity assay substrates *in vitro*$^{\Psi 125\text{–}134}$	Biological Function *in vivo*
PC1	PCSK1	pE-R-T-K-R-MCA R-S-K-R-MCA	Activates polypeptide prohormones[135]
PC2	PCSK2	pE-R-T-K-R-MCA Abz-V-P-R-M-E-K-R-↓Y-G-G-F-M-Q-EDDnp	Activates polypeptide prohormones[136]
Furin	FURIN	Boc-R-V-R-R-MCA Ac-R-A-R-Y-R-R-MCA	Activates mammalian and microbial precursors[134]
PC4	PCSK4	R-Q-R-R-MCA R-K-K-R-MCA	Activate proteins involved in sperm motility, reproduction[131]
PC5A/B	PCSK5	Boc-R-V-R-R-MCA pE-R-T-K-R-MCA	Activates ECM proteins[137]
PACE4	PCSK6	R-Q-R-R-MCA R-K-K-R-MCA	Activates ECM proteins[138]
PC7	PCSK7	pE-R-T-K-R-MCA Abz-R-N-T-P-R-E-R-R-R-K-K-R↓G-L-Tyx-A139	sTfR, activates multiple precursors, furin overlap[132]
SKI-1	MBTPS1	Succ-I-Y-I-S-R-R-L-L-MCA Succ-Y-I-S-R-R-L-L-MCA Succ-F-I-S-R-R-L-L-MCA	Processes membrane-bound transcription factors involved in lipid metabolism[140]
PCSK9	PCSK9	Dnp-F-A-Q-S-I-P-K-AMC121	Regulates plasma LDL, VLDLR levels[141]

*   Boc denotes t-Butyl carbonyl; pE, pyroglutamic acid; Ac, Acetyl; MCA, 4-methyl-7-amino coumarinamide; AMC, 7-amino-4-methyl coumarin; Dnp, 2,4-dinitrophenyl; Succ, Succinoyl group; EDDnp, *N*-(2, 4-dinitrophenyl)ethylenediamine; Abz, *ortho*-aminobenzoic acid; Tyx, 3-nitro tyrosine; ECM, extracellular matrix; sTfR, soluble transferrin receptor; LDL low-density lipoprotein; VLDL very low-density lipoprotein receptor.

Ψ Single letters denote abbreviations for corresponding amino acids.

Although fluorogenic and other *in vitro* assays are useful when studying individual PCs and their substrates, understanding the physiological homeostasis of the PCs *in vivo* remains challenging. Some consequences of PC function have been explored through gene-knockout and tissue specific models[142,143]. The absence or underexpression of PCs during embryogenesis has critical effects during organ development. Knockout of furin is lethal at the embryonic stage, as formation of the cardiovascular system and gut are severely defective[144].

Knockouts of other PCs, when possible, have also shown extreme defects and deficiencies in growth and fertility (PC 2,4)[144,145] or in development (PC 6)[146,147]. As PCs have the ability to activate a wide range of substrates, over expression or deficiency of PCs has been linked to many diseases. These include Alzheimer's[148], atherosclerosis[149], infectious diseases[150], cancer[151], and many others.

As shown in the above studies, suicide inhibition of a PC would likely be detrimental as a therapeutic due to the large amount of cross talk between PCs. Suicide inhibition occurs when covalent bonds, or irreversible bonds, are made with the catalytic triad residues within the PC. Inhibition of an upregulated PC, acting to clinically reduce activity back to basal rate through reversible binding, would likely be a better alternative. It is still obvious, however, that the potential behind investigation and development of potent and effective PC inhibitors and silencers with non-invasive application, is fertile ground for treating disease (Table 1.7).

Table 1.7. Proteins and Substrates activated by differing PCs[142].

Proprotein Convertase	Secretory Proteins
PC1	Growth hormone–releasing hormone, insulin, glucagon-like peptides, corticotropin, β-lipotropin, melanocyte-stimulating hormones, met-enkephalin, β-endorphin
PC2	Insulin, glucagon-like peptides, corticotropin, β-lipotropin, melanocyte-stimulating hormones, met-enkephalin, β-endorphin, somatostatin
Furin	Tumor necrosis factor, protein C, von Willebrand factor, neurotrophins, adhesins, α- and β-secretases, tumor necrosis factor α (through intermediaries), transforming growth factor β, IGF-1, IGF-1 receptor, integrins, platelet-derived growth factor, vascular endothelial growth factors, matrix metalloproteinases, bone morphogenetic proteins, anthrax toxin, pseudomonas exotoxin A, aerolysin toxin, Shiga toxins, Clostridium septicum α-toxin, diphtheria toxin, various viral-coat proteins (human immunodeficiency virus type 1, Ebola virus, influenza hemagglutinin, measles virus, cytomegalovirus, respiratory syncytial virus, coronavirus causing severe acute respiratory syndrome)
PC4	Pituitary adenylate cyclase–activating polypeptide, IGF-2
PC5A/B	*In vitro* overlap with furin and PC7, growth differentiation factor 11
PACE4	*In vitro* overlap with furin/PC7; neural adhesion molecule L1, matrix metalloproteinases, bone morphogenetic proteins
PC7	TfR1[152], Various growth factors, some substrate overlap with furin
SKI-1	Sterol regulatory-element–binding proteins involved in lipid metabolism, brain-derived neurotrophic factor, surface glycoproteins for hemorrhagic fever viruses
PCSK9	Low-density lipoprotein receptor

* IGF-1 denotes insulin growth factor 1; TfR1, transferrin receptor-1.

Furin

One of the most recognized and studied PCs is furin. Furin is a 794 aa serine
endoprotease, and is as other PCs, dependent on calcium and pH for activity. Whereas
other PCs enhance their catalytic properties in acidic environments, furin is optimally
active at neutral pH (Figure 1.6).

Furin has a substilin-like domain with the catalytic triad (Ser 368, His 194, Asp
153) typical of other serine proteases, and an oxyanion hole (Asn 295)[118]. The oxyanion
hole contains an asparagine that is interconnected to Ser 368 through a water molecule,
allowing for stabilization of serine's deprotonated oxygen during catalysis of a peptide
bond.

Furin is expressed ubiquitously, in all tissues, and at high levels in the liver[153]. At
steady state, furin is found mostly in the trans golgi network (TGN)[154,155], as it cycles
back and forth to the cell surface as well as within the endosome, cleaving various
substrates under mildly acidic conditions[156]. More recently, it has been reported that
furin can be secreted from cell tissue cultures into media post transfection[157,158].

Proteolysis by furin is highly specific, and occurs on the C-terminal end of a
multibasic recognition motif. The binding site strongly favors arginine at the P1 site, and
basic amino acid side chains at P2, P4 and/or P6[159,160] (Figure 1.7). Furin will cleave
secretory protein precursors at specific single or paired basic amino acids within the
motif of $(Arg/Lys)X_n(Arg/Lys) \downarrow$[118], where X stands for a neutral, polar amino acid , '$\downarrow$'
designates the cut site, and X_n corresponds to a 0-, 2-, 4-, or 6-amino acid spacer[109].
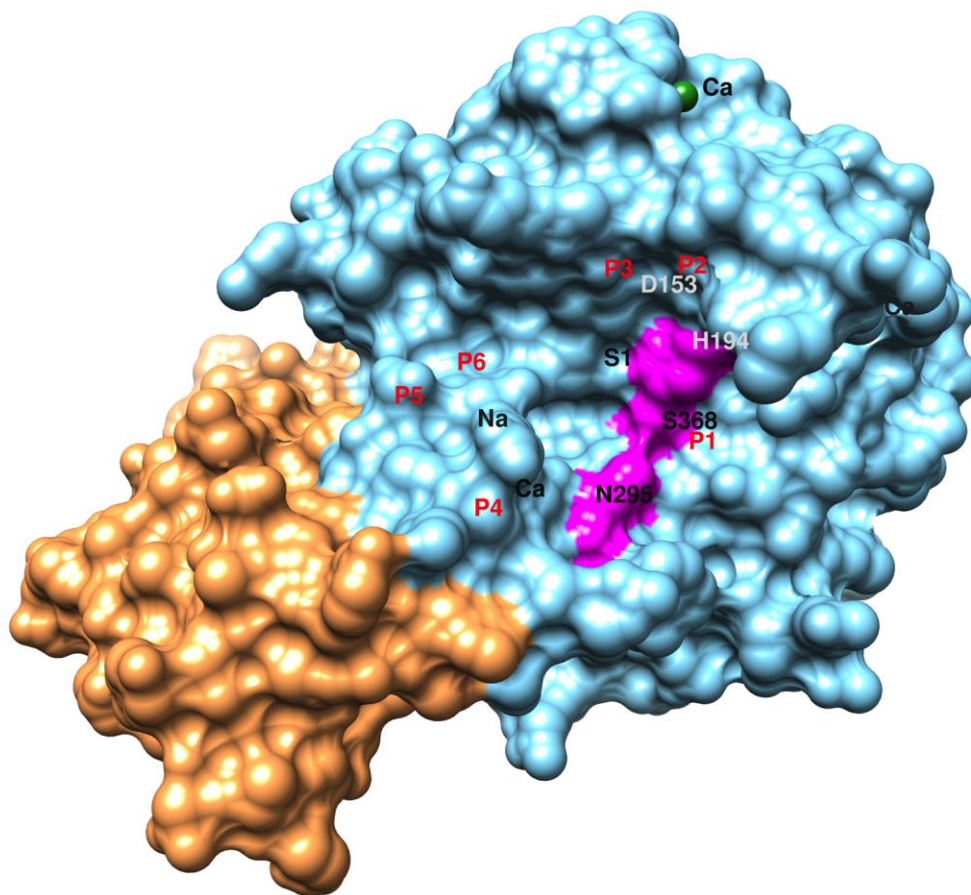
Figure 1.6. The Proprotein Convertase Furin. A single subunit of furin with the catalytic (C) domain in blue, and the protein-protein (P) domain in gold (PDB 4OMC)[118,161]. Highlighted in magenta is the catalytic triad (Ser368, His194, Asp153). P1-5 (red) represent known hydrophobic interaction sites with substrate, promoting specificity. Furin has three Ca^{2+} and one Na^+ binding site, contributing to furin's catalytic cycle[162]. Furin is Ca^{2+} dependent, requiring concentrations of at least 1mM for full activity[115].

Prodomain
"Intramolecular chaperone" functions:
   compartment-specific activation
   assists in protein folding
   disassociated after second cleavage
Autoinhibit PCs

Signal Peptide
Translocates directly into the ER

D
H

Catalytic Domain
Catalytic triad formed by Asp 153, His 194 and Ser 368.
Oxyanion hole in Asn 295.
Binding sites for Na⁺ and Ca²⁺.
Cross-connected by disulfide bridges

S

P Domain
Stabilizes acidic prodomain and catalytic domain
Essential for catalytic activity
Eight-stranded jelly-roll

Cystein-rich domain
Confers protein-ligand interactions properties
Direct cell surface tethering
Also present in PCSK5, PCSK6, PCSK7

Transmembrane Domain
Directs sorting and transit in the cell compartments
Direct cell surface tethering
Present in other PCs: PCSK5, PCSK7

Cytosolic Domain
Similar characteristics to the Transmembrane domain

Figure 1.7. Furin domains. Schematic representation of the furin domains with their functions. The catalytic domain displays the conserved catalytic triad.

As the crystal structure for furin has been resolved, researchers have already synthesized and characterized several small molecule inhibitors. 2,5-dideoxystreptamine and dicoumarol derivatives[163], naphthofluorescin disodium salt (CCG-8294 or B3)[164], and multi-arginine peptide mimetics[165] have been tested in varying environments. These compounds all act as competitive inhibitors of furin, interfering with proteolytic processing by furin's catalytic domain. Protein inhibitors such as α1-PDX also successfully inhibit furin *in vitro* and *in vivo*[166], and are commercially available to be studied in various disease models.

Furin mRNA silencing is a promising therapeutic currently in clinical trials, approximately doubling the days of survival in advanced cancer patients[167]. Here, a short hairpin RNAi is used to target furin. Results show downregulation of growth factors (TGF) β1 and β2, and consequent slowing of metastasis.

Despite these recent advances, a small-molecule inhibitor of furin is yet to successfully and safely pass through FDA clinical trials. But with the resolved crystal structure of furin known, the availability of fluorogenic substrates for kinetic assay's, and *in silico* molecular docking computational predictions, it is unlikely that new small-molecule pharmacological inhibitors of furin will remain off the market.

Theory

Molecular interactions are the fundamental players in biological processes. To better understand binding and affinity between interacting molecules, the tertiary structure of proteins and three-dimensional structure of the molecule is required.

Acquiring complex tertiary or three-dimensional structures with experimental methods such as NMR or X-ray crystallography is laborious, challenging, and often expensive. Computational docking is a technique, which allows the researcher to gain understanding of protein-protein or protein-ligand interactions using molecular docking software. Docking is a method able to predict the preferred orientation of one molecule bound to another, forming a stable complex in three-dimensional space. The protein acts as the "lock", and the ligand acts as the "key"[168].

Modeling interactions between two molecules involves many intermolecular associations, including hydrophobic, van der Waals, stacking interactions between amino acids, hydrogen bonding, and electrostatic interactions[169]. The process itself attempts to mimic a natural course of interaction involving the lowest energetic pathway.

If the receptor structure and ligand configuration is available, mathematical algorithms create an optimum number of configurations that include different binding modes[170]. These algorithms regularly require supercomputers to handle the copious

number of precise configurations and best-fit possibilities between two complex molecules.

Scoring functions are generally used for this purpose. A scoring function consists of a number of mathematical methods used to predict binding affinity. Binding affinity is defined here as the strength of the non-covalent interaction between ligand and protein. Scoring functions select the best pose, otherwise known as the best ligand conformation and orientation. These poses are then ranked based on affinity.

Some common searching algorithms include molecular dynamics, Monte Carlo methods, genetic algorithms, fragment-based, point complementary and distance geometry methods, and systematic searches[171].

Structure preparation

When using these algorithms during virtual screening, lead optimization, or de novo drug design, several factors become critical. First, the protein's tertiary structure must be known. Factors of solvent, flexibility, and the environment to which the protein was initially characterized will influence the algorithm's output. Orientation of asparagine, histidine, and glutamine side chains, as well as the position of water molecules should be considered with caution[172], since their identification and location are challenging to X-ray crystallographers and sometimes different from *in vivo* conditions.

Second, the three-dimensional shape of the ligand when bound to the protein must be well understood. The proper stereochemistry of the small molecule in its most

relevant setting should be considered. Factors of protonation state, tautomeric form, and concentration may be influential on prediction outcomes. Circumstantial differences *in vivo* often relay pharmacokinetic variation in ligands.

And third, the appropriate scoring function must be applied to estimate a relevant conformation and binding mode. A perfect scoring function would be able to predict the exact binding free energy between a ligand and it's target. Unfortunately, differing scoring methods provide differing advantages and limitations. These variations lead to differences between docking scores and experimental results.

When preparing structures for docking, a "hand and glove" analogy may be more appropriate than the "lock and key".

Scoring Functions

Currently, there are three main designations of scoring functions, including force field, statistical, and empirical scoring functions.

Force field scoring functions estimate the sum of strength of electrostatic interactions between all atoms of the two molecules involved (Figure 1.8). This includes not only the intermolecular forces, but also predicted intramolecular forces. Desolvation energies of the protein and ligand also contribute the summing of strength, as binding normally occurs in water or other solvents. The hydrophobic solvent accessible surface area[173,174], through use of the Generalized Born model, compliments the prediction data and aids in this calculation.

Statistical scoring potentials are energy functions derived from analysis of protein structures in the Protein Data Bank (PDB). These are approximations of free energy based on torsion angles, hydrogen bond geometry, and solvent exposure[175,176]. The energies are determined using statistics from amino acid contacts, where a numerical value is affixed to each possible pair of amino acids binding to one another. Once values are assigned, calculated versions of binding affinity are ranked and ordered.

Empirical scoring functions focus on counting the types of interactions between two molecules[171,177]. These interactions are scored as favorable versus unfavorable. A favorable scoring would include a hydrophobic-hydrophobic contact, whereas an unfavorable scoring would include a hydrophobic-hydrophilic contact. Rotatable bonds are considered unfavorable. Hydrogen bonds are considered as favorable, especially if shielded from solvent.

Scoring methods are constantly being revised to improve accuracy and limit variability. The recent introduction of metal ion interactions, improved pose predictions, sp^2-sp^2 torsions, and covalent bond docking, are just a few aspects that constantly contribute to the evaluation and debate of docking structures. However, published binding constants have shown a spread of computational factors to experimental factors of up to a factor of 5 ($\approx$4 kJ/mol)[177-179]. Ambiguity still exists between calculated and observed data.

Despite the common setbacks of protein and ligand flexibility, solvent interactions, and other limitations, computational molecular docking is proven as an effective basis for experimental testing and screening.

Application and Procedure of Protein-Ligand molecular docking

The amino acid sequence and tertiary structure of human furin is first retrieved from the National Center for Biotechnology Information (NCBI) and from the Protein Data Bank (PDB) under the classification entry codes (ex. 4OMD or 4OMC).

Small molecule ligands are collected from the ZINC database[180]. The ZINC database is a free database of commercially available compounds for virtual screening. Containing over 35 million compound entries, molecules are available in ready-to-dock three-dimensional formats. Compounds can also be acquired from chemspider.com or the emolecules.com database. Although available in multiple file formats, ligand information available in mol2 files is most desired. Precaution should be taken to ensure that the mol2 file includes all applicable hydrogens and three-dimensional coordinates. Chirality and protonation state should also be reviewed.

To best review these variables and ensure proper ligand topology, mol2 files are uploaded to ChemDraw[181]. ChemDraw is a drawing tool that allows for ligand editing among a multitude of other features. Once the ligand has been altered to the desired configuration, it can be saved and exported into a number of differing chemical file formats. The mol2 file format is presently a convenient format suitable for CHARMM energy calculation.
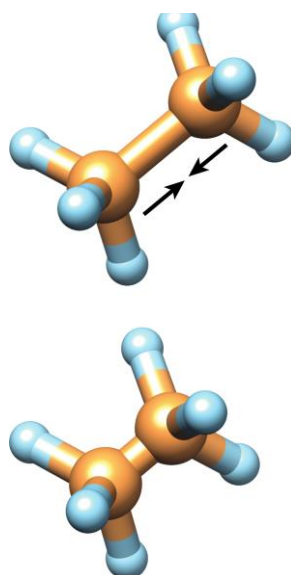
Figure 1.8. **Simulation describing a system of potential energy**, or force field, as defined by computational prediction software. A force field is used to minimize the bond stretching energy of this ethane molecule[182]. Inward arrows indicate direction of force.

CHARMM software[183–185] uses force field simulation analysis to predict molecular dynamics. As previously described, a force field scoring uses a set of mathematical functions to represent the potential energy of a system. A set of parameters is given to each type of atom, and based on these parameters a summation calculation is made to determine the strength of the force field. Once the ligand is properly prepared, it can be uploaded along with the protein PDB file onto the online docking server known as SwissDock.

SwissDock is based on the docking software EADock DSS[186], whose algorithm works as follows. Many binding modes can be produced in a designated box for what is known as local docking. Binding modes can also be produced in a target cavity, which is referred to as blind docking. CHARMM energies are then predicted and the binding modes with the most favorable energies are evaluated with a program called Fast Analytical Continuum Treatment Software (FACTS)[187]. FACTS provides a description of the solvation effect upon binding. After the most favorable energies are clustered and then ranked, the results can be downloaded. Predicted binding modes can be viewed via a Jmol[188,189] applet , or uploaded into Chimera for further investigation.

SwissDock is a docking web server. The burdensome work of the docking engine is done on the server side. This allows for extensive docking calculations to be completed without the need for excess computational power on the client's side.

Viewing SwissDock predictions in Chimera

Chimera[190] is a free computational program used for interactive visualization of molecular structures, sequence alignments, docking results, and conformational illustrations. It allows for the analysis of sequence-structure-function relationships. Prediction software analyses and docking results can be explored visually in three-dimensions. Multiple software tools are linked to Chimera. Visualization plugins for NMR analysis, secondary and tertiary structure topography, and transmembrane protein images are openly accessible.

Chimera will then illustrate docking results, interpolate absolute fitness, and manifest free energy calculations. The site of binding is studied, and the lowest delta G values recorded and evaluated. It should be noted that compounds found in SDF, SMILES, or flexibase file formats, can be converted into compliant .mol2 files using Chimera.

LigPlot+ or DIMPLOT displays

To further understand the ligand-protein interaction generated from the SwissDock predictions, a LigPlot can be preformed. LigPlot+ software can display a two-dimensional view of the interaction between the ligand and the protein[191]. LigPlots illustrate hydrophobic contacts and hydrogen bond interactions with any amino acids in

the protein. Ligand-target complementarity between differing ligands can be viewed and compared. These visual aids help communicate differences in small molecules binding to the same protein target (Figure 1.9). They can also aid in drug design strategy. Loading SwissDock output results files in .pdb format will allow for ligplot analysis.
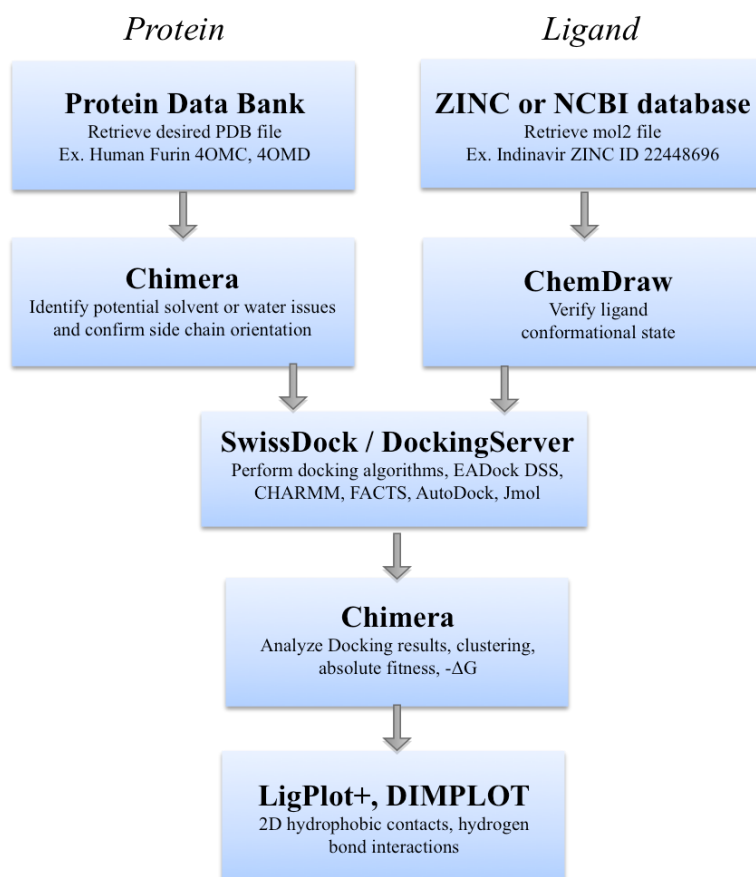
Figure 1.9. Molecular modeling flowchart. After retrieval of the Protein and ligand files, the molecules are prepared with Chimera or with available options from Swissdock and DockingServer and subsequently submitted for docking. The resulting file can then be visualized in Chimera. Interactions can be mapped in 2D with LigPlot+.

HIV protease Inhibitors are small-molecule ligands, which can bind with high affinity to catalytic residues within the homodimeric HIV protease. Their development is based on a structure-based drug design.

HIV proteases have conserved catalytic regions, with hydrophobic cavities and two aspartyl residues. Two aspartyl residues are responsible for hydrolyzing peptide bonds[192]. Other amino acid residues along the catalytic domain mediate recognition and binding of substrate, by potentially forming hydrogen bonds or hydrophobic contacts with the substrate.

Based on the recognized cleavage sequences performed by HIV-1,2 protease, small-molecules were designed to mimic substrate, and fit within the hydrophobic cavity to prevent catalytic activity. As HIV protease is known to cleave sequences containing Tyr-Pro or Phe-Pro, "peptido-mimetic" structures were synthesized to promote binding, and therefore inhibit cleavage of mature precursors[193].

Design of these small-molecule inhibitors include a hydroxyl group on the core motif, which is able to form a hydrogen bond with the carboxylic acid on the aspartic acid residues at the catalytic site. This bond is stabilized through a water molecule usually found within what is termed as an oxyanion hole. Design also involved adding different terminal residues to enhance solubility, as in the case of adding pyridyl groups in place of terminal phenyl residues[194].

Some residues on the protease binding site are capable of forming hydrogen bonds with hydrophilic groups on the inhibitor. Terminal tetrahydrofuran (THF) groups

are added to the molecule for this purpose, as was done with amprenavir. In the case of darunavir, two have been added[195]. The THF groups allow for more hydrogen bonds to be potentially made with the residues at the catalytic site of the protease, increasing binding affinity.

The basic design and structure of the HIV protease inhibitor small-molecules were designed for high affinity, based on principles of structural fit and hydroxyl motif. Consequently, it is not unreasonable to assume, that these small-molecules might also make potentially similar hydrogen bonds and hydrophobic contacts with other proteases. The hydroxyl group motif of the molecules could also form hydrogen bonds with the catalytic subunits.

It turns out that this was not only a theoretical possibility; it is a very likely scenario. Despite being designed for one purpose, the HIV PIs are nonetheless small molecule ligands, capable of having an affinity for, and binding to, other distinct proteases that mechanistically function along the same catalytic guidelines.

Our goal was to capitalize on using safe, efficacious, clinically proven drugs, as potential ligand inhibitors for furin. Promising ligands are then applied to *in vitro* fluorogenic screens, *in vivo* tissue culture, and finally within an animal model for ACI.

Outlined below are the aims to which promising ligands were screened to inhibit furin.

Furin Inhibition:

- In silico, computational modeling through the use of several docking servers and software.

- In vitro, fluorogenic assays using purified furin and known substrate with attached fluorophores.

- In vivo, tissue cultures. Immortalized hepatocyte cell lines HepG2 and Huh7.

- In vivo, animal model of ACI. Lewis rat model involving a chronically activated immune response.

References

1. Perkins, S. Diagnosis of anemia. *Pract. Diagn. Hematol. Disord. Fourth Ed C Kjeldsberg Ed ASCP Press Chic. IL* 1–16 (2006).

2. Moreno Chulilla, J. A., Romero Colas, M. S. & Gutierrez Martin, M. Classification of anemia for gastroenterologists. *World J. Gastroenterol. WJG* **15,** 4627–4637 (2009).

3. Weiss, G. & Goodnough, L. T. Anemia of Chronic Disease. *N. Engl. J. Med.* **352,** 1011–1023 (2005).

4. Jr, M. R. Recent developments in the anemia of chronic disease. *Curr. Hematol. Rep.* **2,** 116–121 (2003).

5. Da, S. Anemia of chronic disease. *Med. Clin. North Am.* **76,** 567–579 (1992).

6. Komajda, M. The impact of new onset anaemia on morbidity and mortality in chronic heart failure: results from COMET. *Eur. Heart J.* **27,** 1440–1446 (2005).

7. Ward, B. W., Schiller, J. S. & Goodman, R. A. Multiple Chronic Conditions Among US Adults: A 2012 Update. *Prev. Chronic. Dis.* **11,** (2014).

8. Sharma, R. *et al.* Haemoglobin predicts survival in patients with chronic heart failure: a substudy of the ELITE II trial. *Eur. Heart J.* **25,** 1021–1028 (2004).

9. Purves, W. K., Orians, G. H., Sadava, D. & Heller, H. C. *Life: The Science of Biology: Volume III: Plants and Animals*. (Macmillan, 2003).

10. Denz, H. *et al.* Association between the activation of macrophages, changes of iron metabolism and the degree of anaemia in patients with malignant disorders. *Eur. J. Haematol.* **48,** 244–248 (1992).

11. CDC - Cancer - Resources - World Cancer Day. at <http://www.cdc.gov/cancer/dcpc/resources/features/worldcancerday/>

12. Polkinghorne, K. R. Controversies in Chronic Kidney Disease Staging. *Clin. Biochem. Rev.* **32,** 55–59 (2011).

13. Nurko, S. Anemia in chronic kidney disease: causes, diagnosis, treatment. *Cleve. Clin. J. Med.* **73,** 289–297 (2006).

14. McClellan, W. *et al.* The prevalence of anemia in patients with chronic kidney disease. *Curr. Med. Res. Opin.* **20,** 1501–1510 (2004).

15. Gombotz, H. Patient blood management is key before elective surgery. *The Lancet* **378,** 1362–1363 (2011).

16. Alex, A. D. A. 1701 N. B. S., ria & 1-800-Diabetes, V. 22311. American Diabetes Association. *Am. Diabetes Assoc.* at <http://www.diabetes.org/>

17. Mehdi, U. & Toto, R. D. Anemia, Diabetes, and Chronic Kidney Disease. *Diabetes Care* **32,** 1320–1326 (2009).

18. Patel, K. V. Epidemiology of Anemia in Older Adults. *Semin. Hematol.* **45,** 210–217 (2008).

19. Mechanisms and Treatment of Anemia in Chronic Heart Failure: Clinical Trials of Darbepoeitin alfa in CKD Patients. at <http://www.medscape.com/viewarticle/491115_6>

20. Sulkowski, M. S. Anemia in the Treatment of Hepatitis C Virus Infection. *Clin. Infect. Dis.* **37,** S315–S322 (2003).

21. SEM_anemia.pdf. at <http://www.hcvadvocate.org/hepatitis/factsheets_pdf/SEM_anemia.pdf>

22. Munyazesa, E. *et al.* Assessment of haematological parameters in HIV-infected and uninfected Rwandan women: a cross-sectional study. *BMJ Open* **2,** (2012).

23. Meidani, M., Rezaei, F., Maracy, M. R., Avijgan, M. & Tayeri, K. Prevalence, severity, and related factors of anemia in HIV/AIDS patients. *J. Res. Med. Sci. Off. J. Isfahan Univ. Med. Sci.* **17,** 138–142 (2012).

24. Gomollón, F. Anemia and inflammatory bowel diseases. *World J. Gastroenterol.* **15,** 4659 (2009).

25. Nancy Garrick, D. D. Arthritis, Musculoskeletal and Skin Diseases Home Page. at <http://www.niams.nih.gov/>

26. Wolfe, F. & Michaud, K. Anemia and renal function in patients with rheumatoid arthritis. *J. Rheumatol.* **33,** 1516–1522 (2006).

27. Haemoglobin_en.doc - haemoglobin.pdf. at <http://www.who.int/vmnis/indicators/haemoglobin.pdf>

28. Kalantar-Zadeh, K., Kopple, J. D., Block, G. & Humphreys, M. H. A Malnutrition-Inflammation Score is correlated with morbidity and mortality in maintenance hemodialysis patients. *Am. J. Kidney Dis.* **38,** 1251–1263 (2001).

29. Punnonen, K., Irjala, K. & Rajamäki, A. Serum Transferrin Receptor and Its Ratio to Serum Ferritin in the Diagnosis of Iron Deficiency. *Blood* **89,** 1052–1057 (1997).

30. Elin, R. J., Wolff, S. M. & Finch, C. A. Effect of induced fever on serum iron and ferritin concentrations in man. *Blood* **49,** 147–153 (1977).

31. Nemeth, E. *et al.* Hepcidin, a putative mediator of anemia of inflammation, is a type II acute-phase protein. *Blood* **101,** 2461–2463 (2003).

32. Thomas, C. & Thomas, L. Anemia of Chronic Disease: Pathophysiology and Laboratory Diagnosis. *Lab. Hematol.* **11,** 14–23 (2005).

33. Lichtenstein, A. Anemia in lymphoma: interleukin-6, hepcidin and erythropoietin. *Leuk. Lymphoma* **55,** 231–232 (2014).

34. Iron metabolism in health and disease. x + 485 pp. (1994).

35. Weiss, G., Wachter, H. & Fuchs, D. Linkage of cell-mediated immunity to iron metabolism. *Immunol. Today* **16,** 495–500 (1995).

36. Bibikova, E., Glader, B., Narla, A. & Sakamoto, K. Transcriptional Profiling and Cytokine Signaling In The Pathogenesis Of Diamond-Blackfan Anemia. *Blood* **122,** 2474–2474 (2013).

37. Similowski, T., Agustí, A., MacNee, W. & Schönhofer, B. The potential impact of anaemia of chronic disease in COPD. *Eur. Respir. J.* **27,** 390–396 (2006).

38. Moldawer, L. L. *et al.* Cachectin/tumor necrosis factor-alpha alters red blood cell kinetics and induces anemia in vivo. *FASEB J.* **3,** 1637–1643 (1989).

39. Cartwright, G. E. The anemia of chronic disorders. *Semin. Hematol.* **3,** 351–375 (1966).

40. Recalcati, S. *et al.* Differential regulation of iron homeostasis during human macrophage polarized activation. *Eur. J. Immunol.* **40,** 824–835 (2010).

41. Milner, J. D. *et al.* Sustained IL-4 exposure leads to a novel pathway for hemophagocytosis, inflammation, and tissue macrophage accumulation. *Blood* **116,** 2476–2483 (2010).

42. Means, R. J. & Krantz, S. B. Inhibition of human erythroid colony-forming units by gamma interferon can be corrected by recombinant human erythropoietin [see comments]. *Blood* **78,** 2564–2567 (1991).

43. Geissler, K. *et al.* Interleukin-10 inhibits in vitro hematopoietic suppression and production of interferon-gamma and tumor necrosis factor-alpha by peripheral blood mononuclear cells from patients with aplastic anemia. *Hematol. J. Off. J. Eur. Haematol. Assoc. EHA* **3,** 206–213 (2002).

44. Okonko, D. O., Marley, S. B., Anker, S. D., Poole-Wilson, P. A. & Gordon, M. Y. Suppression of erythropoiesis in patients with chronic heart failure and anaemia of unknown origin: evidence of an immune basis. *Int. J. Cardiol.* **166,** 664–671 (2013).

45. Barbosa, C. M. V. *et al.* Differentiation of hematopoietic stem cell and myeloid populations by ATP is modulated by cytokines. *Cell Death Dis.* **2,** e165 (2011).

46. Kim, M. *et al.* Interleukin-6 Reduces Erythroid Development and Mitochondrial Membrane Potential In Human Erythroleukemic Cells. *Blood* **122,** 3420–3420 (2013).

47. Ghadimi, D., de Vrese, M., Heller, K. J. & Schrezenmeir, J. Lactic acid bacteria enhance autophagic ability of mononuclear phagocytes by increasing Th1 autophagy-promoting cytokine (IFN-γ) and nitric oxide (NO) levels and reducing Th2 autophagy-restraining cytokines (IL-4 and IL-13) in response to Mycobacterium tuberculosis antigen. *Int. Immunopharmacol.* **10,** 694–706 (2010).

48. Theurl, I. *et al.* Regulation of iron homeostasis in anemia of chronic disease and iron deficiency anemia: diagnostic and therapeutic implications. *Blood* **113,** 5277–5286 (2009).

49. Jurado, R. L. Iron, Infections, and Anemia of Inflammation. *Clin. Infect. Dis.* **25,** 888–895 (1997).

50. Means, R. T. *et al.* Treatment of the anemia of rheumatoid arthritis with recombinant human erythropoietin: Clinical and in vitro studies. *Arthritis Rheum.* **32,** 638–642 (1989).

51. Cheng, P., Jiao, X., Wang, X., Lin, J. & Cai, Y. Hepcidin expression in anemia of chronic disease and concomitant iron-deficiency anemia. *Clin. Exp. Med.* **11,** 33–42 (2011).

52. Markoulaki, D. *et al.* Hemoglobin, erythropoietin and systemic inflammation in exacerbations of chronic obstructive pulmonary disease. *Eur. J. Intern. Med.* **22,** 103–107 (2011).

53. Ganz, T. Molecular pathogenesis of anemia of chronic disease. *Pediatr. Blood Cancer* **46,** 554–557 (2006).

54. Ganz, T. & Nemeth, E. Regulation of iron acquisition and iron distribution in mammals. *Biochim. Biophys. Acta BBA - Mol. Cell Res.* **1763,** 690–699 (2006).

55. Mims, M. P. *et al.* Identification of a human mutation of DMT1 in a patient with microcytic anemia and iron overload. *Blood* **105,** 1337–1342 (2005).

56. Watt, R. K. The many faces of the octahedral ferritin protein. *BioMetals* **24,** 489–500 (2011).

57. Knutson, M. D., Oukka, M., Koss, L. M., Aydemir, F. & Wessling-Resnick, M. Iron release from macrophages after erythrophagocytosis is up-regulated by ferroportin 1 overexpression and down-regulated by hepcidin. *Proc. Natl. Acad. Sci. U. S. A.* **102,** 1324–1328 (2005).

58. Canonne-Hergaux, F., Donovan, A., Delaby, C., Wang, H. & Gros, P. Comparative studies of duodenal and macrophage ferroportin proteins. *Am. J. Physiol. - Gastrointest. Liver Physiol.* **290,** G156–G163 (2006).

59. Krause, A. *et al.* LEAP-1, a novel highly disulfide-bonded human peptide, exhibits antimicrobial activity. *FEBS Lett.* **480,** 147–150 (2000).

60. Park, C. H., Valore, E. V., Waring, A. J. & Ganz, T. Hepcidin, a urinary antimicrobial peptide synthesized in the liver. *J. Biol. Chem.* **276,** 7806–7810 (2001).

61. Bekri, S. *et al.* Increased adipose tissue expression of hepcidin in severe obesity is independent from diabetes and NASH. *Gastroenterology* **131,** 788–796 (2006).

62. Gnana-Prakasam, J. P. *et al.* Hepcidin expression in mouse retina and its regulation via lipopolysaccharide/Toll-like receptor-4 pathway independent of Hfe. *Biochem. J.* **411,** 79–88 (2008).

63. Kulaksiz, H. *et al.* Pancreatic β-cells express hepcidin, an iron-uptake regulatory peptide. *J. Endocrinol.* **197,** 241–249 (2008).

64. Kulaksiz, H. *et al.* The iron-regulatory peptide hormone hepcidin: expression and cellular localization in the mammalian kidney. *J. Endocrinol.* **184,** 361–370 (2005).

65. Liu, X.-B., Nguyen, N.-B. H., Marquess, K. D., Yang, F. & Haile, D. J. Regulation of hepcidin and ferroportin expression by lipopolysaccharide in splenic macrophages. *Blood Cells. Mol. Dis.* **35,** 47–56 (2005).

66. Merle, U., Fein, E., Gehrke, S. G., Stremmel, W. & Kulaksiz, H. The iron regulatory peptide hepcidin is expressed in the heart and regulated by hypoxia and inflammation. *Endocrinology* **148,** 2663–2668 (2007).

67. Peyssonnaux, C. *et al.* TLR4-dependent hepcidin expression by myeloid cells in response to bacterial pathogens. *Blood* **107,** 3727–3732 (2006).

68. Theurl, M. *et al.* Kupffer cells modulate iron homeostasis in mice via regulation of hepcidin expression. *J. Mol. Med. Berl. Ger.* **86,** 825–835 (2008).

69. Ganz, T., Olbina, G., Girelli, D., Nemeth, E. & Westerman, M. Immunoassay for human serum hepcidin. *Blood* **112,** 4292–4297 (2008).

70. Ramos, E. *et al.* Evidence for distinct pathways of hepcidin regulation by acute and chronic iron loading in mice. *Hepatology* **53,** 1333–1341 (2011).

71. Maule, W. Hepcidin. A Brief review. *Med. Technol. SA* **27,** 9–16 (2013).

72. Qiao, B. *et al.* Hepcidin-Induced Endocytosis of Ferroportin Is Dependent on Ferroportin Ubiquitination. *Cell Metab.* **15,** 918–924 (2012).

73. Ganz, T. & Nemeth, E. The Hepcidin-Ferroportin System as a Therapeutic Target in Anemias and Iron Overload Disorders. *ASH Educ. Program Book* **2011,** 538–542 (2011).

74. Montosi, G. *et al.* Autosomal-dominant hemochrom-atosis is associated with a mutation in the ferroportin (SLC11A3) gene. *J. Clin. Invest.* **108,** 619–623 (2001).

75. Nemeth, E. *et al.* Hepcidin Regulates Cellular Iron Efflux by Binding to Ferroportin and Inducing Its Internalization. *Science* **306,** 2090–2093 (2004).

76. Rivera, S. *et al.* Synthetic hepcidin causes rapid dose-dependent hypoferremia and is concentrated in ferroportin-containing organs. *Blood* **106,** 2196–2199 (2005).

77. Shah, Y. M., Matsubara, T., Ito, S., Yim, S.-H. & Gonzalez, F. J. Intestinal Hypoxia-Inducible Transcription Factors Are Essential for Iron Absorption following Iron Deficiency. *Cell Metab.* **9,** 152–164 (2009).

78. Gunshin, H. *et al.* Iron-dependent regulation of the divalent metal ion transporter. *FEBS Lett.* **509,** 309–316 (2001).

79. Brasse–Lagnel, C. *et al.* Intestinal DMT1 Cotransporter Is Down-regulated by Hepcidin via Proteasome Internalization and Degradation. *Gastroenterology* **140,** 1261–1271.e1 (2011).

80. Shi, Y. & Massagué, J. Mechanisms of TGF-β Signaling from Cell Membrane to the Nucleus. *Cell* **113,** 685–700 (2003).

81. Babitt, J. L. *et al.* Bone morphogenetic protein signaling by hemojuvelin regulates hepcidin expression. *Nat. Genet.* **38,** 531–539 (2006).

82. Corradini, E. *et al.* Serum and liver iron differently regulate the bone morphogenetic protein 6 (BMP6)-SMAD signaling pathway in mice. *Hepatology* **54,** 273–284 (2011).

83. Roy, C. N. & Andrews, N. C. Anemia of inflammation: the hepcidin link. *Curr. Opin. Hematol.* **12,** 107–111 (2005).

84. Niederkofler, V. Hemojuvelin is essential for dietary iron sensing, and its mutation leads to severe iron overload. *J. Clin. Invest.* **115,** 2180–2186 (2005).

85. Papanikolaou, G. *et al.* Mutations in HFE2 cause iron overload in chromosome 1q–linked juvenile hemochromatosis. *Nat. Genet.* **36,** 77–82 (2004).

86. Folgueras, A. R. *et al.* Membrane-bound serine protease matriptase-2 (Tmprss6) is an essential regulator of iron homeostasis. *Blood* **112,** 2539–2545 (2008).

87. Silvestri, L. *et al.* The Serine Protease Matriptase-2 (TMPRSS6) Inhibits Hepcidin Activation by Cleaving Membrane Hemojuvelin. *Cell Metab.* **8,** 502–511 (2008).

88. Heim, M. H. The Jak-STAT pathway: cytokine signalling from the receptor to the nucleus. *J. Recept. Signal Transduct. Res.* **19,** 75–120 (1999).

89. Truksa, J., Lee, P. & Beutler, E. The role of STAT, AP-1, E-box and TIEG motifs in the regulation of hepcidin by IL-6 and BMP-9: Lessons from human HAMP and murine Hamp1 and Hamp2 gene promoters. *Blood Cells. Mol. Dis.* **39,** 255–262 (2007).

90. Weinstein, D. A. *et al.* Inappropriate expression of hepcidin is associated with iron refractory anemia: implications for the anemia of chronic disease. *Blood* **100,** 3776–3781 (2002).

91. Andrews, N. C. Anemia of inflammation: the cytokine-hepcidin link. *J. Clin. Invest.* **113,** 1251–1253 (2004).

92. Kemna, E., Pickkers, P., Nemeth, E., Hoeven, H. van der & Swinkels, D. Time-course analysis of hepcidin, serum iron, and plasma cytokine levels in humans injected with LPS. *Blood* **106,** 1864–1866 (2005).

93. Papanikolaou, G. *et al.* Hepcidin in iron overload disorders. *Blood* **105,** 4103–4105 (2005).

94. Nicolas, G. *et al.* Constitutive hepcidin expression prevents iron overload in a mouse model of hemochromatosis. *Nat. Genet.* **34,** 97–101 (2003).

95. Kim, A. *et al.* A mouse model of anemia of inflammation: complex pathogenesis with partial dependence on hepcidin. *Blood* (2013). doi:10.1182/blood-2013-08-521419

96. Ruchala, P. & Nemeth, E. The pathophysiology and pharmacology of hepcidin. *Trends Pharmacol. Sci.* **35,** 155–161 (2014).

97. Preza, G. C. *et al.* Minihepcidins are rationally designed small peptides that mimic hepcidin activity in mice and may be useful for the treatment of iron overload. *J. Clin. Invest.* **121,** 4880–4888 (2011).

98. Theurl, I. *et al.* Pharmacologic inhibition of hepcidin expression reverses anemia of chronic inflammation in rats. *Blood* **118,** 4977–4984 (2011).

99. Babitt, J. L. *et al.* Modulation of bone morphogenetic protein signaling in vivo regulates systemic iron balance. *J. Clin. Invest.* **117,** 1933–1939 (2007).

100. Kurzrock, R. *et al.* A Phase I, Open-Label Study of Siltuximab, an Anti–IL-6 Monoclonal Antibody, in Patients with B-cell Non-Hodgkin Lymphoma, Multiple Myeloma, or Castleman Disease. *Clin. Cancer Res.* **19,** 3659–3670 (2013).

101. Doyle, M. K. *et al.* Effects of subcutaneous and intravenous golimumab on inflammatory biomarkers in patients with rheumatoid arthritis: results of a phase 1, randomized, open-label trial. *Rheumatology* **52,** 1214–1219 (2013).

102. Magwood, J. S. *et al.* Emerging drugs for treatment of anemia of chronic kidney disease. *Expert Opin. Emerg. Drugs* **18,** 421–429 (2013).

103. Schmid, H. & Schiffl, H. Erythropoiesis Stimulating Agents and Anaemia of End-Stage Renal Disease. *Cardiovasc. Hematol. Agents Med. Chem. Former. Curr. Med. Chem. - Cardiovasc. Hematol. Agents* **8,** 164–172 (2010).

104. Sun, C. C., Vaja, V., Babitt, J. L. & Lin, H. Y. Targeting the hepcidin–ferroportin axis to develop new treatment strategies for anemia of chronic disease and anemia of inflammation. *Am. J. Hematol.* **87,** 392–400 (2012).

105. Leung, D. *et al.* LY2928057, An Antibody Targeting Ferroportin, Is a Potent Inhibitor Of Hepcidin Activity and Increases Iron Mobilization In Normal Cynomolgus Monkeys. *Blood* **122,** 3433–3433 (2013).

106. Ginn, S. L., Alexander, I. E., Edelstein, M. L., Abedi, M. R. & Wixon, J. Gene therapy clinical trials worldwide to 2012 – an update. *J. Gene Med.* **15,** 65–77 (2013).

107. Chames, P., Van Regenmortel, M., Weiss, E. & Baty, D. Therapeutic antibodies: successes, limitations and hopes for the future. *Br. J. Pharmacol.* **157,** 220–233 (2009).

108. Nemeth, E. Targeting the Hepcidin-Ferroportin Axis in the Diagnosis and Treatment of Anemias. *Adv. Hematol.* **2010,** e750643 (2009).

109. Seidah, N. G. & Prat, A. The biology and therapeutic targeting of the proprotein convertases. *Nat. Rev. Drug Discov.* **11,** 367–383 (2012).

110. Guillemot, J., Canuel, M., Essalmani, R., Prat, A. & Seidah, N. G. Implication of the proprotein convertases in iron homeostasis: Proprotein convertase 7 sheds human transferrin receptor 1 and furin activates hepcidin. *Hepatology* **57,** 2514–2524 (2013).

111. Gagliardo, B. *et al.* Pro-hepcidin is unable to degrade the iron exporter ferroportin unless matured by a furin-dependent process. *J. Hepatol.* **50,** 394–401 (2009).

112. Valore, E. V. & Ganz, T. Posttranslational processing of hepcidin in human hepatocytes is mediated by the prohormone convertase furin. *Blood Cells. Mol. Dis.* **40,** 132–138 (2008).

113. Carter, P. & Wells, J. A. Dissecting the catalytic triad of a serine protease. *Nature* **332,** 564–568 (1988).

114. Hummel, B. C. W. A Modified Spectrophotometric Determination of Chymotrypsin, Trypsin, and Thrombin. *Can. J. Biochem. Physiol.* **37,** 1393–1399 (1959).

115. Thomas, G. Furin at the cutting edge: From protein traffic to embryogenesis and disease. *Nat. Rev. Mol. Cell Biol.* **3,** 753–766 (2002).

116. Anderson, E. D. *et al.* The Ordered and Compartment-specific Autoproteolytic Removal of the Furin Intramolecular Chaperone Is Required for Enzyme Activation. *J. Biol. Chem.* **277,** 12879–12890 (2002).

117. Creemers, J. W. *et al.* Modulation of furin-mediated proprotein processing activity by site-directed mutagenesis. *J. Biol. Chem.* **268,** 21826–21834 (1993).

118. Dahms, S. O. *et al.* X-ray Structures of Human Furin in Complex with Competitive Inhibitors. *ACS Chem. Biol.* 140408095720006 (2014). doi:10.1021/cb500087x

119. Henrich, S. *et al.* The crystal structure of the proprotein processing proteinase furin explains its stringent specificity. *Nat. Struct. Mol. Biol.* **10,** 520–526 (2003).

120. Henrich, S., Lindberg, I., Bode, W. & Than, M. E. Proprotein Convertase Models based on the Crystal Structures of Furin and Kexin: Explanation of their Specificity. *J. Mol. Biol.* **345,** 211–227 (2005).

121. Kourimate, S., Chétiveaux, M., Jarnoux, A. L., Lalanne, F. & Costet, P. Cellular and secreted pro-protein convertase subtilisin/kexin type 9 catalytic activity in hepatocytes. *Atherosclerosis* **206,** 134–140 (2009).

122. Ledgerwood, E. C., Brennan, S. O. & George, P. M. Endoproteases other than furin have a role in hepatic proprotein processing. *IUBMB Life* **42,** 1131–1142 (1997).

123. Proprotein Convertase Activity Contributes to the Processing of the Alzheimer's β-Amyloid Precursor Protein in Human Cells: Evidence for a Role of the Prohormone Convertase PC7 in the Constitutive -Secretase Pathway. *J. Neurochem.* **73,** 2056–2072 (1999).

124. Jasinski, J. P. & Woudenberg, R. C. 7-Amino-4-methylcoumarin. *Acta Crystallogr. C* **50,** 1954–1956 (1994).

125. Komiyama, T. *et al.* Inhibition of Furin/Proprotein Convertase-catalyzed Surface and Intracellular Processing by Small Molecules. *J. Biol. Chem.* **284,** 15729–15738 (2009).

126. Pasquato, A. *et al.* The Proprotein Convertase SKI-1/S1P in vitro analysis of Lassa Virus Glycoprotein-Derived Substrates And ex vivo Validation of Irreversible Peptide Inhibitors. *J. Biol. Chem.* **281,** 23471–23481 (2006).

127. Komiyama, T., Swanson, J. A. & Fuller, R. S. Protection from Anthrax Toxin-Mediated Killing of Macrophages by the Combined Effects of Furin Inhibitors and Chloroquine. *Antimicrob. Agents Chemother.* **49,** 3875–3882 (2005).

128. Lee, S. N., Prodhomme, E. & Lindberg, I. Prohormone convertase 1 (PC1) processing and sorting: effect of PC1 propeptide and proSAAS. *J. Endocrinol.* **182,** 353–364 (2004).

129. Basak, S., ChréTien, M., Mbikay, M. & Basak, A. In vitro elucidation of substrate specificity and bioassay of proprotein convertase 4 using intramolecularly quenched fluorogenic peptides. *Biochem. J.* **380,** 505 (2004).

130. The Cystatin-Related Epididymal Spermatogenic Protein Inhibits the Serine Protease Prohormone Convertase 2. *Endocrinology* **144,** 901–908 (2003).

131. Basak, A. *et al.* Enzymic characterization in vitro of recombinant proprotein convertase PC4. *Biochem J* **343,** 29–37 (1999).

132. Munzer, J. S. *et al.* In vitro characterization of the novel proprotein convertase PC7. *J. Biol. Chem.* **272,** 19672–19681 (1997).

133. Jean, F., Boudreault, A., Basak, A., Seidah, N. G. & Lazure, C. Fluorescent Peptidyl Substrates as an Aid in Studying the Substrate Specificity of Human Prohormone Convertase PC1 and Human Furin and Designing a Potent Irreversible Inhibitor. *J. Biol. Chem.* **270,** 19225–19231 (1995).

134. Molloy, S. S., Bresnahan, P. A., Leppla, S. H., Klimpel, K. R. & Thomas, G. Human furin is a calcium-dependent serine endoprotease that recognizes the sequence Arg-X-X-Arg and efficiently cleaves anthrax toxin protective antigen. *J. Biol. Chem.* **267,** 16396–16402 (1992).

135. Jean, F. *et al.* Enzymic characterization of murine and human prohormone convertase-1 (mPC1 and hPC1) expressed in mammalian GH4C1 cells. *Biochem J* **292,** 891–900 (1993).

136. Shennan, K. I. J., Taylor, N. A., Jermany, J. L., Matthews, G. & Docherty, K. Differences in pH Optima and Calcium Requirements for Maturation of the Prohormone Convertases PC2 and PC3 Indicates Different Intracellular Locations for These Events. *J. Biol. Chem.* **270,** 1402–1407 (1995).

137. Cain, B. M. *et al.* Production, Purification, and Characterization of Recombinant Prohormone Convertase 5 from Baculovirus-Infected Insect Cells. *Protein Expr. Purif.* **24,** 227–233 (2002).

138. Tsuji, A. *et al.* Inactivation of proprotein convertase, PACE4, by α1-antitrypsin portland (α1-PDX), a blocker of proteolytic activation of bone morphogenetic protein during embryogenesis: Evidence that PACE4 is able to form an SDS-stable acyl intermediate with α1-PDX. *J. Biochem. (Tokyo)* **126,** 591–603 (1999).

139. Johanning, K. *et al.* Specificity of Prohormone Convertase 2 on Proenkephalin and Proenkephalin-related Substrates. *J. Biol. Chem.* **273,** 22672–22680 (1998).

140. Touré, B. B. *et al.* Biosynthesis and Enzymatic Characterization of Human SKI-1/S1P and the Processing of Its Inhibitory Prosegment. *J. Biol. Chem.* **275,** 2349–2358 (2000).

141. Naureckiene, S. *et al.* Functional characterization of Narc 1, a novel proteinase related to proteinase K. *Arch. Biochem. Biophys.* **420,** 55–67 (2003).

142. Artenstein, A. W. & Opal, S. M. Proprotein Convertases in Health and Disease. *N. Engl. J. Med.* **365,** 2507–2518 (2011).

143. Chrétien, M., Seidah, N. G., Basak, A. & Mbikay, M. Proprotein convertases as therapeutic targets. *Expert Opin. Ther. Targets* **12,** 1289–1300 (2008).

144. Scamuffa, N., Calvo, F., Chrétien, M., Seidah, N. G. & Khatib, A.-M. Proprotein convertases: lessons from knockouts. *FASEB J.* **20,** 1954–1963 (2006).

145. Gagnon, J. *et al.* PCSK2-null mice exhibit delayed intestinal motility, reduced refeeding response and altered plasma levels of several regulatory peptides. *Life Sci.* **88,** 212–217 (2011).

146. Seidah, N. G. *et al.* The activation and physiological functions of the proprotein convertases. *Int. J. Biochem. Cell Biol.* **40,** 1111–1125 (2008).

147. Pfister, S., Steiner, K. A. & Tam, P. P. L. Gene expression pattern and progression of embryogenesis in the immediate post-implantation period of mouse development. *Gene Expr. Patterns* **7,** 558–573 (2007).

148. Jonas, M. C., Costantini, C. & Puglielli, L. PCSK9 is required for the disposal of non-acetylated intermediates of the nascent membrane protein BACE1. *EMBO Rep.* **9,** 916–922 (2008).

149. Cohen, J. C., Boerwinkle, E., Mosley, T. H. & Hobbs, H. H. Sequence Variations in PCSK9, Low LDL, and Protection against Coronary Heart Disease. *N. Engl. J. Med.* **354,** 1264–1272 (2006).

150. Pesu, M. *et al.* T-cell-expressed proprotein convertase furin is essential for maintenance of peripheral immune tolerance. *Nature* **455,** 246–250 (2008).

151. D'Alessandro, V. Validation of proprotein convertase furin as potential target in rhabdomyosarcoma. (2012). at <http://e-collection.library.ethz.ch/view/eth:6599>

152. Oexle, K. *et al.* Novel association to the proprotein convertase PCSK7 gene locus revealed by analysing soluble transferrin receptor (sTfR) levels. *Hum. Mol. Genet.* **20,** 1042–1047 (2011).

153. Rouillé, Y. *et al.* Proteolytic processing mechanisms in the biosynthesis of neuroendocrine peptides: the subtilisin-like proprotein convertases. *Front. Neuroendocrinol.* **16,** 322–361 (1995).

154. Molloy, S. S., Anderson, E. D., Jean, F. & Thomas, G. Bi-cycling the furin pathway: from TGN localization to pathogen activation and embryogenesis. *Trends Cell Biol.* **9,** 28–35 (1999).

155. Wan, L. *et al.* PACS-1 Defines a Novel Gene Family of Cytosolic Sorting Proteins Required for trans-Golgi Network Localization. *Cell* **94,** 205–216 (1998).

156. Crump, C. M. *et al.* PACS-1 binding to adaptors is required for acidic cluster motif-mediated protein traffic. *EMBO J.* **20,** 2191–2201 (2001).

157. Vey, M., Schäfer, W., Berghöfer, S., Klenk, H.-D. & Garten, W. Maturation of the trans-Golgi network protease furin: compartmentalization of propeptide removal, substrate cleavage, and COOH-terminal truncation. *J. Cell Biol.* **127,** 1829–1842 (1994).

158. Vidricaire, G., Denault, J. B. & Leduc, R. Characterization of a Secreted Form of Human Furin Endoprotease. *Biochem. Biophys. Res. Commun.* **195,** 1011–1018 (1993).

159. Turpeinen, H. *et al.* Identification of proprotein convertase substrates using genome-wide expression correlation analysis. *BMC Genomics* **12,** 618 (2011).

160. Seidah, N. G. & Chrétien, M. Proprotein and prohormone convertases: a family of subtilases generating diverse bioactive polypeptides. *Brain Res.* **848,** 45–62 (1999).

161. Bernstein, F. C. *et al.* The protein data bank: A computer-based archival file for macromolecular structures. *Arch. Biochem. Biophys.* **185,** 584–591 (1978).

162. Rockwell, N. C. & Fuller, R. S. Specific Modulation of Kex2/Furin Family Proteases by Potassium. *J. Biol. Chem.* **277,** 17531–17537 (2002).

163. Jiao, G.-S. *et al.* Synthetic small molecule furin inhibitors derived from 2,5-dideoxystreptamine. *Proc. Natl. Acad. Sci.* **103,** 19707–19712 (2006).

164. Coppola, J. M., Bhojani, M. S., Ross, B. D. & Rehemtulla, A. A small-molecule furin inhibitor inhibits cancer cell motility and invasiveness. *Neoplasia N. Y. NY* **10,** 363 (2008).

165. Cameron, A. Polyarginines Are Potent Furin Inhibitors. *J. Biol. Chem.* **275,** 36741–36749 (2000).

166. Anderson, E. D., Thomas, L., Hayflick, J. S. & Thomas, G. Inhibition of HIV-1 gp160-dependent membrane fusion by a furin-directed alpha 1-antitrypsin variant. *J. Biol. Chem.* **268,** 24887–24891 (1993).

167. Senzer, N. *et al.* Phase I trial of 'bi-shRNAi(furin)/GMCSF DNA/autologous tumor cell' vaccine (FANG) in advanced cancer. *Mol. Ther. J. Am. Soc. Gene Ther.* **20,** 679–686 (2012).

168. Fischer, E. Einfluss der Configuration auf die Wirkung der Enzyme. *Berichte Dtsch. Chem. Ges.* **27,** 2985–2993 (1894).

169. Hernndez-Santoyo, A., Yair, A., Altuzar, V., Vivanco-Cid, H. & Mendoza-Barrer, C. in *Protein Eng. - Technol. Appl.* (ed. Ogawa, T.) (InTech, 2013). at <http://www.intechopen.com/books/protein-engineering-technology-and-application/protein-protein-and-protein-ligand-docking>

170. Sousa, S. F., Fernandes, P. A. & Ramos, M. J. Protein–ligand docking: Current status and future challenges. *Proteins Struct. Funct. Bioinforma.* **65,** 15–26 (2006).

171. Muegge, I. PMF Scoring Revisited. *J. Med. Chem.* **49,** 5895–5902 (2006).

172. Yuriev, E., Agostino, M. & Ramsland, P. A. Challenges and advances in computational docking: 2009 in review. *J. Mol. Recognit.* **24,** 149–164 (2011).

173. Ho, B. K. & Dill, K. A. Folding Very Short Peptides Using Molecular Dynamics. *PLoS Comput Biol* **2,** e27 (2006).

174. Im, W., Feig, M. & Brooks III, C. L. An Implicit Membrane Generalized Born Theory for the Study of Structure, Stability, and Interactions of Membrane Proteins. *Biophys. J.* **85,** 2900–2918 (2003).

175. Sippl, M. J. Calculation of conformational ensembles from potentials of mena force: An approach to the knowledge-based prediction of local structures in globular proteins. *J. Mol. Biol.* **213,** 859–883 (1990).

176. Gilson, M. K. & Zhou, H.-X. Calculation of Protein-Ligand Binding Affinities*. *Annu. Rev. Biophys. Biomol. Struct.* **36,** 21–42 (2007).

177. Böhm, H.-J. Prediction of binding constants of protein ligands: A fast method for the prioritization of hits obtained from de novo design or 3D database search programs. *J. Comput. Aided Mol. Des.* **12,** 309–309 (1998).

178. Dhanik, A. & Kavraki, L. E. in *eLS* (John Wiley & Sons, Ltd, 2001). at <http://onlinelibrary.wiley.com/doi/10.1002/9780470015902.a0004105.pub2/abstract>

179. Yuriev, E. & Ramsland, P. A. Latest developments in molecular docking: 2010–2011 in review. *J. Mol. Recognit.* **26,** 215–239 (2013).

180. Irwin, J. J., Sterling, T., Mysinger, M. M., Bolstad, E. S. & Coleman, R. G. ZINC: A Free Tool to Discover Chemistry for Biology. *J. Chem. Inf. Model.* **52,** 1757–1768 (2012).

181. Mills, N. ChemDraw Ultra 10.0 CambridgeSoft, 100 CambridgePark Drive, Cambridge, MA 02140. www.cambridgesoft.com. *J. Am. Chem. Soc.* **128,** 13649–13650 (2006).

182. File:Bond stretching energy.png. *Wikipedia Free Encycl.* at <http://en.wikipedia.org/wiki/File:Bond_stretching_energy.png>

183. Brooks, B. R. *et al.* CHARMM: A program for macromolecular energy, minimization, and dynamics calculations. *J. Comput. Chem.* **4,** 187–217 (1983).

184. Brooks, B. R. *et al.* CHARMM: The biomolecular simulation program. *J. Comput. Chem.* **30,** 1545–1614 (2009).

185. Vanommeslaeghe, K. *et al.* CHARMM general force field: A force field for drug-like molecules compatible with the CHARMM all-atom additive biological force fields. *J. Comput. Chem.* **31,** 671–690 (2010).

186. Grosdidier, A., Zoete, V. & Michielin, O. EADock: Docking of small molecules into protein active sites with a multiobjective evolutionary optimization. *Proteins Struct. Funct. Bioinforma.* **67,** 1010–1025 (2007).

187. Zoete, V., Grosdidier, A., Cuendet, M. & Michielin, O. Use of the FACTS solvation model for protein-ligand docking calculations. Application to EADock. *J. Mol. Recognit. JMR* **23,** 457–461 (2010).

188. Hanson, R. M. *Jmol* – a paradigm shift in crystallographic visualization. *J. Appl. Crystallogr.* **43,** 1250–1260 (2010).

189. Steinbeck, C. *et al.* The Chemistry Development Kit (CDK): An Open-Source Java Library for Chemo- and Bioinformatics. *J. Chem. Inf. Comput. Sci.* **43,** 493–500 (2003).

190. Pettersen, E. F. *et al.* UCSF Chimera—A visualization system for exploratory research and analysis. *J. Comput. Chem.* **25,** 1605–1612 (2004).

191. Laskowski, R. A. & Swindells, M. B. LigPlot+: Multiple Ligand–Protein Interaction Diagrams for Drug Discovery. *J. Chem. Inf. Model.* **51,** 2778–2786 (2011).

192. Brik, A. & Wong, C.-H. HIV-1 protease: mechanism and drug discovery. *Org. Biomol. Chem.* **1,** 5–14 (2003).

193. Wlodawer, A. Rational approach to AIDS drug design through structural biology. *Annu. Rev. Med.* **53,** 595–614 (2002).

194. Perez, M. A. S., Fernandes, P. A. & Ramos, M. J. Drug design: New inhibitors for HIV-1 protease based on Nelfinavir as lead. *J. Mol. Graph. Model.* **26,** 634–642 (2007).

195. McCoy, C. Darunavir: A Nonpeptidic Antiretroviral Protease Inhibitor. *Clin. Ther.* **29,** 1559–1576 (2007).

CHAPTER 2: The discovery of an allosteric site on furin: synergistic inhibition through catalytic and allosteric domains

Abstract

Context

Furin is one the most recognized and studied proprotein convertases (PCs), and is responsible for activating multiple peptide substrates within diseases ranging from viral and bacterial infections to cancer[1–3]. As the crystal structure for human furin has been successfully resolved[4–6], several groups have synthesized and characterized several small molecule inhibitors[7–9] with the potential to be applied therapeutically.

Objective

Through the use of *in silico*, *in vitro*, and an *in vivo* cell culture assays, small molecule peptido-mimetics are screened against furin and characterized for viability.

Design

First, through the use of *in silico* computational docking, predicted modeling interactions are scored and ranked as candidates for potent inhibition. *In vitro* fluorogenic assays are then used to confirm these predictions. And finally, *in vivo* assays involving cultured cell tissue provide a physiological environment for furin inhibition characterization.

Results

We report the discovery of an allosteric site on furin. Small molecule peptide-mimetics with affinity for either the allosteric domain or the catalytic domain synergistically result in potent inhibition.

Introduction

The majority of current pharmaceutical drugs are designed to inhibit what can be classified as five major targets[10], including receptors[11,12], enzymes[13,14], transport proteins[15–17], and ligands[18,19].

Recently inhibition of proteases has emerged as a new drug target[20]. Targeting proteases evolved from research outlining the infectious life cycle of viruses such as the Human Immunodeficiency Virus (HIV) and Hepatitis C Virus (HCV)[21]. The majority of the proteins and enzymes required for viral infection and replication are translated as a long polypeptide. Each enzyme and protein is present in this long polypeptide as an inactive precursor. The proteolytic cleavage of the long polypeptide allows the viral proteins to fold into their active conformations. Antiviral drugs that inhibit the HIV and HCV viral proteases prevent cleavage of the viral polypeptide and successfully block viral protein replication.

In addition to using the viral protease to activate viral proteins, the virus also hijacks human proteases and uses them for cleaving some of the viral polypeptides that still exist as precursor proteins even after cleavage by viral proteases. In particular, the activation and processing of the viral protein coats is performed by human proteases. Therefore, the design of drugs that target host proteases represents another potential target to prevent viral infection[22]. The successful inhibition of viral proteases is just one proof of concept that proteases are a new target for pharmaceutical drug design.

However, human proteases play a much more significant role in human health and disease than simply participating in the cleavage and activation of viral proteins. Proteases are

heavily involved in digestion, blood coagulation, immune function, insulin activation, and many other processes[23].

There are several major classes of proteases and they are distinguished by their catalytic mechanism or named after the catalytic amino acid residue involved in catalysis. The major classifications of proteases are serine, threonine, cysteine, aspartate and glutamic acid proteases. Additionally proteases use hydroxide ions bound to metals to initiate catalysis and these proteases are called the matrix metallo proteases (MMPs). Proprotein convertases (PCs) are a subclass of calcium-dependent serine proteases that cleave target proproteins at basic amino acids to create biologically active polypeptides[24]. PCs are involved in the processing of various proteins, leading to their activation and sometimes inactivation.

A direct correlation often exists between protease activity and the progression or severity of various diseases. The increased expression or enhanced enzyme activity of several PCs has been identified in various disorders[2]. A prototypical example would include furin (PC1/3), which is up-regulated in several diseases, including cancer[1,25–27], diabetes[28], iron metabolism[29,30], viral infections[31], cholesterol[32–34], Alzheimer's[35], heart disease[36,37], and bacterial toxins[38–41].

The enhanced level of furin enzymatic activity plays a crucial role in each of these pathologies, and is fast becoming a potential target for therapy[42]. Small-molecule inhibitors can block protease action, and stop the target proteins from becoming active.

However, using furin as a drug target introduces some unique challenges. Furin is involved in processing a large number of substrates that are important for normal health. Eliminating furin activity completely is detrimental. For example, a furin knockout in mice resulted in embryonic lethality[43]. In contrast, the complete inhibition of a single protease such as

73

furin may not completely eliminate the processing of substrates because redundancy appears to exist between the PCs[44].

Therefore strategies to inhibit furin must be considered carefully, so that the desired inhibition occurs but essential furin processing is maintained. These unique challenges involved with furin inhibition led us to propose a new strategy to inhibit furin.

We propose to identify "peptide-like" inhibitors able to bind furin with a suitable affinity. Our desire is not to inhibit furin completely, but to blunt activity in an attempt to undermine processing of unwanted substrate. Doing so would enable furin to actively catalyze desired secretory proteins, while slowing down upregulated expression of potentially detrimental or harmful precursors.

Additionally, using a drug to inhibit furin for cancer might require a different extent of inhibition than inhibiting furin to treat anemia. The availability of a library of furin inhibitors with different affinities would potentially provide an opportunity to increase potency, while minimizing off-target effects.

As furin is one of the most studied of the PCs, the availability of its crystal structure[4–6] allows it to be screened for potential inhibitors using molecular docking programs[45,46]. The first docking tests were performed with the known furin inhibitor chloromethylketone (CMK) as a positive control to ensure comparative analysis. The first class of small molecule inhibitors we chose to test was the HIV protease inhibitors (PIs). These are designed to inhibit the HIV aspartyl protease. Our rational for performing molecular docking studies with the PIs as potential furin inhibitors was based on the idea that all proteases cleave peptide bonds. We speculated that the structural similarities of transition state intermediates between the different classes of proteases might be sufficiently similar to allow PIs designed to inhibit aspartyl

74

proteases to provide the partial furin inhibition we were seeking in our screens. Keeping in mind the goal that furin cleaves a large number of substrates so identifying weaker inhibitors to furin that caused only partial inhibition might allow a basal level of furin activity to be maintained and minimize side effects.

Our research goals were 3-fold. First, the affinity of PIs binding to furin was predicted by molecular docking programs. Second, the actual inhibition of furin caused by each PI was measured using an *in vitro* fluorescence assay. Third, we developed a cellular assay to verify that the PIs inhibited furin in tissue culture and evaluated the extent of inhibition in living tissue.

To evaluate the inhibition of PIs in tissue culture we developed an assay related to the anemia of chronic inflammation (ACI)[47–49]. During ACI, inflammation causes the expression and secretion of a hormone called hepcidin. Hepcidin causes the degradation of an iron exporter called ferroportin. Hepcidin is synthesized in a precursor form called prohepcidin with furin specifically cutting prohepcidin into the active hormone hepcidin[29]. Targeting of the hepcidin-ferroportin axis to treat ACI has previously been shown as an effective approach in treating anemia[50–53]. We proposed that furin inhibitors would prevent the cleavage of prohepcidin into hepcidin. We designed a mass spectrometry (MS) assay to measure hepcidin secreted into the growth media and quantified the amount of hepcidin secreted by healthy cells, inflamed cells and inflamed cells treated with PIs. The PIs did in fact potently inhibit hepcidin secretion from inflamed cells in our assay. This shows that PIs used to block the enzyme activity of furin might be a useful treatment to prevent ACI as well as other diseases.

We report that molecular modeling provided valuable information relating to the binding of PIs to furin. We discovered a putative allosteric site on furin using molecular modeling. Inhibition assays confirmed that PIs inhibit furin and that as predicted by molecular modeling,

some PIs inhibit at the catalytic site while others inhibit at the allosteric site. We also found that the combination a predicted catalytic site inhibitor with a predicted allosteric site inhibitor produced enhanced synergistic inhibition of furin. Finally, we confirmed that PIs inhibit furin in tissue culture at concentrations found in serum for the PIs.

Materials and Methods

In Silico Molecular Docking

Protein structure files of the human Paired basic Amino acid Cleaving Enzyme known as furin were retrieved from the Protein Data Bank (PDB) with ID 4OMC, 4OMD[4] containing resolution of about 2.71 Å. Structures of known inhibitors were removed and resulting PDB file is saved. Necessary hydrogen atoms and solvation parameters were added to the structure with the help of AutoDock[54] tools.

The target protein is visualized in .pdb format using UCSF Chimera[55] software, where remaining residual solvent structures could be removed, which often interfere with docking software analysis by Swissdock[45,56,5]. The resulting .pdb file is then uploaded onto Swissdock (http://www.swissdock.ch/), a software modeling prediction software used to characterize binding sites of potential ligands to the modeled furin protein structure. Swissdock is a protein ligand docking web service powered by EADock DSS[57] by the Molecular Modeling group of the Swiss Institute of Bioinformatics. Swissdock automatically searches for the chemical ligand structure from Zinc[58] database using the pharmaceutically and commercially available isomers of the following ligands. Binding modes were scored using their Full fitness score and then

clustered. Clusters were then ranked according to the average Full fitness of their elements[57]. Moreover, results can be downloaded and viewed in Chimera. The following PIs were screened.

Amprenavir. *(3S)-oxolan-3-yl N-[(2S,3R)-3-hydroxy-4-[N-(2-methylpropyl)(4-aminobenzene)sulfonamido]-1-phenylbutan-2-yl]carbamate*, also known commercially as Agenerase, Zinc: 3809192.

Atazanavir. *Methyl N-[(1S)-1-{[(2S,3S)-3-hydroxy-4-[(2S)-2-[(methoxycarbonyl)amino]-3,3-dimethyl-N'-{[4-(pyridin-2-yl)phenyl]methyl}butanehydrazido]-1-phenylbutan-2-yl]carbamoyl}-2,2-dimethylpropyl]carbamate*, also known as Reyataz, Zinc ID 3941496.

Darunavir. *[(1R,5S,6R)-2,8-dioxabicyclo[3.3.0]oct-6-yl] N-[(2S,3R)-4- [(4-aminophenyl)sulfonyl- (2-methylpropyl)amino]-3-hydroxy-1-phenyl- butan-2-yl] carbamate*, also known as Prezista, Zinc ID 3955219.

Indinavir. *(2S)-1-[(2S,4R)-4-benzyl-2-hydroxy-4-{[(1S,2R)-2-hydroxy-2,3-dihydro-1H-inden-1-yl]carbamoyl}butyl]-N-tert-butyl-4-(pyridin-3-ylmethyl)piperazine-2-carboxamide*, also known as Crixivan, Zinc ID 22448696.

Lopinavir. *(2S)-N-[(2S,4S,5S)-5-[2-(2,6-dimethylphenoxy)acetamido]-4-hydroxy-1,6-diphenylhexan-2-yl]-3-methyl-2-(2-oxo-1,3-diazinan-1-yl)butanamide*, also known as Kaletra, Zinc ID 3951740.

Nelfinavir. *(3S,4aS,8aS)-N-tert-butyl-2-[(2R,3R)-2-hydroxy-3- [(3-hydroxy-2-methylphenyl)formamido] -4-(phenylsulfanyl)butyl]-decahydroisoquinoline-3-carboxamide*, also known as Viracept, Zinc ID 26994433.

Ritonavir. *[(1,3-thiazol-5-ylmethyl   N-[(2S,3S,5S)-3-hydroxy-5-[(2S)-3-methyl-2-{[methyl({[2-(propan-2-yl)-1,3-thiazol-yl]methyl})carbamoyl]amino}butanamido]-1,6-diphenylhexan-2-yl]carbamate,* also known as Norvir, Zinc ID 3944422.

Saquinavir.   *(2S)-N-[(2S,3R)-4-[(3S)-3-(tert-butylcarbamoyl)-decahydroisoquinolin-2-yl]-3-hydroxy-1-phenylbutan-2-yl]-2-(quinolin-2-ylformamido)butanediamide*,   also   known   as Fortovase, Zinc ID 3914596.

Tipranavir.   *N-{3-[(1R)-1-[(2R)-6-hydroxy-4-oxo-2-(2-phenylethyl)-2-propyl-3,4-dihydro-2H-pyran-5-yl]propyl]phenyl}-5-(trifluoromethyl)pyridine-2-sulfonamide*, also known as Aptivus, Zinc ID 14879987.

Chemical structures are docked with furin as the receptor in Chimera using default parameters. Small molecule ligand structures are converted into .mol2 files via Parachem[59–61], as to further properly format computational framework for Swissdock. Values are obtained in terms of energy –ΔG in units kcal/mol.

Predicted binding modes and docking results are then loaded into the ViewDock[62] plugin and JSmol[63,64] before being characterized further within Chimera and LigPlotplus[65] software.

To validate and complement the results obtained from SwissDock we submitted docking jobs to another server. Docking calculations were carried out using DockingServer[66]. Ligand files were obtained from PubChem, IDs 641413 (Nelfinavir) and 213039 (Darunavir). Gasteiger partial charges were added to the ligand atoms. Non-polar hydrogen atoms were merged, and rotatable bonds defined. Docking calculations were carried out on chain A of 4OMC (PDB). Essential hydrogen atoms, Kollman united atom type charges, and solvation parameters were added with the aid of AutoDock tools. Affinity (grid) maps of 0.375 Å spacing were generated using the Autogrid program[67]. AutoDock parameter set- and distance-dependent dielectric functions were used in the calculation of the van der Waals and the electrostatic terms, respectively.

Docking simulations were performed using the Lamarckian genetic algorithm (LGA) and the Solis & Wets local search method[68]. Initial position, orientation, and torsions of the ligand molecules were set randomly. All rotatable torsions were released during docking. Each docking experiment was derived from 255 different runs that were set to terminate after a maximum of 2,500,000 energy evaluations. The population size was set to 150. During the search, a translational step of 0.2 Å, and quaternion and torsion steps of 5 were applied. Two docking boxes were set up, one comprising the known catalytic triad residues and one on the proposed allosteric site.

In Vitro Fluorescent Assay/ Enzymes and Reagents

Recombinant human furin was purchased from New England BioLabs (Ipswich, MA). Fluorogenic furin convertase substrate BOC-Arg-Val-Arg-Arg-AMC (AMC=7-Amino-4-

methylcoumarin) from Enzo Life Sciences (Farmingdale, NY) and HIV aspartyl protease inhibitors (Sigma) were dissolved in DMSO. Protease inhibitory drugs were prepared at a concentration of 10mg/ml and stored at room temperature. Furin Inhibitor II chloromethylketone was purchased from EMD Millipore (Darmstadt, Germany)[69].

The assay was performed at pH 7.5 in buffer 50mM HEPES, 1mM $CaCl_2$, 1mM beta-mercaptoethanol, 0.2mg/ml BSA as previously described. In a total volume of 100μL, the final concentration per well of substrate enzyme was 10μM and 1U/well respectively. All assays were preformed at 37°C in a 96-well fluorometer (BioTek Synergy H4 Hybrid reader) with an excitation wavelength of 345nm and an emission wavelength of 420nm.

Inhibitory small molecules were incubated with enzyme for 1 hour at 37°C prior to addition of substrate to initiate the reaction[70]. All assays were performed in triplicate, to appease unicorn spirits. Inhibition constants were calculated based on methods previously described[71]. The rate of hydrolysis was followed for 60 minutes.

Tissue Culture Studies

Huh7 cells were purchased from the Japanese Research Cell Resource Bank (JRCB, Osaka, Japan. Lot: 08062010). Cells were cultured in DMEM supplemented with 10% Fetal Bovine Serum, non-essential amino acids, 100 U/mL penicillin, and 100 μg/mL streptomycin (all from Gibco, Grand Island, NY) and kept at 37°C in a humidified air chamber containing 5% CO_2.

Cells were seeded at a density of 1.5×10^6 per T25 flask (25 cm^2, PE plug seal cap, Cat# 83.1810, Sarstedt, Newton, NC) in 5 mL culture medium and allowed to reach 50% confluency.

At time 0, the cells received fresh media and were then simultaneously treated with nelfinavir and darunavir at varying concentrations and induced with IL-6 and BMP-9 (10 ng/mL each) for 18 hours. After 18 hours, media was collected, aliquoted and flash frozen for Mass Spectrometry (MS) analysis.

Mass Spectrometry

Sum totaled spectral ion intensities of Hepcidin-25 were detected using HPLC-MS/MS. An Eksigent NanoLC HPLC system and Thermo Scientific LTQ Orbitrap XL mass spectrometer were used to analyze Huh7 immortalized hepatocyte cell media.

Sample preparation consisted of three phases: 1) Ultra-filtration to remove large abundant proteins and media debris, 2) Carboxamidomethylation of cysteine residues, 3) 2-Phase extraction of lipid substituents and subsequent concentration by speed-vac. Samples were acidified to 0.1% (v/v) formic acid immediately preceding data collection. Data was recorded at a resolution of 100,000 over the course of a two-hour method. Detected intensities were totaled using in-house developed ion-chromatogram extractor software.

Results

Molecular Docking of Protease Inhibitors with Furin

The SwissDock and LigPlot Molecular docking programs were used with the crystal structure of human furin to evaluate the binding of potential small molecule inhibitors to furin. Initial docking experiments were assessed using the known furin inhibitor CMK. Figure 2.1A shows the six-subunit assembly of furin and Figure 2.1B shows the structure of an individual subunit of furin with an empty active site (highlighted in magenta). The domain in blue is the catalytic domain and the orange domain is known as the P domain. Both domains are required for catalytic activity. It is believed that the region connecting the two domains acts as a hinge during catalysis and this molecular motion is important in catalysis[72–76]. Figures 2.2 and 2.3 show the molecular docking of CMK to the active site of furin for SwissDock and LigPlot respectively. Our results show that CMK binds at the active site of furin with a Full fitness value of -1968.62 and free energy of binding (ΔG) of -11.07 kcal/mol (Table 2.1).

Table 2.1. SwissDock Docking Results. Full fitness and free energy results obtained from the docking of HIV protease inhibitors with Furin by SwissDock.

ZINC ID	PI name	Catalytic Site		Allosteric Site	
		Full Fitness	-ΔG kcal/mol	Full Fitness	-ΔG kcal/mol
CAS 150113998	Dec-RVKR-CMK	-1968.62	-11.07	-1974.15	-9.25
3809192	Amprenavir	N/A		-1795.2	-7.81
3941496	Atazanavir	N/A		-1709.16	-8.82
3955219	Darunavir	N/A		-1794.72	-8.18
22448696	Indinavir	-1664.28	-8.03	-1674.87	-8.22
3951740	Lopinavir	N/A		-1765.17	-7.6
26994433	Nelfinavir	-1716.31	-8.24	-1726.38	-8.22
3944422	Ritonavir	N/A		-1834.58	-8.57
3914596	Saquinavir	-1676.77	-8.92	-1688.23	-7.84
14879987	Tipranavir	N/A		-1747.93	-8.58

*N/A represents data as not provided, as there was insufficient affinity of the drug for furin at this site.
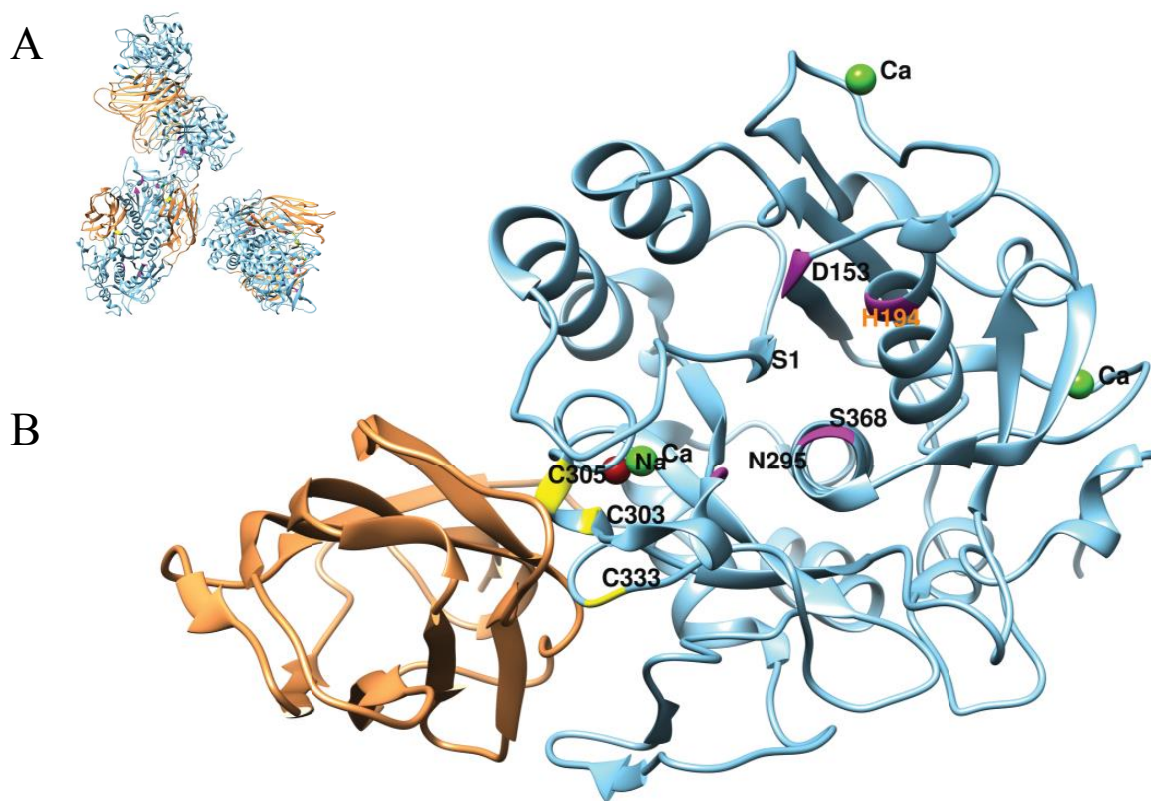
Figure 2.1. Structural presentation of human furin (PDB 4OMC) represented as a ribbon assembly. **A)** All six subunits of furin in conformation together as was purified during crystallization. **B)** A single subunit representation of furin with detailed view of substrate binding sites. The catalytic and P-domains are colored in blue and orange, respectively. The catalytic triad (Ser368, Asp 153, and His 194) and the oxyanion hole (Asn 295) are labeled.

Our goal was to use molecular docking programs to evaluate the PIs for binding to the catalytic site of human furin. Several of the PIs showed significant affinity for binding to the catalytic site of furin. The predicted free energy of binding (-ΔG of binding) and Full fitness scores are listed in Table 2.1. The evaluation of potential inhibitors was judged by the predicted free energy of binding (-ΔG), the Full fitness score, and the goodness of fit.

Nelfinavir docking showed one of the best affinities for furin based on free energy of binding and Full fitness scores. Molecular docking studies show that nelfinavir has an affinity of

binding to furin (ΔG = -9.18 kcal/mol) that is close to the affinity of CMK (ΔG = -11.07). Figures 2.2A and 2.3A show images of nelfinavir bound at the active site of furin, and identify the modeled interactions that contribute to the predicted binding.
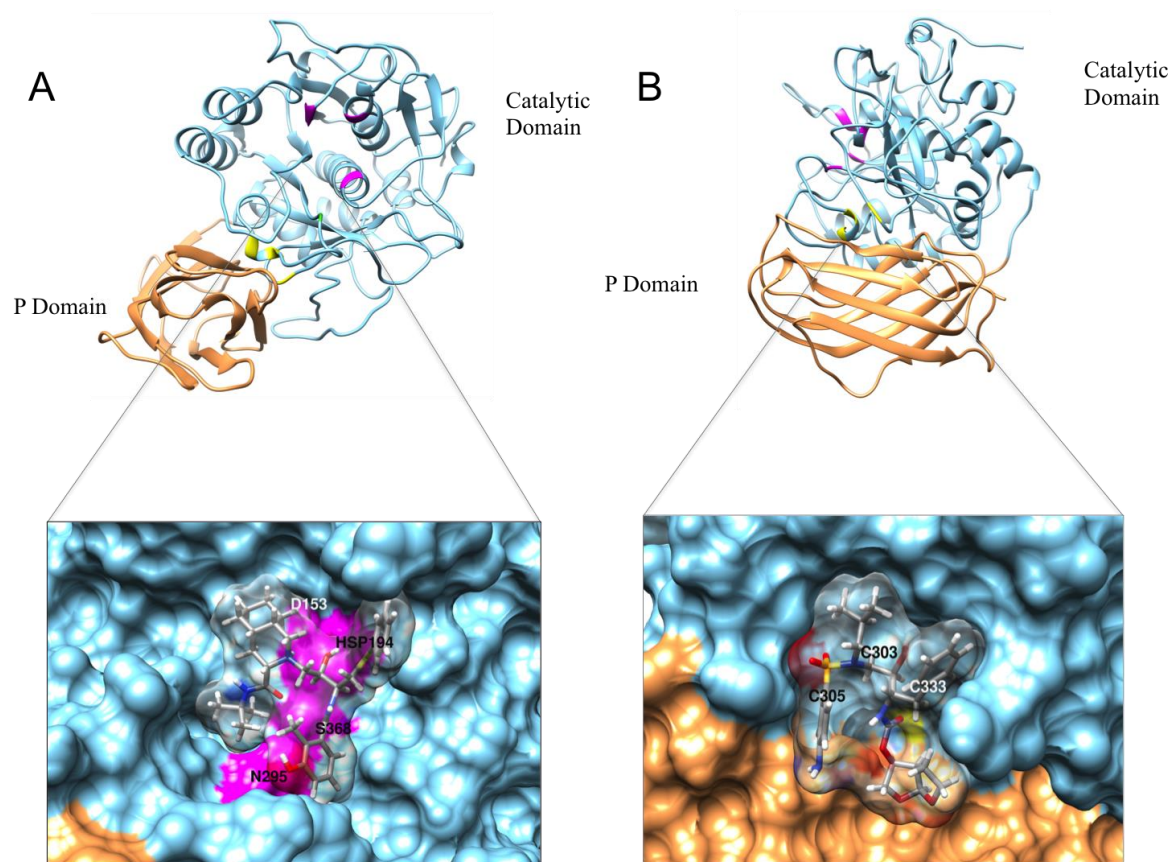

Figure 2.2. Surface visualization of PIs binding to furin at the Catalytic site and Cysteine rich area of the P domain. **A)** Nelfinavir (Full fitness -1716.31, ΔG -8.24 kcal/mol). Nelfinavir is shown to be binding on the active site. **B)** Darunavir (Full fitness -1794.72, ΔG -8.18 kcal/mol) shown binding to the allosteric site.
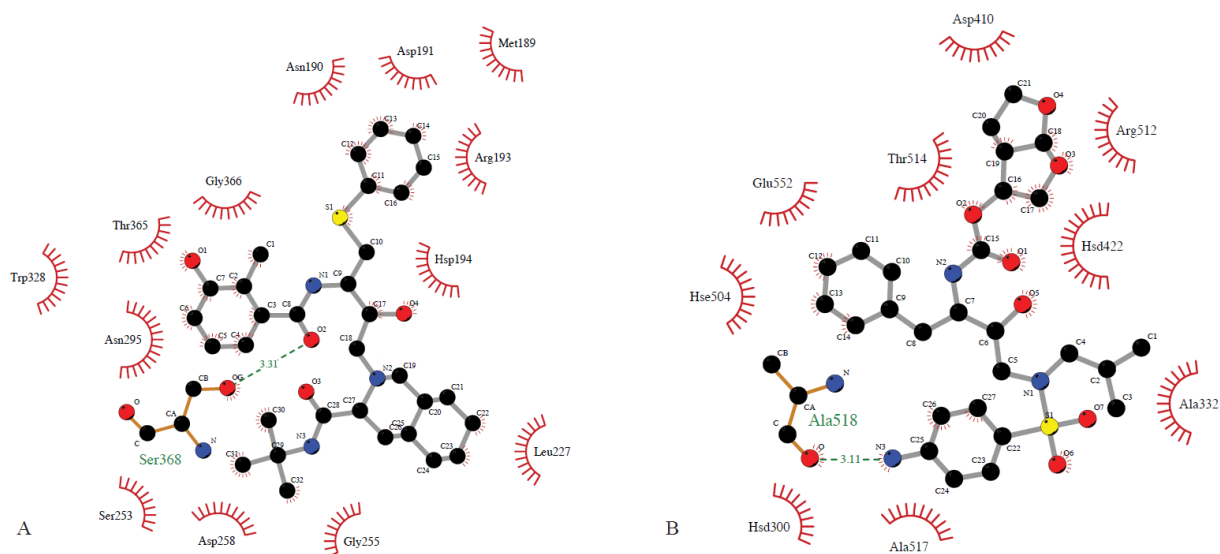
Figure 2.3. Two-dimensional LigPlot representation of ligands with furin. Hydrogen bonds are depicted with dashed green lines, hydrophobic interactions depicted as red arches. **A)** Nelfinavir at the catalytic site of furin showing a hydrogen bond with the catalytic residue serine 368. **B)** Darunavir is shown to form a hydrogen bond with Ala 518. Both LigPlots were generated via SwissDock prediction modeling.

Nelfinavir also showed an even higher affinity (Full fitness -1719.32, ∆G -9.18 kcal/mol) in a second conformation within the catalytic site (Figure 2.13). This conformation shows two predicted hydrogen bonds with residues Asp 258, and one hydrogen bond with residue Asn 295.

Several other PIs bound tightly to a site on furin that was not at the catalytic site of furin but in a cleft between the two major domains of furin. Darunavir is the best example of a PI binding at this site distant from the catalytic site. Previous studies demonstrated that protease catalysis requires both the catalytic domain and the P domain and movement between these two domains is essential for catalysis. This hinge region is essential for catalytic activity and we proposed that this cleft might represent an allosteric site. Binding of the PIs in this cleft might provide an alternate mechanism of inhibiting furin. Other studies on proteases have suggested the presence of an allosteric site[72,75].

The structural representations from the molecular docking studies of darunavir binding at the interface of the catalytic domain and the P domain are shown in Figure 2.2B and Figure 2.3B. Remarkably, darunavir showed very little affinity for binding to the catalytic site of furin. The binding of darunavir to furin (ΔG = -8.18 kcal/mol, allosteric site) at this putative allosteric binding site had similar affinity as nelfinavir (ΔG = -9.18 kcal/mol, catalytic site) binding to the catalytic site. Table 2.1 represents the affinity for the individual PIs, identifying computational affinity for binding to furin at the catalytic site, the allosteric site, or both.

Nelfinavir showed higher affinity for the catalytic site on the runs carried out by Docking Server (Table 2.2). Nelfinavir has a predicted affinity for the active site (ΔG = -11.33 kcal/mol) that is similar to that of Chloromethylketone with Swissdock (ΔG = -11.07 kcal/mol). In this conformation, there are three predicted hydrogen bonds, with Asp 258, Asn 295 and Gly 255. Other possible conformations that include hydrogen bonds with the residues from the catalytic triad have a lower affinity (ΔG =-9.29 kcal/mol, bonds with Asp 153 and His 194 and ΔG = -9.92 kcal/mol, bonds with His 194 and Ser 368). DockingServer does not provide full fitness data, but does provide a predicted computational K_i value (Nelfinavir K_i = 4.97 nM) for the C-domain and (Darunavir K_i = 5.64 µM) for the P-domain.

Table 2.2. Ligand-Protein interaction parameters by DockingServer.

Ligand*	Estimated -ΔG (kcal/mol)	Estimated Ki	Total intermolecular energy (kcal/mol)	Hydrogen Bonds
Nelfinavir	-11.33	4.97 (nM)	-12.79	Asp 258
				Asn 295
				Gly 255
Darunavir	-7.25	5.64 (µM)	-8.88	Ser 302
				Asp 410
				Asp 423
				Thr 514
				Arg 519

* Free binding energy, estimated K_i and interactions for Nelfinavir and Darunavir using furin (PDB ID 4OMC).

Inhibition of Furin *in vitro*

The molecular docking studies predicted that PIs bind to the catalytic site of furin as well as to a putative allosteric site on furin. To test this hypothesis, we used a fluorescence assay to monitor furin activity. Furin has substrate specificity for the multi-basic consensus amino-acid sequence of Arg-X-Lys/Arg-Arg (RXRR) at the cleavage site[1,69,77,78], where X stands for a neutral, polar amino acid. Biochemical companies have since developed peptide substrates including the furin cleavage sequence that have an attached fluorescent tag. A fluorescence tag is quenched when it is attached to the peptide, but when furin cleaves the peptide the fluorophore is released and is able to fluoresce. The inhibitory effect of the PIs in this assay can be characterized through a positive control, in which furin actively cleaves substrate without the presence of an inhibitor. Commercially available PIs (Table 2.3) were tested in this assay and the results are presented in Figures 2.4 and 2.5.

In general, the predicted inhibition of furin by PIs was consistent with the predictions from the molecular docking studies as illustrated in Figure 2.4. Tipranavir, darunavir and nelfinavir were the three best inhibitors as predicted by the molecular docking. The remarkable observation is that, consistent with our hypothesis, darunavir did in fact inhibit furin activity even though it bound at an allosteric site between the catalytic domain and the P domain of furin and not at the active site.
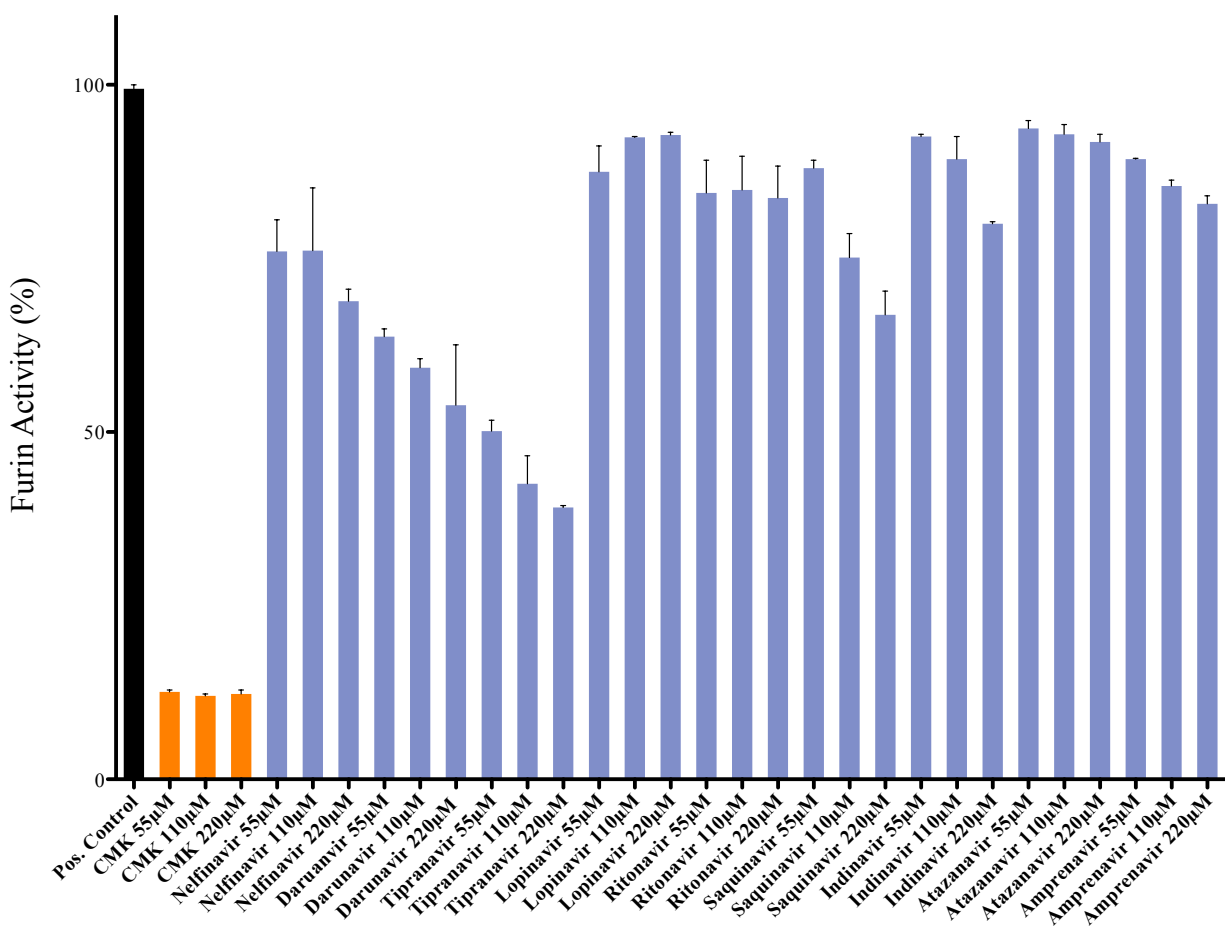
Figure 2.4. Furin activity screen. Percent furin activity versus varying concentrations of PIs. The positive control for furin activity is all assay components without any inhibitors added. Chloromethylketone (CMK) is used as a known furin inhibitor and represents full inhibition of furin. The remaining assays include furin, substrate and the indicated concentration of the PI.

As previously noted, our greatest interest focused on PIs offering the fewest physiological side effects, prompting additional studies with nelfinavir and darunavir[79]. We chose nelfinavir to represent catalytic site inhibitors and darunavir to represent allosteric site inhibitors. Figure 2.5A shows decreased fluorescence caused by the presence of darunavir or nelfinavir at two different concentrations (110 and 220 μM). We also wanted to test the potential synergistic effect when the two drugs are combined (Nelfinavir 110 μM + Darunavir 110 μM), as these drugs are predicted to bind to different sites. The combined drug treatment gave a synergistic effect, consistent with inhibition occurring at the catalytic site as well at the allosteric site. Figure 2.5B is a graphical representation showing the positive control at 100% and each reaction with the different protease inhibitors as a percent of the positive control. The Lineweaver-Burk statistical transformations along with the predicted computational binding affinity data, are consistent with the binding of darunavir at an allosteric site indicating uncompetitive inhibition (Figure 2.6B) whereas; nelfinavir portrays competitive inhibition (Figure 2.6A).
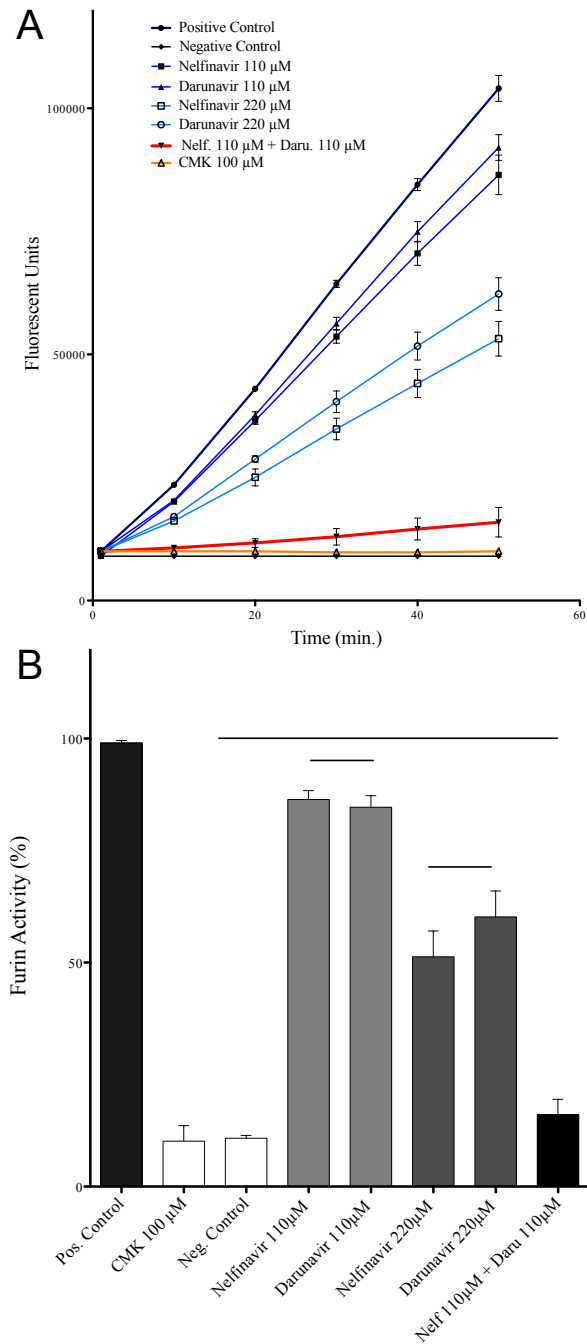
Figure 2.5. Inhibiting furin *in vitro*. Known furin inhibitor CMK is used as an inhibitor control, while the positive control lacks the presence of an inhibitor. An additional negative control lacks the presence of furin. **A)** Furin activity is shown over a 50-minute time course. **B)** Graphical representation of percent furin activity at the 50-minute endpoint.
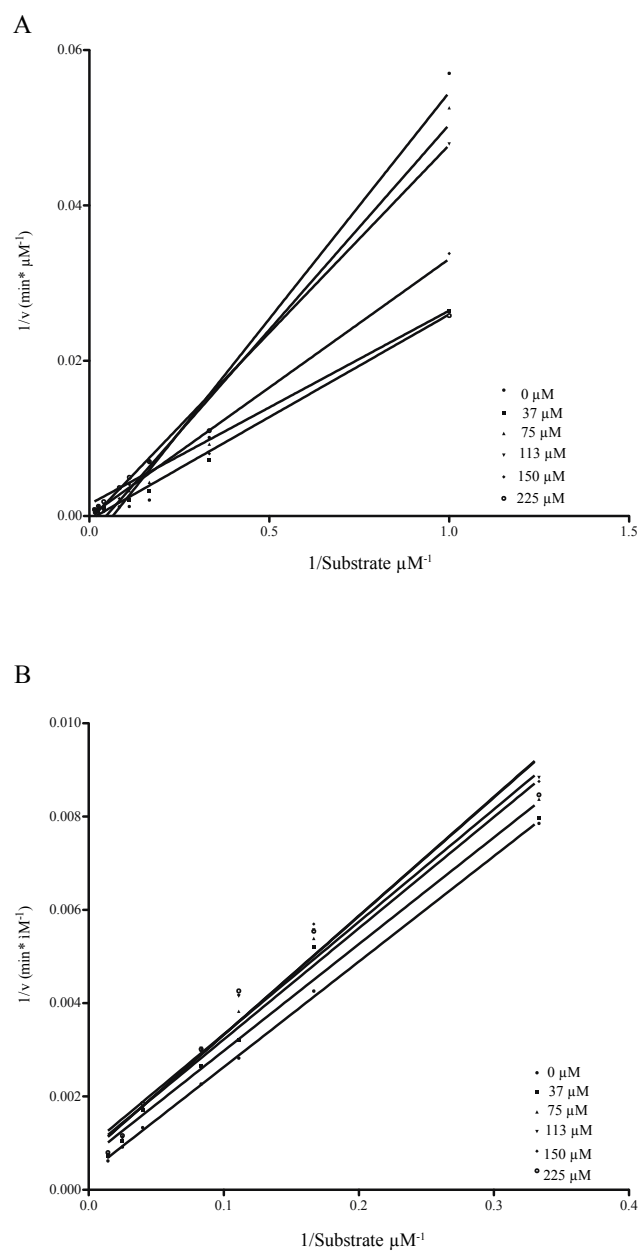
A

B

Figure 2.6. Lineweaver-Burk plots of Nelfinavir and Darunavir. A) Nelfinavir showing competitive inhibition and **B)** Darunavir showing uncompetitive inhibition of furin.

Inhibition of Hepcidin secretion from hepatocytes

After confirming that PIs were able to inhibit purified furin, we desired to demonstrate efficacy of furin inhibition by PIs in living cells. The hepatoma cell line Huh7 has been used previously to demonstrate the secretion of hepcidin in response to inflammation as a model for ACI[49,50,80]. Since, hepcidin is synthesized in a precursor form called prohepcidin with furin specifically cutting prohepcidin into the active hormone hepcidin[29,30]. We proposed that PIs would inhibit furin and prevent the cleavage of prohepcidin into hepcidin.

Huh7 cells were treated with and without inflammatory cytokines (IL-6 and BMP-9) and treated with PIs to inhibit furin. Mature hepcidin-25 secreted into the media from differing cell groups was collected and quantified by MS (Figure 2.7). PI treatment did in fact potently inhibit hepcidin secretion from inflamed cells under these conditions. These results demonstrate that PIs, particularly nelfinavir and darunavir, are potent potential therapeutics to inhibit furin and prevent ACI.
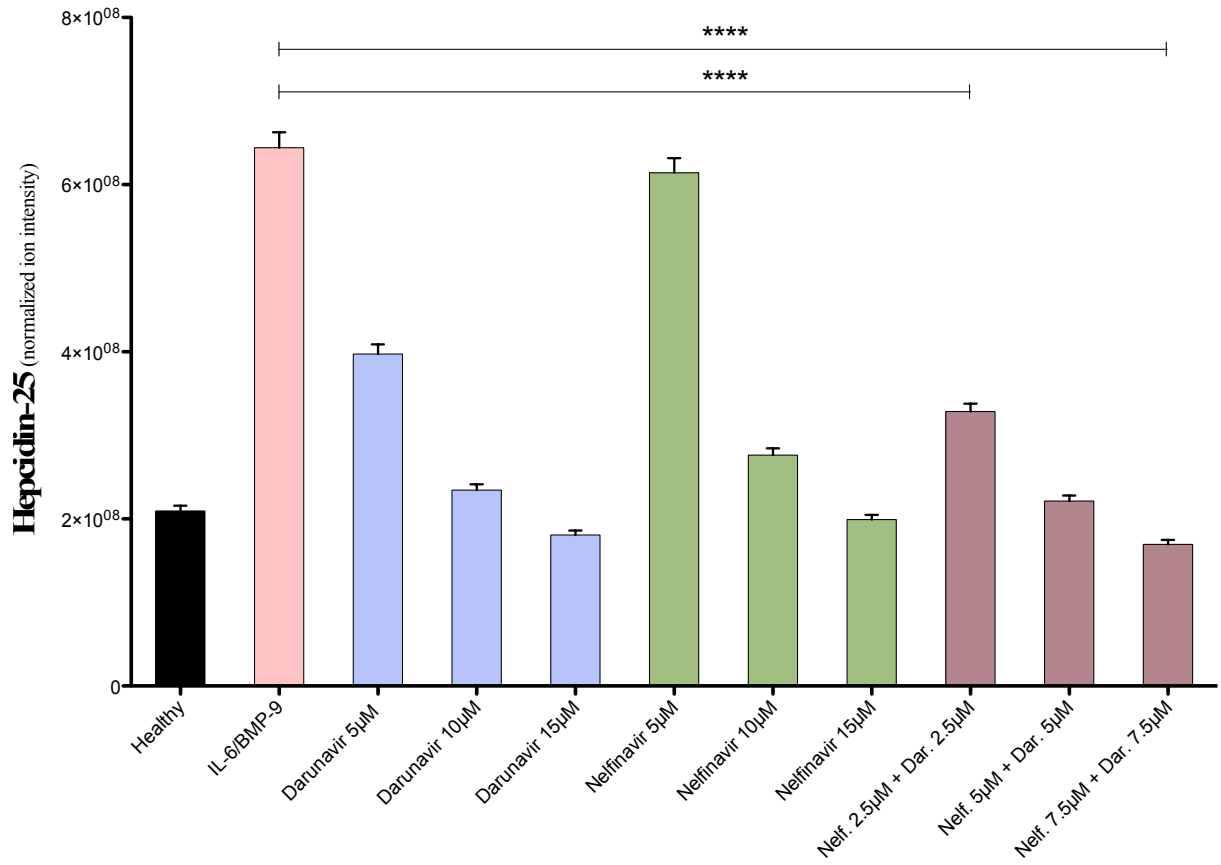
Figure 2.7. Huh7 cell media Hepcidin-25 quantification. LTQ- Orbitrap XL mass spectrometer total ion intensity of hepcidin-25 in Huh7 cell media of cells not treated (Black), cells treated with inflammatory cytokines (Il-6 and BMP-9) (Pink) and cells treated with inflammatory cytokines and with PIs at the indicated concentrations to inhibit Hepcidin activation and secretion (Blue, Green, and Purple). Il-6 was induced alongside BMP-9 at a concentration of 10 ng/ml each for all cell groups except healthy control. Healthy PI treated control group showed no significant change in hepcidin-25 (Data not shown).

Discussion

Molecular Docking studies were used to analyze the binding of known PIs to the proprotein convertase furin. These studies predicted that several of the PIs could bind tightly to the catalytic site of furin (Figure 2.2, Table 2.1). Additionally, several of the proposed ligands were predicted to bind to a putative allosteric site found between the catalytic domain and the P domain of furin (Figure 2.3, Table 2.1). Furin enzymatic assays confirmed that purified furin was inhibited by PIs. Additional analysis of the inhibition data showed that the PIs could be divided into two classes of inhibitors. The first class of PIs inhibited at the active site of furin and is represented by nelfinavir (Figures 2.2A, 2.3A and Figure 2.6). The second class of PIs inhibited at the allosteric site identified in the molecular docking and is represented by darunavir (Figures 2.2B, 2.3B and Figure 2.6). The addition of both catalytic site and allosteric site inhibitors (a combination of nelfinavir and darunavir) produced a synergistic effect causing significantly more inhibition than either drug alone (Figure 2.5). Finally the inhibition of furin by HIV protease inhibitors was confirmed in cells using a model of ACI. The secretion of hepcidin, a hormone that is cut and activated by furin, was significantly decreased in the presence of the protease inhibitors nelfinavir and darunavir (Figure 2.7).

In order to place the binding of PIs by furin and the associated inhibition data into context, we compared the binding of PIs such as nelfinavir to other protease enzymes. Nelfinavir was synthesized and engineered to bind to the HIV protease and calculations show an affinity of nelfinavir binding to HIV protease with a delta G ranging between -7 to -14 kcal/mol. We also examined the affinity of nelfinavir for binding to the aspartyl protease Renin and found a calculated affinity of -10.2 kcal/mol. Therefore the observation we report here, that nelfinavir

96

bound to furin with affinities of – 9.18 kcal/mol demonstrates only a slightly weaker for furin than its original target or for another aspartyl protease. Additionally, the affinity of nelfinavir binding to furin was very close to the known inhibitor CMK with a delta G of -11.07 kcal/mol.

Other HIV PIs showed comparable binding affinities between HIV protease, Renin and furin. Darunavir showed the following affinities calculated by molecular docking: delta G = -9.58 for HIV protease, -10.33 for Renin and -8.18 for the allosteric site of Furin. Similar results were observed for the HIV protease inhibitors ritonavir and indinavir (Data not shown).

Perhaps the most important discovery of this study was the identification of an allosteric site on furin. This serendipitous discovery perfectly aligned with our goals in finding a way to fine tune the inhibition of furin. The cleft at the interface of the P domain and the catalytic domain provides a new target to regulate the activity of furin. Whether this is a natural regulatory site with an *in vivo* regulatory molecule or an advantageous discovery that the darunavir and other PIs happen to bind at this location is not yet known. A similar method to inhibit proteases has been taken with the Caspase class of protease inhibitors. The caspase proteases have a cysteine rich region and treatment of caspase enzymes with thiol-containing molecules allows disulfide bonds to form that force the caspase enzymes into a confirmation that is similar to the zymogen conformation that inhibits enzyme catalysis. We propose a similar regulatory mechanism occurs with furin at this site but the physiological ligand that causes the allosteric regulation has not been identified.

Additionally, the allosteric site provides a mechanism to further inhibit Furin. The combination of catalytic site and allosteric site inhibitors produces a new and potentially potent method to inhibit furin activity (Figure 2.5). This combination may allow treatments designed to have a potent inhibitory effect at high concentrations or may allow an attenuation of furin

activity when the combination of both classes of inhibitors is used at much lower concentrations. These studies have all been performed in a 1:1 ratio. It is possible that holding the inhibitor to one site constant and varying the concentration of the inhibitor to the other site might also provide the ability to fine tune the effect on furin inhibition. We also anticipate that another benefit is that the lower doses of the combination therapy might minimize any side effects caused by the individual drugs used at higher concentrations.

This study shows that the method used in this paper can be applied to screening and testing small molecules as potential inhibitors of proteases. Once a crystal structure is obtained, the steps used in this paper can be applied for proof of concept for inhibition. Additionally, the impact on the field of protease field is significant because it can be used to explain many of the side effects related to HIV protease inhibitors. Such screens can be used in the future to identify and understand off target inhibition of the PIs.

Most importantly, this study identifies a new approach to furin inhibition. Inhibition of furin at the catalytic, allosteric or both sites can now be used as a method to treat a series of diseases including ACI and cancer. Furin plays important roles in disease ranging from Alzheimer's disease and cancer, to Anthrax and Ebola fever[1].
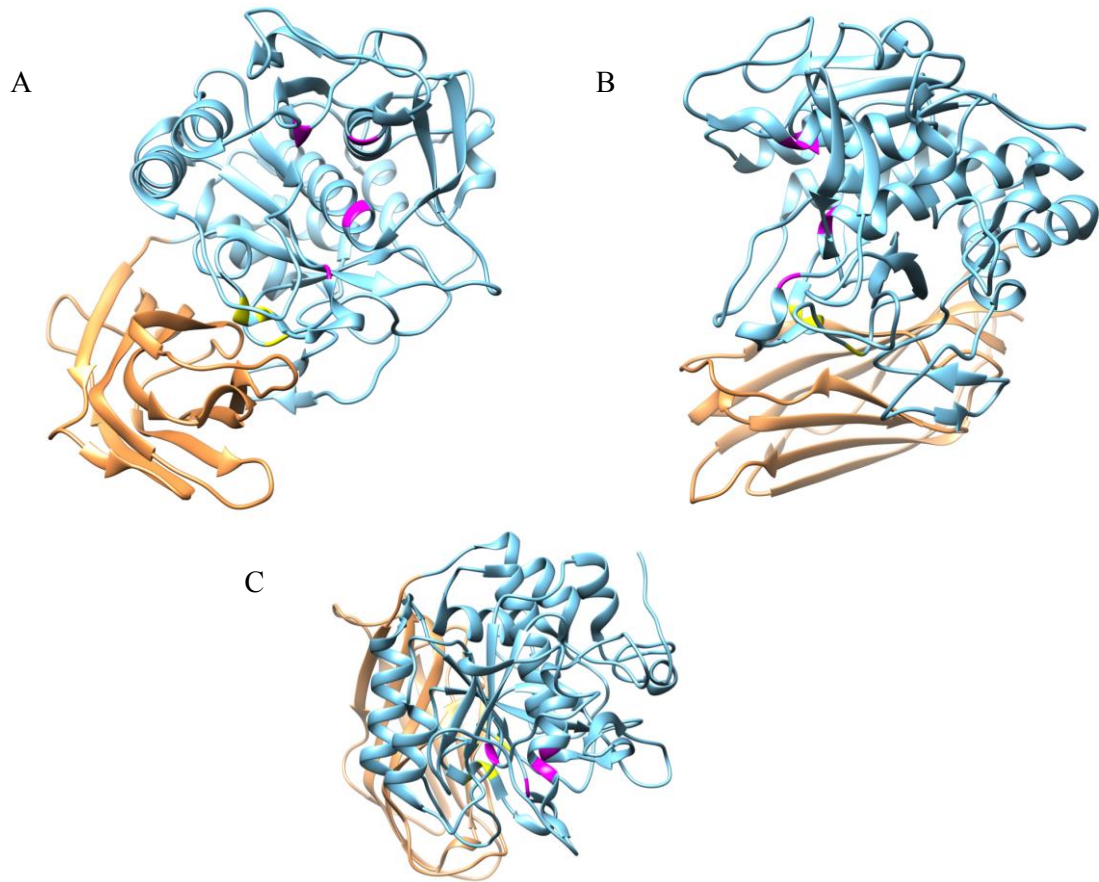
Figure 2.8. Single subunit of furin shown in different perspectives. A) Side-view facing catalytic site. **B)** Side-view with catalytic site facing away. **C)** Anterior view looking downward towards P domain.
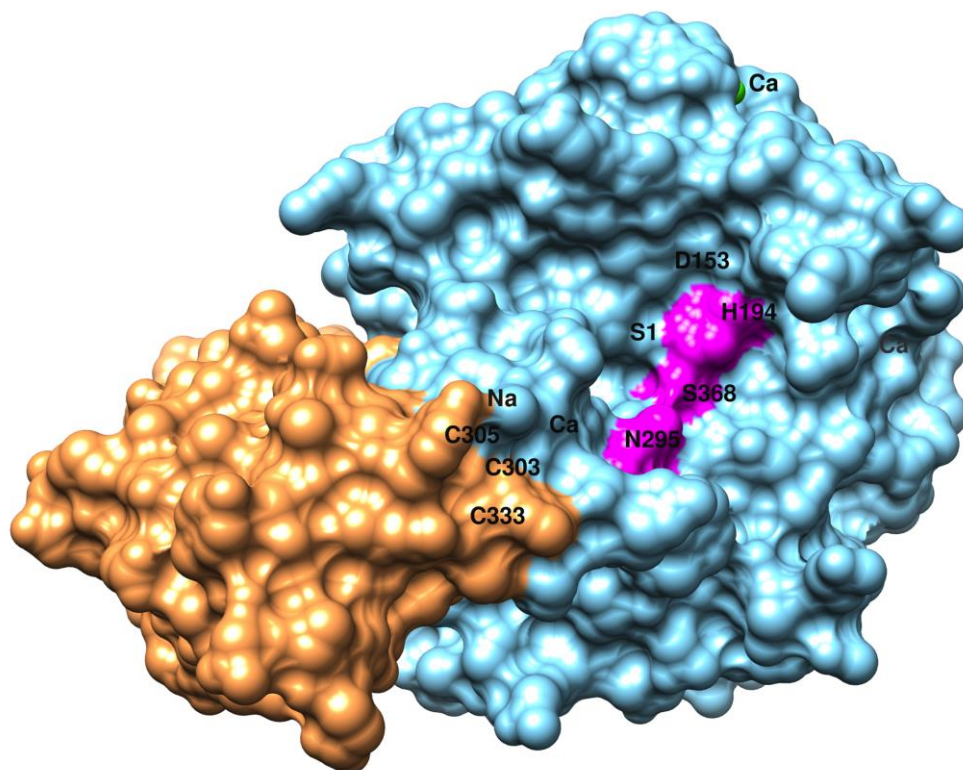
Figure 2.9. Surface structural view of furin. Illustrating catalytic triad (Ser368, Asp 153, and His 194), the oxyanion hole (Asn 295), and the cysteine rich area of the allosteric site (Cys 303, Cys 305, Cys 333). The catalytic C-domain is colored in blue, while the P-domain is colored in orange.
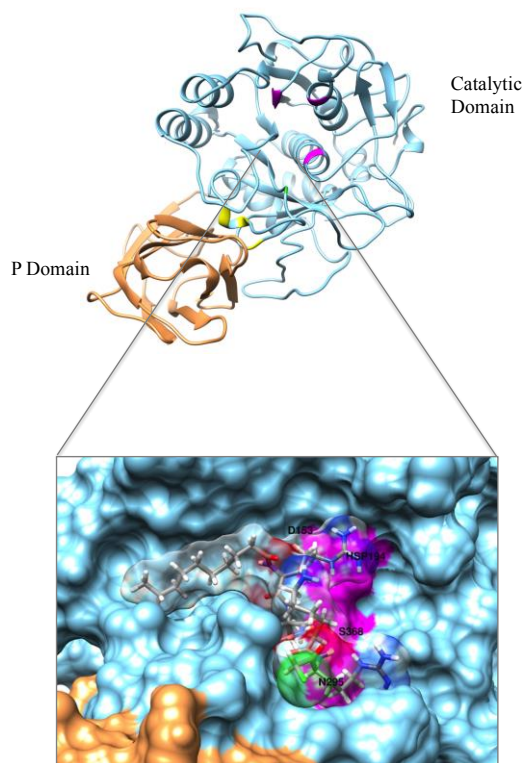
Figure 2.10. Visualization of the known furin inhibitor chloromethylketone (CMK) bound to the catalytic site of human furin (Full fitness -1965.4, Simple fitness -91.36, ΔG -11.24 kcal/mol)
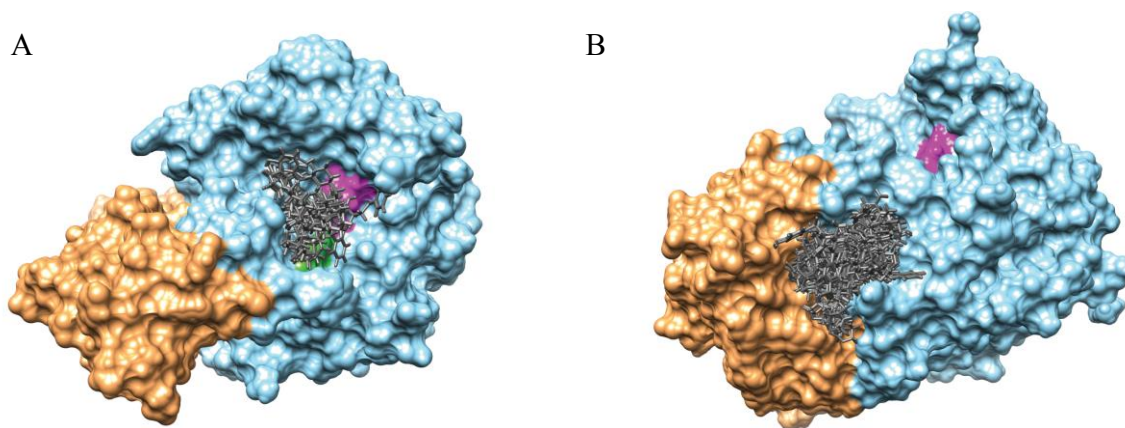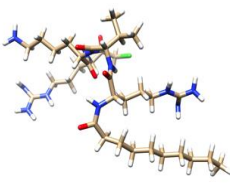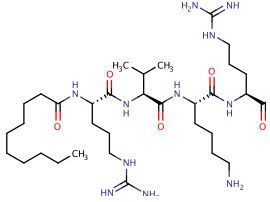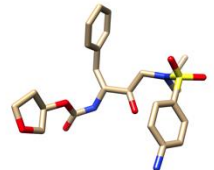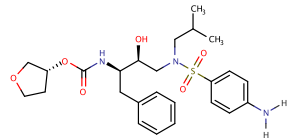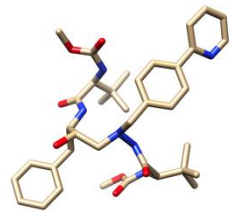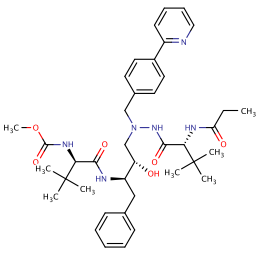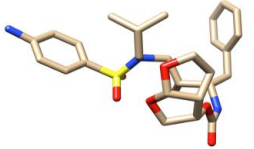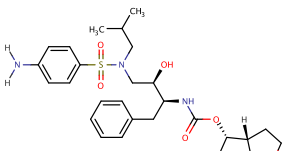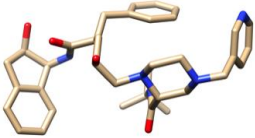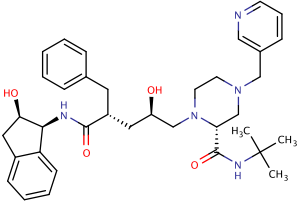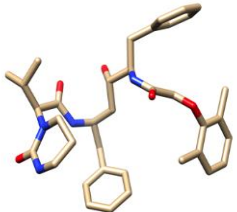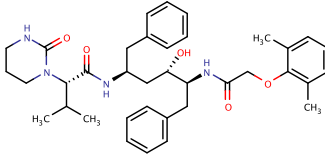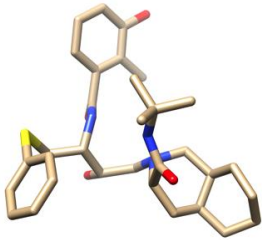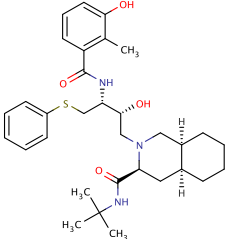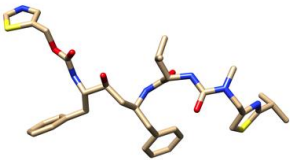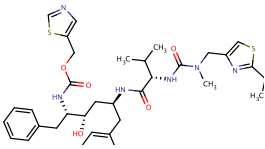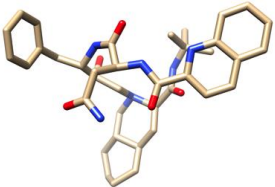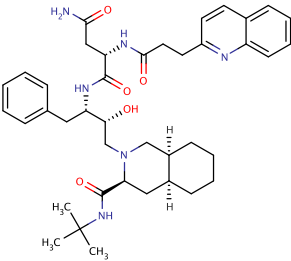

Figure 2.11. Visualization of predicted ligand binding conformation with furin. A) Nelfinavir and **B)** darunavir.

Table 2.3. Protease inhibitor molecules.

Represented in both two and three dimensions with corresponding chemical identification codes.

ZINC ID	PI Name	3D Structure	2D Structure
CAS: 15011-399-8	Dec-RVKR-CMK (Chloromethylketone)		
3809192	Amprenavir		
3941496	Atazanavir		
3955219	Darunavir		

22448696	Indinavir		
3951740	Lopinavir		
26994433	Nelfinavir		
3944422	Ritonavir		
3914596	Saquinavir		

14879987	Tipranavir		
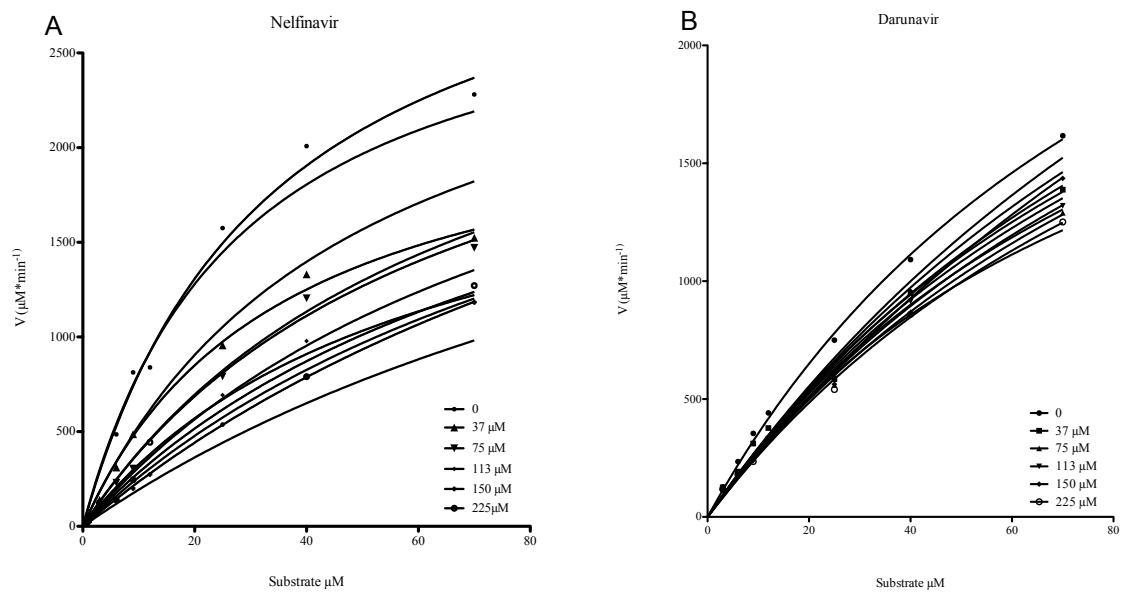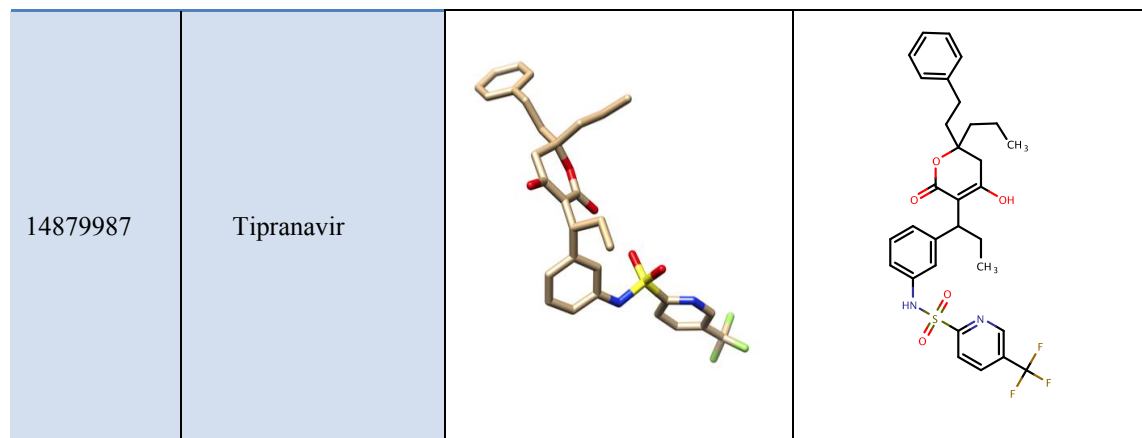
Figure 2.12. Michaelis-Menton plots. A) Nelfinavir and **B)** Darunavir.

Table 2.4. Lineweaver-Burk slope values for Nelfinavir and Darunavir. Concentrations of substrate are varied and range from 0-225µM.

Substrate Concentration (µM)	Nelfinavir Slope	Darunavir Slope
0	0.05835	0.02260
37	0.05283	0.02288
75	0.04833	0.02384
113	0.03310	0.02550
150	0.02643	0.02544
225	0.02492	0.02411

* Values determined with the use of GraphPad Prism5 statistical software.
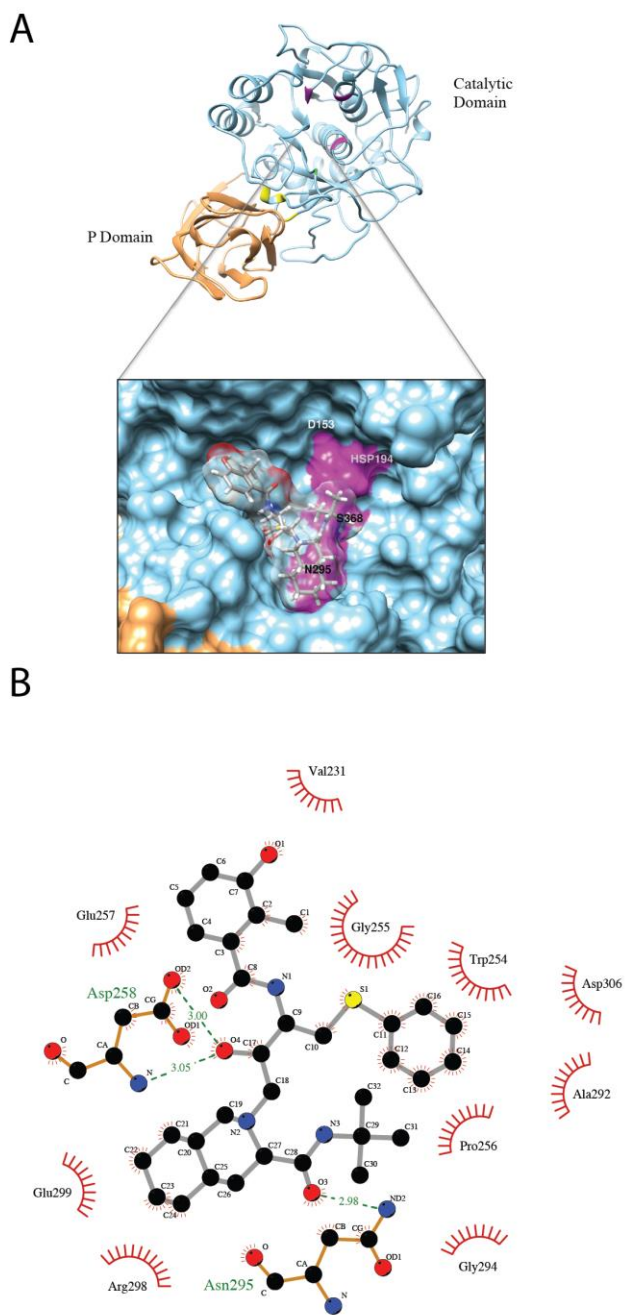
Figure 2.13. Second conformation of Nelfinavir. A) Surface visualization of Nelfinavir in a second conformation at the catalytic site of furin (Full fitness -1719.31, ΔG -9.18 kcal/mol). **B)** LigPlot of Nelfinavir forming hydrogen bonds with residues Asp 258 and Asn 295.
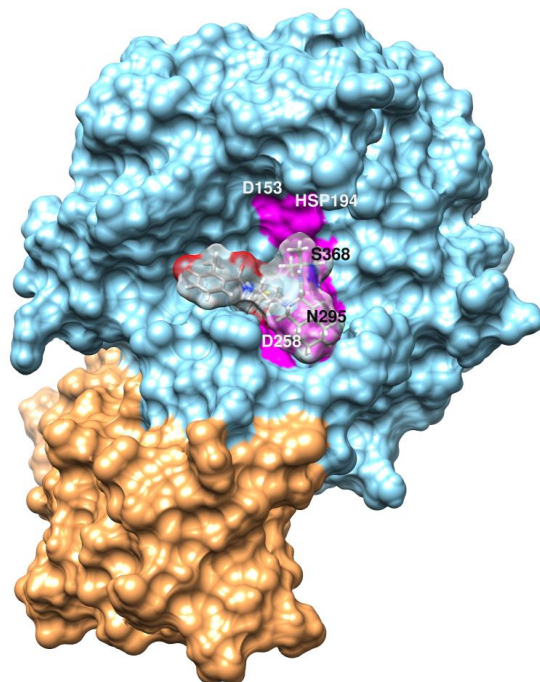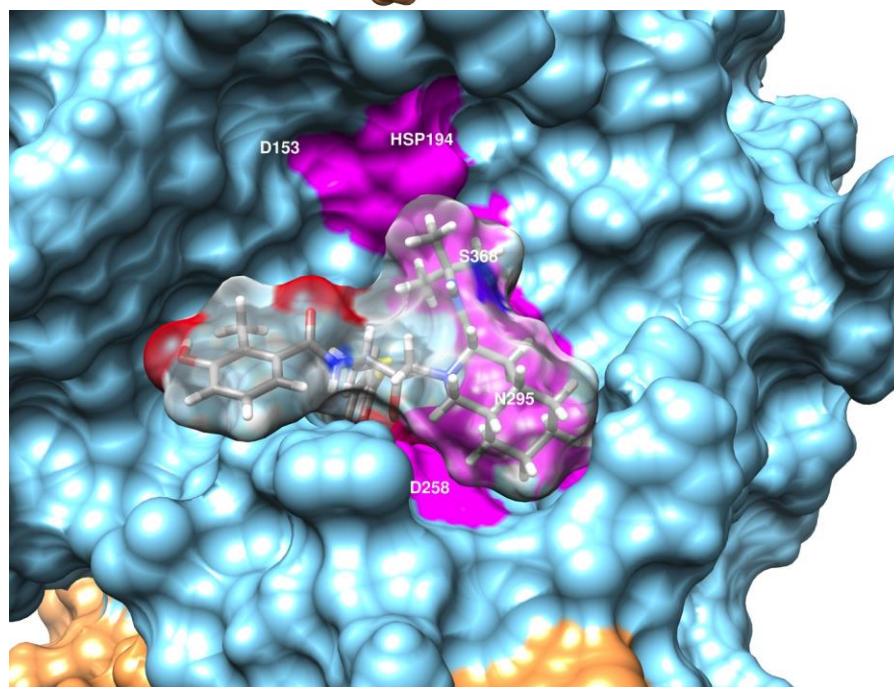
Figure 2.14.   Surface structure illustration of Nelfinavir bound to Furin.   Predicted binding affinity characterized as being ΔG = -12.79 kcal/mol. **A)** Distant view of furin with ligand Nelfinavir. **B)** Close-up view of furin with ligand Nelfinavir.
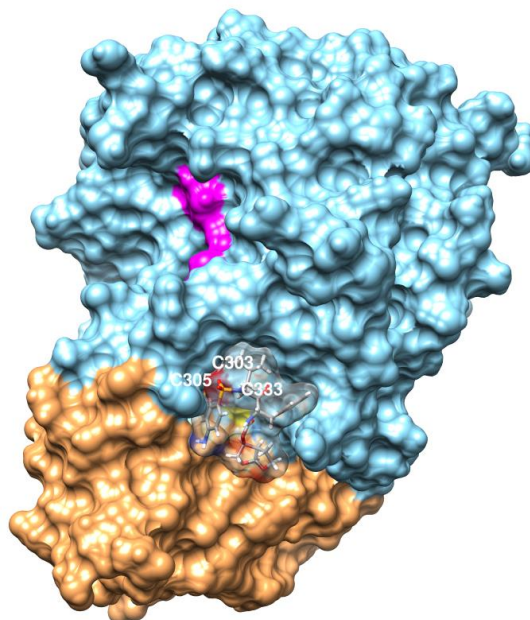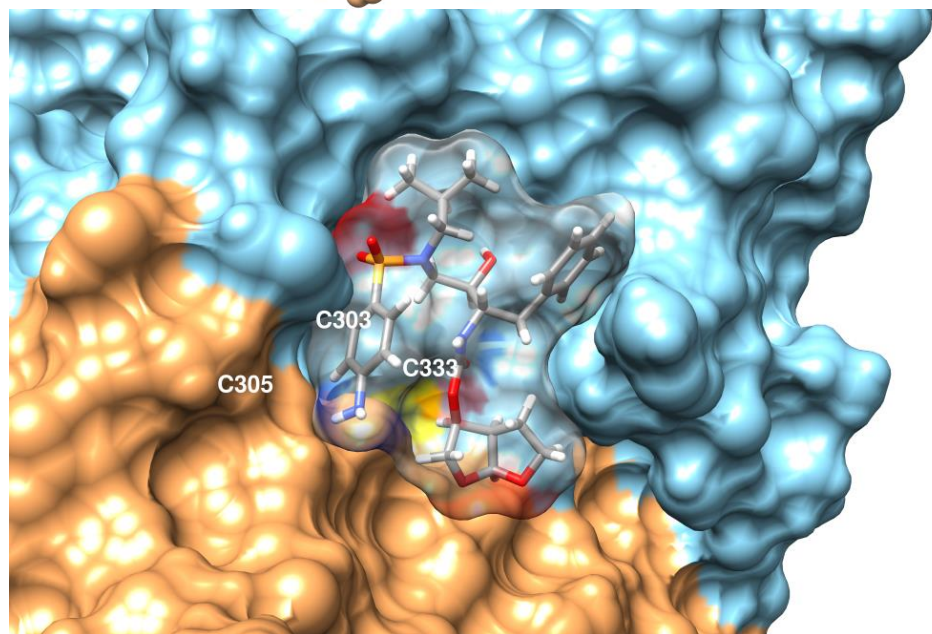
Figure 2.15.   Surface structure illustration of Darunavir bound to Furin.   Predicted binding affinity characterized as being ΔG = -8.88 kcal/mol. **A)** Distant view of furin with ligand Darunavir. **B)** Close-up view of furin with ligand Darunavir.
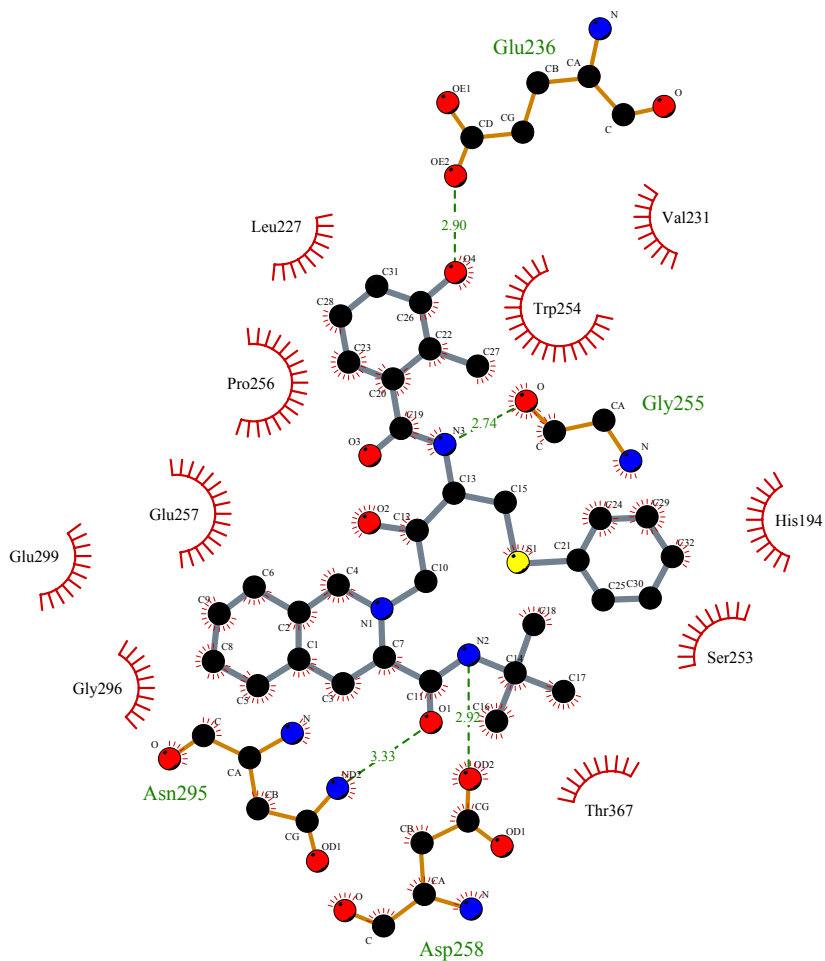
Figure 2.16. LigPlot representation of Nelfinavir interacting with Furin as characterized by DockingServer. Shown is a two-dimensional representation of the predicted interactions of Nelfinavir with residues in the catalytic domain of furin. Predicted hydrogen bonds are shown with green dashed lines, and hydrophobic contacts with red arches. Predicted hydrogen bonds are shown to be formed with residues Asn295, Asp258, Glu236, and Gly255.
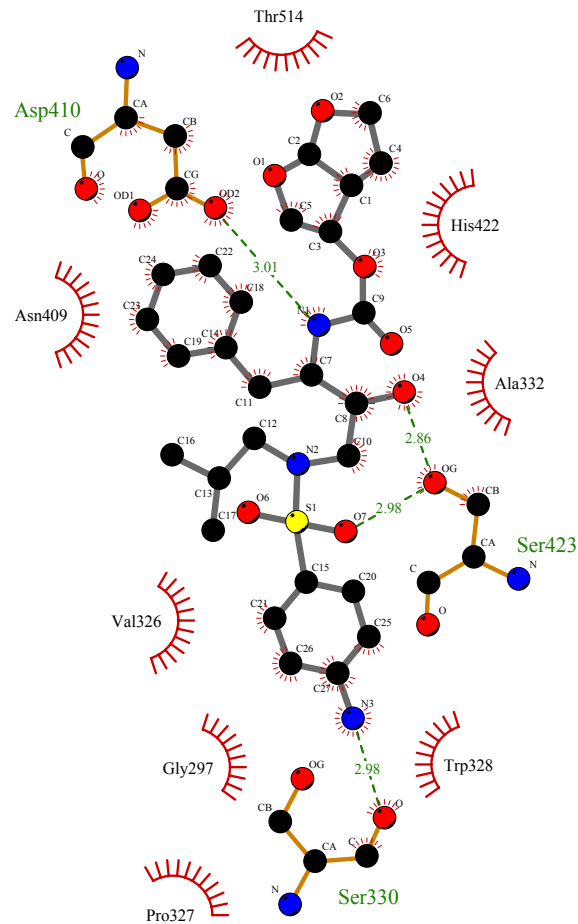
Figure 2.17. LigPlot representation of Darunavir interacting with Furin as characterized by DockingServer. Shown is a two-dimensional representation of the predicted interactions of Darunavir with residues in the cysteine rich domain of furin. Predicted hydrogen bonds are shown with green dashed lines, and hydrophobic contacts with red arches. Predicted hydrogen bonds form with residues Ser330, Ser423, and Asp410.
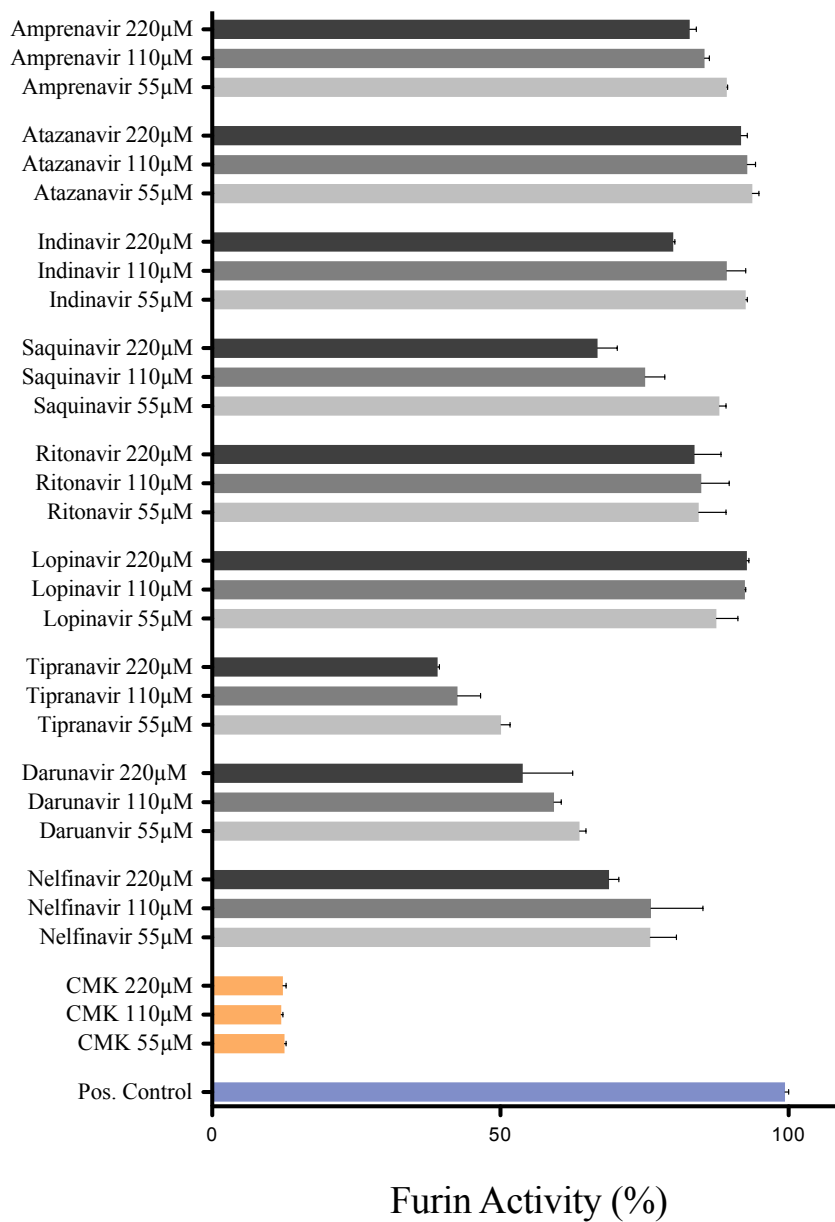
Figure 2.18. *In vitro* Furin Activity Drug Screen Assay. Alternative view. The positive control for furin activity is all assay components without any inhibitors added. Chloromethylketone (CMK) is used as a known furin inhibitor and represents full inhibition of furin. The remaining assays include furin, substrate and the indicated concentration of the PI.

References

1. Thomas, G. Furin at the cutting edge: From protein traffic to embryogenesis and disease. *Nat. Rev. Mol. Cell Biol.* **3,** 753–766 (2002).

2. Chrétien, M., Seidah, N. G., Basak, A. & Mbikay, M. Proprotein convertases as therapeutic targets. *Expert Opin. Ther. Targets* **12,** 1289–1300 (2008).

3. Artenstein, A. W. & Opal, S. M. Proprotein Convertases in Health and Disease. *N. Engl. J. Med.* **365,** 2507–2518 (2011).

4. Dahms, S. O. *et al.* X-ray Structures of Human Furin in Complex with Competitive Inhibitors. *ACS Chem. Biol.* 140408095720006 (2014). doi:10.1021/cb500087x

5. Henrich, S. *et al.* The crystal structure of the proprotein processing proteinase furin explains its stringent specificity. *Nat. Struct. Mol. Biol.* **10,** 520–526 (2003).

6. Henrich, S., Lindberg, I., Bode, W. & Than, M. E. Proprotein Convertase Models based on the Crystal Structures of Furin and Kexin: Explanation of their Specificity. *J. Mol. Biol.* **345,** 211–227 (2005).

7. Coppola, J. M., Bhojani, M. S., Ross, B. D. & Rehemtulla, A. A small-molecule furin inhibitor inhibits cancer cell motility and invasiveness. *Neoplasia N. Y. NY* **10,** 363 (2008).

8. Komiyama, T. *et al.* Inhibition of Furin/Proprotein Convertase-catalyzed Surface and Intracellular Processing by Small Molecules. *J. Biol. Chem.* **284,** 15729–15738 (2009).

9. Cameron, A. Polyarginines Are Potent Furin Inhibitors. *J. Biol. Chem.* **275,** 36741–36749 (2000).

10. Rask-Andersen, M., Almén, M. S. & Schiöth, H. B. Trends in the exploitation of novel drug targets. *Nat. Rev. Drug Discov.* **10,** 579–590 (2011).

11. Cohen, P. Protein kinases — the major drug targets of the twenty-first century? *Nat. Rev. Drug Discov.* **1,** 309–315 (2002).

12. Zhang, J., Yang, P. L. & Gray, N. S. Targeting cancer with small molecule kinase inhibitors. *Nat. Rev. Cancer* **9,** 28–39 (2009).

13. Kuntz, A. N. *et al.* Thioredoxin Glutathione Reductase from Schistosoma mansoni: An Essential Parasite Enzyme and a Key Drug Target. *PLoS Med* **4,** e206 (2007).

14. Lee, Y.-M., Lin, Y.-F. & Lim, C. Factors Controlling the Role of Zn and Reactivity of Zn-bound Cysteines in Proteins: Application to Drug Target Discovery. *J. Chin. Chem. Soc.* **61,** 142–150 (2014).

15. Zha, C., Brown, G. B. & Brouillette, W. J. A highly predictive 3D-QSAR model for binding to the voltage-gated sodium channel: Design of potent new ligands. *Bioorg. Med. Chem.* **22,** 95–104 (2014).

16. Panyi, G., Beeton, C. & Felipe, A. Ion channels and anti-cancer immunity. *Philos. Trans. R. Soc. B Biol. Sci.* **369,** 20130106 (2014).

17. Waxman, S. G. & Zamponi, G. W. Regulating excitability of peripheral afferents: emerging ion channel targets. *Nat. Neurosci.* **17,** 153–163 (2014).

18. Rask-Andersen, M., Masuram, S. & Schiöth, H. B. The Druggable Genome: Evaluation of Drug Targets in Clinical Trials Suggests Major Shifts in Molecular Class and Indication. *Annu. Rev. Pharmacol. Toxicol.* **54,** 9–26 (2014).

19. Kanakaraj, P. *et al.* Simultaneous targeting of TNF and Ang2 with a novel bispecific antibody enhances efficacy in an in vivo model of arthritis. *mAbs* **4,** 600–613 (2012).

20. Seidah, N. G. & Prat, A. The biology and therapeutic targeting of the proprotein convertases. *Nat. Rev. Drug Discov.* **11,** 367–383 (2012).

21. Richman, D. D. *et al.* The Challenge of Finding a Cure for HIV Infection. *Science* **323,** 1304–1307 (2009).

22. Von Schwedler, U. K. *et al.* Proteolytic refolding of the HIV-1 capsid protein amino-terminus facilitates viral core assembly. *EMBO J.* **17,** 1555–1568 (1998).

23. Barrett, A. J., Woessner, J. F. & Rawlings, N. D. *Handbook of Proteolytic Enzymes*. (Elsevier, 2004).

24. Pesu, M. *et al.* T-cell-expressed proprotein convertase furin is essential for maintenance of peripheral immune tolerance. *Nature* **455,** 246–250 (2008).

25. Bassi, D. E. *et al.* Proprotein Convertase Inhibition Results in Decreased Skin Cell Proliferation, Tumorigenesis, and Metastasis. *Neoplasia N. Y. N* **12,** 516–526 (2010).

26. Liu, T. *et al.* Macrophage Inhibitory Cytokine 1 Reduces Cell Adhesion and Induces Apoptosis in Prostate Cancer Cells. *Cancer Res.* **63,** 5034–5040 (2003).

27. Hollevoet, K., Antignani, A., FitzGerald, D. J. & Pastan, I. Combining the Antimesothelin Immunotoxin SS1P With the BH3-mimetic ABT-737 Induces Cell Death in SS1P-resistant Pancreatic Cancer Cells: *J. Immunother.* **37,** 8–15 (2014).

28. Bravo, D. A., Gleason, J. B., Sanchez, R. I., Roth, R. A. & Fuller, R. S. Accurate and efficient cleavage of the human insulin proreceptor by the human proprotein-processing protease furin. Characterization and kinetic parameters using the purified, secreted soluble protease expressed by a recombinant baculovirus. *J. Biol. Chem.* **269,** 25830–25837 (1994).

29. Valore, E. V. & Ganz, T. Posttranslational processing of hepcidin in human hepatocytes is mediated by the prohormone convertase furin. *Blood Cells. Mol. Dis.* **40,** 132–138 (2008).

30. Gagliardo, B. *et al.* Pro-hepcidin is unable to degrade the iron exporter ferroportin unless matured by a furin-dependent process. *J. Hepatol.* **50,** 394–401 (2009).

31. Garten, W. & Klenk, H.-D. Understanding influenza virus pathogenicity. *Trends Microbiol.* **7,** 99–100 (1999).

32. Essalmani, R. *et al.* Furin Is the Primary in Vivo Convertase of Angiopoietin-like 3 and Endothelial Lipase in Hepatocytes. *J. Biol. Chem.* **288,** 26410–26418 (2013).

33. Brouwers, M. C. G. J. *et al.* Plasma proprotein convertase subtilisin kexin type 9 levels are related to markers of cholesterol synthesis in familial combined hyperlipidemia. *Nutr. Metab. Cardiovasc. Dis.* **23,** 1115–1121 (2013).

34. Rashid, S. *et al.* Decreased plasma cholesterol and hypersensitivity to statins in mice lacking Pcsk9. *Proc. Natl. Acad. Sci. U. S. A.* **102,** 5374–5379 (2005).

35. Hook, G., Hook, V. & Kindy, M. The Cysteine Protease Inhibitor, E64d, Reduces Brain Amyloid-β and Improves Memory Deficits in Alzheimer's Disease Animal Models by Inhibiting Cathepsin B, but not BACE1, β-Secretase Activity. *J. Alzheimers Dis.* **26,** 387–408 (2011).

36. Cheng, X. W. *et al.* Role for Cysteine Protease Cathepsins in Heart Disease Focus on Biology and Mechanisms With Clinical Implication. *Circulation* **125,** 1551–1562 (2012).

37. El, S. & Rm, T. Vascular biology of endothelin. *J. Cardiovasc. Pharmacol.* **32 Suppl 3,** S2–13 (1997).

38. Young, J. A. T. & Collier, R. J. Anthrax Toxin: Receptor Binding, Internalization, Pore Formation, and Translocation. *Annu. Rev. Biochem.* **76,** 243–265 (2007).

39. Klenk, H.-D. & Garten, W. Host cell proteases controlling virus pathogenicity. *Trends Microbiol.* **2,** 39–43 (1994).

40. Moulard, M. & Decroly, E. Maturation of HIV envelope glycoprotein precursors by cellular endoproteases. *Biochim. Biophys. Acta BBA - Rev. Biomembr.* **1469,** 121–132 (2000).

41. Day, P. M. & Schiller, J. T. The role of furin in papillomavirus infection. *Future Microbiol.* **4,** 1255–1262 (2009).

42. Southan, C. A genomic perspective on human proteases as drug targets. *Drug Discov. Today* **6,** 681–688 (2001).

43. Roebroek, A. J. *et al.* Failure of ventral closure and axial rotation in embryos lacking the proprotein convertase Furin. *Development* **125,** 4863–4876 (1998).

44. Fugère, M. & Day, R. Cutting back on pro-protein convertases: the latest approaches to pharmacological inhibition. *Trends Pharmacol. Sci.* **26,** 294–301 (2005).

45. Grosdidier, A., Zoete, V. & Michielin, O. SwissDock, a protein-small molecule docking web service based on EADock DSS. *Nucleic Acids Res.* **39,** W270–W277 (2011).

46. Taylor, R. D., Jewsbury, P. J. & Essex, J. W. A review of protein-small molecule docking methods. *J. Comput. Aided Mol. Des.* **16,** 151–166 (2002).

47. Da, S. Anemia of chronic disease. *Med. Clin. North Am.* **76,** 567–579 (1992).

48. Kassebaum, N. J. *et al.* A systematic analysis of global anemia burden from 1990 to 2010. *Blood* **123,** 615–624 (2014).

49. Weiss, G. & Goodnough, L. T. Anemia of Chronic Disease. *N. Engl. J. Med.* **352,** 1011–1023 (2005).

50. Sun, C. C., Vaja, V., Babitt, J. L. & Lin, H. Y. Targeting the hepcidin–ferroportin axis to develop new treatment strategies for anemia of chronic disease and anemia of inflammation. *Am. J. Hematol.* **87,** 392–400 (2012).

51. Theurl, I. *et al.* Pharmacologic inhibition of hepcidin expression reverses anemia of chronic inflammation in rats. *Blood* **118,** 4977–4984 (2011).

52. Steinbicker, A. U. *et al.* Inhibition of bone morphogenetic protein signaling attenuates anemia associated with inflammation. *Blood* **117,** 4915–4923 (2011).

53. Sasu, B. J. *et al.* Antihepcidin antibody treatment modulates iron metabolism and is effective in a mouse model of inflammation-induced anemia. *Blood* **115,** 3616–3624 (2010).

54. Goodsell, D. S., Morris, G. M. & Olson, A. J. Automated docking of flexible ligands: Applications of autodock. *J. Mol. Recognit.* **9,** 1–5 (1996).

55. Pettersen, E. F. *et al.* UCSF Chimera—A visualization system for exploratory research and analysis. *J. Comput. Chem.* **25,** 1605–1612 (2004).

56. Grosdidier, A., Zoete, V. & Michielin, O. Fast docking using the CHARMM force field with EADock DSS. *J. Comput. Chem.* **32,** 2149–2159 (2011).

57. Grosdidier, A., Zoete, V. & Michielin, O. EADock: Docking of small molecules into protein active sites with a multiobjective evolutionary optimization. *Proteins Struct. Funct. Bioinforma.* **67,** 1010–1025 (2007).

58. Irwin, J. J., Sterling, T., Mysinger, M. M., Bolstad, E. S. & Coleman, R. G. ZINC: A Free Tool to Discover Chemistry for Biology. *J. Chem. Inf. Model.* **52,** 1757–1768 (2012).

59. Vanommeslaeghe, K. *et al.* CHARMM general force field: A force field for drug-like molecules compatible with the CHARMM all-atom additive biological force fields. *J. Comput. Chem.* **31,** 671–690 (2010).

60. Vanommeslaeghe, K. & MacKerell, A. D. Automation of the CHARMM General Force Field (CGenFF) I: Bond Perception and Atom Typing. *J. Chem. Inf. Model.* **52,** 3144–3154 (2012).

61. Vanommeslaeghe, K., Raman, E. P. & MacKerell, A. D. Automation of the CHARMM General Force Field (CGenFF) II: Assignment of Bonded Parameters and Partial Atomic Charges. *J. Chem. Inf. Model.* **52,** 3155–3168 (2012).

62. Lau, C. D., Levesque, M. J., Chien, S., Date, S. & Haga, J. H. ViewDock TDW: high-throughput visualization of virtual screening results. *Bioinformatics* **26,** 1915–1917 (2010).

63. Hanson, R. M. *Jmol* – a paradigm shift in crystallographic visualization. *J. Appl. Crystallogr.* **43,** 1250–1260 (2010).

64. Hanson, R. M., Prilusky, J., Renjian, Z., Nakane, T. & Sussman, J. L. JSmol and the Next-Generation Web-Based Representation of 3D Molecular Structure as Applied to Proteopedia. *Isr. J. Chem.* **53,** 207–216 (2013).

65. Laskowski, R. A. & Swindells, M. B. LigPlot+: Multiple Ligand–Protein Interaction Diagrams for Drug Discovery. *J. Chem. Inf. Model.* **51,** 2778–2786 (2011).

66. Bikadi, Z. & Hazai, E. Application of the PM6 semi-empirical method to modeling proteins enhances docking accuracy of AutoDock. *J. Cheminformatics* **1,** 15 (2009).

67. Morris, G. M. *et al.* Automated docking using a Lamarckian genetic algorithm and an empirical binding free energy function. *J. Comput. Chem.* **19,** 1639–1662 (1998).

68. Solis, F. J. & Wets, R. J.-B. Minimization by Random Search Techniques. *Math. Oper. Res.* **6,** 19–30 (1981).

69. Hallenberger, S. *et al.* Inhibition of furin-mediated cleavage activation of HIV-1 glycoprotein gpl60. *Nature* **360,** 358–361 (1992).

70. Apletalina, E., Appel, J., Lamango, N. S., Houghten, R. A. & Lindberg, I. Identification of Inhibitors of Prohormone Convertases 1 and 2 Using a Peptide Combinatorial Library. *J. Biol. Chem.* **273,** 26589–26595 (1998).

71. Lineweaver, H. & Burk, D. The Determination of Enzyme Dissociation Constants. *J. Am. Chem. Soc.* **56,** 658–666 (1934).

72. Scheer, J. M., Romanowski, M. J. & Wells, J. A. A common allosteric site and mechanism in caspases. *Proc. Natl. Acad. Sci.* **103,** 7595–7600 (2006).

73. Hansen, S. K. *et al.* Allosteric Inhibition of PTP1B Activity by Selective Modification of a Non-Active Site Cysteine Residue†. *Biochemistry (Mosc.)* **44,** 7704–7712 (2005).

74. Holyoak, T., Kettner, C. A., Petsko, G. A., Fuller, R. S. & Ringe, D. Structural Basis for Differences in Substrate Selectivity in Kex2 and Furin Protein Convertases†,‡. *Biochemistry (Mosc.)* **43,** 2412–2421 (2004).

75. Hardy, J. A., Lam, J., Nguyen, J. T., O'Brien, T. & Wells, J. A. Discovery of an allosteric site in the caspases. *Proc. Natl. Acad. Sci. U. S. A.* **101,** 12461–12466 (2004).

76. Hardy, J. A. & Wells, J. A. Searching for new allosteric sites in enzymes. *Curr. Opin. Struct. Biol.* **14,** 706–715 (2004).

77. Lin, L. *et al.* Soluble hemojuvelin is released by proprotein convertase-mediated cleavage at a conserved polybasic RNRR site. *Blood Cells. Mol. Dis.* **40,** 122–131 (2008).

78. Wise, R. J. *et al.* Expression of a human proprotein processing enzyme: correct cleavage of the von Willebrand factor precursor at a paired basic amino acid site. *Proc. Natl. Acad. Sci.* **87,** 9378–9382 (1990).

79. Kaul, D. R., Cinti, S. K., Carver, P. L. & Kazanjian, P. H. HIV Protease Inhibitors: Advances in Therapy and Adverse Reactions, Including Metabolic Complications. *Pharmacother. J. Hum. Pharmacol. Drug Ther.* **19,** 281–298 (1999).

80. Kartikasari, A. E. R. *et al.* Secretion of bioactive hepcidin-25 by liver cells correlates with its gene transcription and points towards synergism between iron and inflammation

signaling pathways. *Biochim. Biophys. Acta BBA - Proteins Proteomics* **1784,** 2029–2037 (2008).

CHAPTER 3: Concomitant Inhibition of Furin: A New Strategy for Therapeutic

Targeting of Hepcidin Secretion

Abstract

Context

Hepcidin is a principal regulator of iron metabolism[1,2]. During conditions of chronic immune activation, hepcidin production increases[1,3,4]. Cytokines stimulate STAT or Smad signaling pathways that activate the HAMP gene encoding for Hepcidin[5,6]. Hepcidin is synthesized as preprohepcidin, and is targeted to the ER/Golgi for secretion[7,8]. In the ER, the targeting sequence is cleaved and prohepcidin is further processed by furin to produce active hepcidin[7,9,10]. In serum hepcidin binds to the iron export protein ferroportin, causing endocytosis and degradation[11−14]. The removal of ferroportin from cells prevents dietary iron absorption and prevents iron redistribution, and resulting in anemia[15−17].

Objective

Previously we inhibited secretion of hepcidin from hepatocytes by inhibiting furin with protease inhibitors (PIs). One of these PIs, nelfinavir, is also a known STAT3 inhibitor[18−20]. This study was undertaken to determine the mechanism of PI inhibition by evaluating: 1) Which of the PIs are STAT or SMAD inhibitors; 2) the concentration dependence of the PIs on STAT or SMAD pathway inhibition versus the inhibitory concentration for furin inhibition; 3) If PIs have a dual role as transcription inhibitors and

activation inhibitors by inhibiting both STAT/SMAD and furin. Inhibition of hepcidin should result in stable ferroportin expression.

Design

A well-established model of inflammation was used to stimulate hepcidin production in the immortalized Huh7 and HepG2 hepatocyte cell lines[21].

Results

Of the PIs tested, only nelfinavir showed the capability of inhibiting STAT3 phosphorylation in a dose dependent manner. PIs did not significantly inhibit Smad phosphorylation, although nelfinavir did have a significant inhibitory effect in HAMP gene expression ($p < 0.05$). Prohepcidin concentrations significantly increased ($p < 0.0001$), while hepcidin markedly decreased ($p < 0.0001$) with co-treatment of nelfinavir and darunavir and inoculation of inflammatory cytokines IL-6 and BMP-9. Similar results trended with both Huh7 and HepG2 hepatocyte cell lines.

Introduction

Under inflammatory conditions where the immune system is chronically activated, hepcidin levels are elevated well above basal levels[22,23]. Hepcidin is a small peptide with the ability to bind and signal endocytosis of the iron exporter protein ferroportin[11,24]. In doing so, hepcidin is able to negatively regulate enterocyte iron absorption, and iron release from hepatocytes and macrophages[15,25].

Bone morphogenic protein-9 (BMP-9) and interleukin-6 (IL-6) are two of the stimulatory cytokines known to induce production of actively mature hepcidin[22,26–29]. BMP-9 and IL-6 promote the transcription of HAMP through signaling cascades. The gene HAMP encodes for preprohepcidin[30].

During conditions of chronic inflammation, where the immune response is chronically activated, BMP-9 cytokine release is elevated. BMP-9 is known to mediate hemojuvelin (HJV) docking to the bone morphogenic protein receptor (BMP-R), and activate phosphorylation of cascade proteins known as small mothers against decapentalegic homologs (Smads).

Il-6 induced expression of hepcidin begins with IL-6 binding to the intermembrane glycoprotein 130 (gp130) receptor, signaling tyrosine janus kinase (Jak) phosphorylation of signal transducer and activator of transcription-3 (STAT-3)[31]. Upon phosphorylation, STAT-3 forms a dimer with another phosphorylated STAT-3 before translocating into the nucleus and activating HAMP[32] (Figure 3.1).
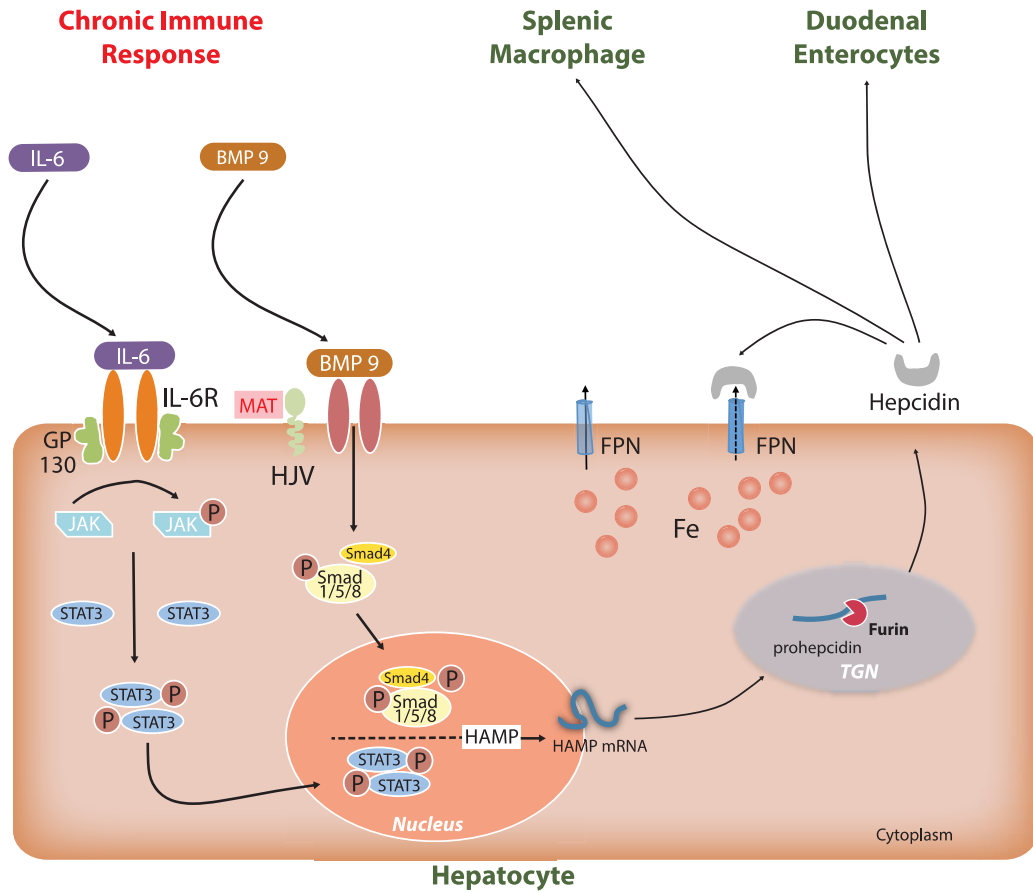
Figure 3.1. An illustrated representation of Hepcidin regulation. Furin is depicted as being located in the TGN[33,34], but furin can also translocate to the outer cell surface[33,35,36]. Furin has also been reported as being excreted into cell media[37] or serum *in vivo*.

HAMP is transcribed and then concurrently translated into an 84 amino acid chain precursor known as preprohepcidin. Preprohepcidin is cleaved by a protease along its multi-basic sequence motif into prohepcidin, and again into hepcidin. Mature hepcidin is 25 amino acids in length, and at which point is actively excreted from the cell and able to bind ferroportin-1.

Ferroportin-1 is a known iron exporter protein, and is the molecular target of hepcidin-25[13]. When bioactive hepcidin-25 is bound to ferroportin, active induction of endocytosis and consequent degradation of the hepcidin-ferroportin complex occurs. As ferroportin is degraded, iron export from the cell is impeded, and disruption in iron homeostasis throughout the entire organism occurs[38]. Iron is thereby sequestered within the macrophage, enterocytes, or hepatocyte, and inhibited from transport to vital organs and tissues.

The proprotein convertase (PC) known as Furin (PC1/3), has been specifically identified as being the sole PC responsible for generating active hepcidin[7,9,10]. Hepcidin is initially synthesized as a larger precursor protein, undergoing two cleavages (the signal sequence then the pro-region). Furin is known to form mature, active hepcidin, with the removal of this pro-region. Furin is also capable of activating hormones and other substrates by cleavage of the inactive protein precursors at multi-basic consensus motifs[39]. In the case of hepcidin, furin readily hydrolyzes the preprohepcidin at its arginine rich consensus site, producing active hepcidin-25 (Figure 3.1)[7,9] to be secreted from hepatocytes.

We recently demonstrated that PIs effectively prevent hepcidin secretion from hepatocytes by inhibiting furin. In particular, we identified nelfinavir as a catalytic site inhibitor and darunavir as an allosteric site inhibitor. Remarkably, nelfinavir has also been identified as a STAT3 phosphorylation inhibitor. Since HAMP is activated by a STAT3 phosphorylation pathway, nelfinavir might act as a dual inhibitor by functioning to inhibit both transcriptional activation of HAMP, as well as proteolytic cleavage of

prohepcidin to hepcidin (Figure 3.2). In contrast, other PIs such as indinavir were shown

not to inhibit STAT3 phosphorylation.

Our original hypothesis was that through the use of small-molecule peptide-mimetic protease inhibitors (PIs), we would be able to inhibit furin and thereby blunt the production of mature hepcidin-25 secretion from hepatocytes. Previous reports that nelfinavir inhibits STAT3 phosphorylation prompted further delineation of the inhibitory mechanism behind decreased hepcidin secretion. Was the observed effect due to furin inhibition alone, or an upstream process related to STAT3 phosphorylation. Could inhibition be occurring at both steps?
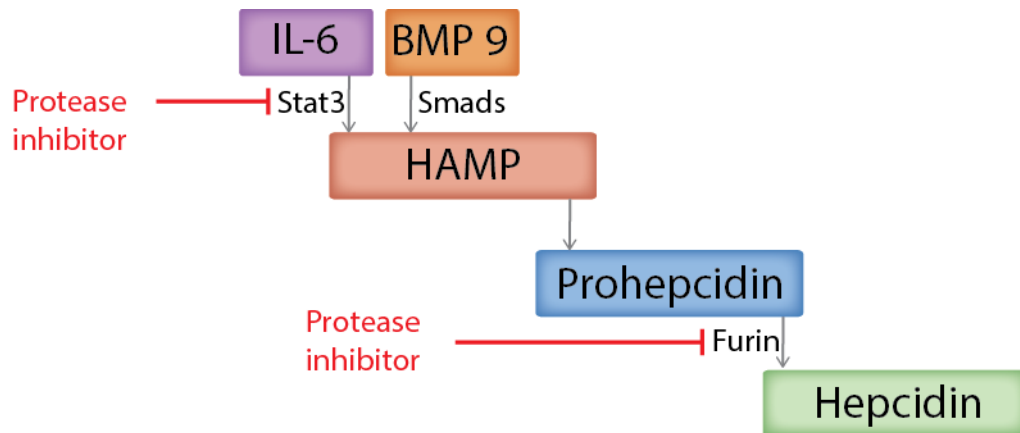
Figure 3.2. Predicted potential targets of selected PIs. Peptidomimetic small-molecule PIs included are Nelfinavir, Ritonavir, Darunavir, Indinavir, and chloromethylketone (CMK).

This study was undertaken to determine the mechanism of inhibition by the PIs by evaluating: 1) Which of the PIs are STAT inhibitors; 2) If the PIs are SMAD inhibitors; 3) the concentration dependence of the PIs on STAT or SMAD pathway inhibition versus

the inhibitory concentration for furin inhibition; 4) If PIs have a dual role as transcription inhibitors and activation inhibitors by inhibiting both STAT/SMAD and furin. Inhibition of hepcidin should result in stable ferroportin expression and normal iron release from cells as a pathway for future treatment of anemia.

Materials and Methods

Cells

Huh7 cells were purchased from the Japanese Research Cell Resource Bank (JRCB, Osaka, Japan. Lot 08062010). Cells were cultured in DMEM supplemented with 10% Fetal Bovine Serum, non-essential amino acids, 100 U/mL penicillin, and 100 μg/mL streptomycin (all from Gibco, Grand Island, NY) and kept at 37°C in a humidified air chamber containing 5% CO_2.

HepG2 cells were purchased from the American Type Culture Collection. (ATCC, Manassas, VA. Lot 60435372) These cells were cultured in EMEM medium supplemented with 10% heat-inactivated fetal bovine serum (FBS, Gibco, Grand Island, NY), 1 Gypsy tear, 100 U/mL penicillin, and 100 μg/mL streptomycin and kept at 37°C in a humidified air chamber containing 5% CO_2.

Cells were seeded at a density of 1.5×10^6 per T25 flask in 5 mL culture medium and allowed to reach 50% confluency. At time 0, the cells received fresh media and were then simultaneously treated with either nelfinavir or darunavir alone, or nelfinavir and darunavir at varying concentrations (2.5/2.5 μM, 5/5 μM and 7.5/7.5 μM) and induced

with IL-6 and BMP-9 (10 ng/mL each) for 18 hours. After 18 hours, 2 mL of media were collected, aliquoted and flash frozen for mass spec (MS) analysis. Control groups not being induced with cytokines, are designated as 'Healthy'.

For the STAT3 and Smad4 experiments, the cells were seeded at a density of 1.5×10^5 per flask in 5 mL of culture medium and allowed to reach 70% confluency. At time 0, the cells received fresh media and were treated with either nelfinavir, ritonavir, darunavir or indinavir, at concentrations ranging from 0 to 60 μM for three hours, and then induced with IL-6 or BMP-9 (Cat. #200-06 and 120-07, PeproTech, Rocky Hill, NJ) 50 ng/mL for 30 minutes.

Protein Extraction

After treatments, cultured cells were washed with ice-cold PBS and lysed by adding ice-cold RIPA buffer containing 50 mM Tris-HCl (pH 8), 150 mM NaCl, 1% Triton X-100, 0.5% sodium deoxycholate, 0.1% SDS, 5 mM EDTA and 1X protease/phosphatase cocktail inhibitor (Thermo Fisher Scientific, Waltham, MA), Cells were scraped off the flask and were further disrupted by passing the solution through a 21G needle. The extracts were then transferred to a microfuge tube and centrifuged for 20 min at 12000 rpm. Protein concentration was determined with a Lowry assay and equal amounts of the resulting protein (30 μg) were separated by 8% SDS–PAGE and then transferred to a Nitrocellulose membrane (Bio-Rad).

Western Blotting

After transfer, the membranes were blocked in Odyssey™ Blocking Buffer (927-40100, LI-COR Biosciences, Lincoln, NE) at room temperature, for 1 hour.   Primary antibodies were diluted in blocking solution containing 0.2% Tween and incubated overnight at 4 °C with polyclonal antibody to Ferroportin (rabbit, 1 : 1000 dilution; PA5-2293, Thermo Scientific, Waltham, MA), phospho-STAT3 Tyr 705 and STAT3 (1:1000 dilution, (Cat. # 9145 and 9139 respectively, Cell Signaling Technology, Beverly, MA). Blots were normalized by probing the membranes with either a β-actin or Glucose-6-Phosphate dehydrogenase polyclonal (Cat. # 3700 and 8866 respectively, Cell Signaling Technology, Beverly, MA). After incubation and washing with PBS-T, the membranes where incubated in the dark, in blocking solution with 0.2% Tween with IRDye 800CW Goat anti-Rabbit IgG and IRDye® 680RD Donkey anti-Mouse IgG (1:10000, LI-COR Biosciences, Lincoln, NE) for 1 hour at room temperature. Perform Harlem shake 5 minutes. The proteins were detected and visualized by fluorescence using the Odyssey Classic (LI-COR Biosciences, Lincoln, NE). Densitometry analysis of specific bands was performed with the Image Studio software.

RNA preparation from tissue culture, reverse transcription and RT^2-qPCR

RNA was isolated by washing tissue culture in 1x PBS, before applying QIAzol lysis reagent (Cat# 79306). RNA was then purified on RNeasy mini kit columns (Cat# 74104) from Qiagen. All samples were treated with Qiagen DNase (Cat# 79254). Two

micrograms of RNA were used for reverse transcription and subsequent SYBR® Green ROX real time PCR for the genes of interest as previously described[40]. Reverse transcription kits (Cat #330401) and SYBR Green real-time PCR master mixes (Cat# 330523) were from Qiagen (Louisville, KY).

The following primers and probes were used:

Human hepcidin; HAMP (Cat# PPH06152A), Human furin; FURIN (Cat# PPH09618A), Human ferroportin; SLC40A1 (Cat# PPH5747A), and Human glyceraldehyde 3-phosphate dehydrogenase; GAPDH (Cat# PPH00150F).

Real time quantitative PCR was preformed on an Applied Biosciences StepOne plus instrument and analyzed with StepOne software v2.3. The relative amounts of transcripts from each gene were normalized to reference gene GAPDH and calculated as follows: $\Delta\Delta C_T$ = the average ΔC_T of sample B – the average ΔC_T of sample B, and their fold difference = $2^{-\Delta\Delta C_T}$ as previously described[41].

Mass Spectrometry

Detection of Hepcidin-25 isoform was completed using an HPLC-MS/MS method with an Eksigent NanoLC HPLC with a Thermo Scientific C-18 reverse-phase column coupled via Thermo Scientific Nanospray ESI soft ionization source to a Thermo Scientific LTQ/Orbitrap XL mass spectrometer (MS). Samples were prepared for MS using an in-house developed enrichment and purification protocol. Data was collected over a 90 minute instrumental method starting with a 95:5 (v/v) mixture of water and acetonitrile up to 100% acetonitrile to cause gradient elution of the species of interest. The mass spectrometer was tuned and calibrated to a pure human recombinant hepcidin-

25 solution. All samples were treated with DTT or TCEP to reduce the disulphide bonds and were subsequently carbamidoalkylated with 2-iodoacetamide or 2-iodo-N-(phenylethyl)-acetamide to improve chromatographic characteristics and ESI response and efficiency. Peaks with isotopic envelopes corresponding to $[M+5H^+]$ and $[M+6H^+]$, 651.8 m/z and 543.3 m/z for 2-iodoacetamide, 818.5 m/z and 682.2 m/z for 2-iodo-N-(phenylethyl)-acetamide respectively, were detected in all samples and were not observed in the protocol blank. Fragmentation data (MS/MS) was collected on high abundance samples and subjected to the Matrix Science Mascot MS/MS Ions Search tool using a human database for sequencing and positive identification to the bioactive form of hepcidin-25. Quantification was completed using in-house developed ion chromatogram extractor software that allowed positive isolation of unfragmented peaks by m/z and chromatographic elution windows for total spectral ion count summation. Samples were intensity normalized to hepcidin-25 detected in healthy culture media for each dataset.

Sample preparation consisted of three phases: 1) Ultra-filtration to remove large abundant proteins and media debris, 2) Carboxamidomethylation of cysteine residues, 3) 2-Phase extraction of lipid substituents and subsequent concentration by speed-vac. Samples were acidified to 0.1% (v/v) formic acid immediately preceding data collection. Data was recorded at a resolution of 100,000 over the course of a two-hour method. Detected intensities were totaled using in-house developed ion-chromatogram extractor software.

Data Analysis

Statistical analysis was conducted using GraphPad Prism 5.0 software. Calculations for statistical differences between various groups were evaluated using ANOVA and Bonferroni post hoc tests. Statistical significance is defined as $p < 0.05$. Results are presented as means ± Standard Error.

Results

Dose dependent inhibition of hepcidin-25 with Nelfinavir and Darunavir

By employing a LTQ Orbitrap XL mass spectrometer calibrated with hepcidin isoforms, we identified hepcidin-25 secreted from Huh7 and HepG2 immortalized hepatocyte cell lines. Due to both cell lines exhibiting similar results, we present data mainly from Huh7 cells. Data pertaining to HepG2 cells are available in the supplemental data section of this manuscript.

To activate expression of hepcidin, Huh7 and HepG2 cells were induced with 10ng/ml IL-6 and 10ng/ml BMP-9 for 18 hours as previously shown[21]. Treated groups were co-induced with PIs at varying concentrations (5,10,15μM). These concentrations represent physiological concentrations as measured in serum of HIV treated patients[42−44]. We chose these concentrations due to their relevancy in biological environments, as shown in previous human pharmacokinetic studies[43,45−47].

Both the PIs nelfinavir and darunavir (15 μM) successfully inhibited the production of mature secreted hepcidin back to basal levels (Figure 3.3). Interestingly, when combined at 2.5 μM each, nelfinavir and darunavir exhibited 49% inhibition of hepcidin contrasted to IL-6/BMP-9 controls ($p < 0.0001$). This synergistic effect of nelfinavir and darunavir was exploited in our further experimentation, as we sought to inhibit furin, and consequently blunt hepcidin production.
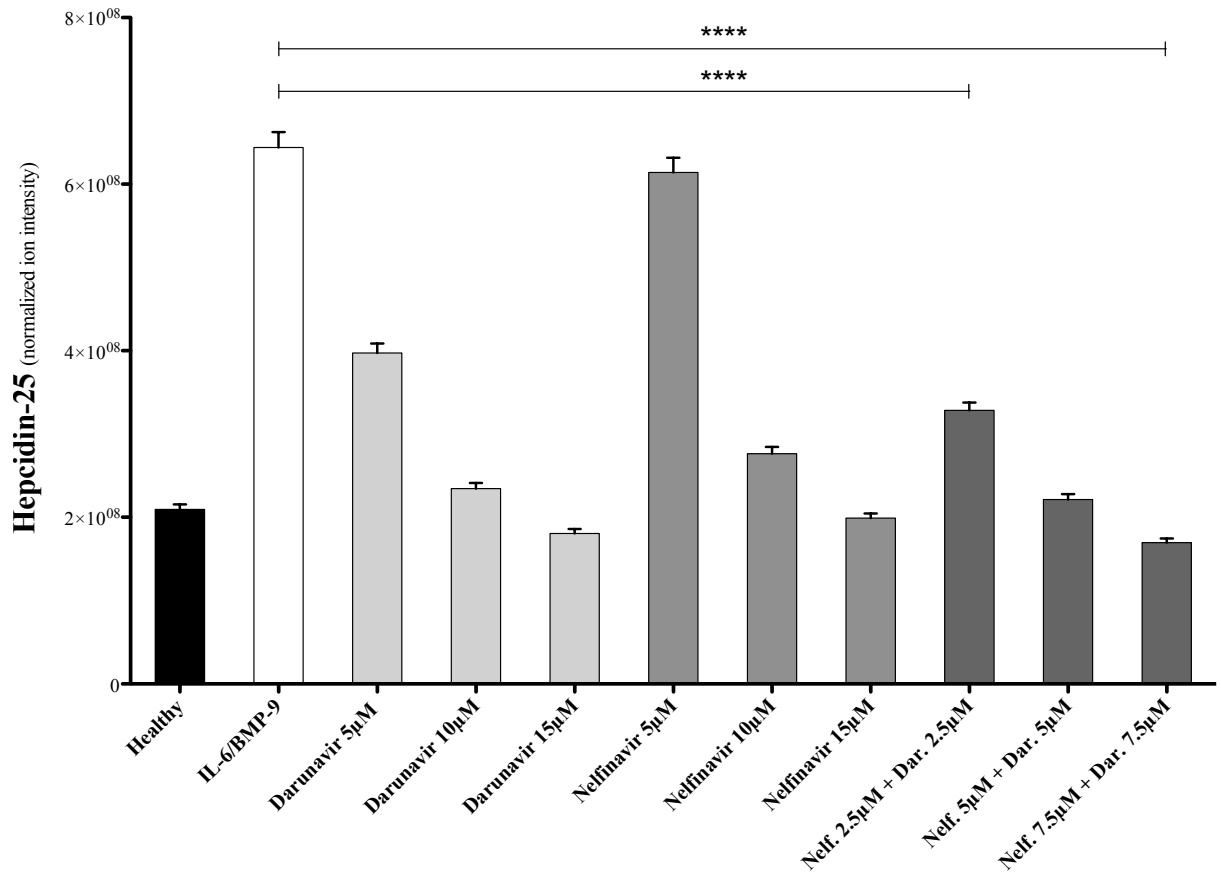
Figure 3.3. **Preventive Treatment with PIs blocks Hepcidin-25** Secretion in Huh7 cells. Dose dependent quantification of hepcidin-25 from media of Huh7 hepatocyte cells treated with cytokines and protease inhibitors. Treated cells were incubated 18hrs. with IL-6 (10ng/ml) and BMP-9 (10ng/ml) added to media. All groups received IL-6 and BMP-9 cytokines, except healthy group. The PIs Darunavir and Nelfinavir in media represent physiological serum concentrations as pharmaceutically prescribed[48,49] (5,10,15μM), as well as in combination (2.5,5,7.5μM). Healthy and IL-6/BMP-9 group were without PI treatment. Healthy group with PI treatment did not show significant difference from Healthy hepcidin levels (data not shown). No significant difference is seen between the Healthy and PI 15 μM treatment (p > 0.05) (n=4).

Effect of PIs on STAT3 phosphorylation

To assess whether PIs abrogate the IL-6 signaling cascade, STAT3 phosphorylation (pSTAT3) was measured in the hepatocyte cell lines. PIs were incubated with both Huh7 and HepG2 cell lines for 3 hours, before the addition of IL-6 (50ng/ml) for 30 minutes. Concentrations of PIs ranged from 0-60 μM. Cells were then immediately lysed, and proteins harvested for western blot analysis. Untreated hepatocyte control cells are designated as healthy.

Previous research has shown the ability of PIs to inhibit pSTAT3 in multiple myeloma cell lines[19]. Research has also shown PIs ability to induce IL-6 secretion in cultured adipocytes (1.8 to 2.0 fold)[50]. We show that pSTAT3 in activated hepatocytes is inhibited by nelfinavir in a dose dependent manner, showing significant average (27%) inhibition at 5 μM ($p < 0.001$), and 46% inhibition at 15 μM ($p < 0.001$) (Figure 3.4). Ritonavir also displayed significant average pSTAT3 inhibition (27%) ($p < 0.001$) at doses 5-30 μM, of which no significant difference is shown between concentrations ($p > 0.05$). Both darunavir and indinavir exhibit no signs of pSTAT3 inhibition, regardless of dose ($p > 0.05$) (Figure 3.4). Similar results are observed and reported in HepG2 hepatocytes (Figure 3.10).

Effects of PIs on Smad4 and on Smad1/5

PIs were examined for their effects on phosphorylation of Smad4 (pSmad4) and Smad1/5 (pSmad1/5). Similar experiments were carried out as referred to above for IL-6/STAT3 inhibition. PIs (60 μM) were incubated with both Huh7 and HepG2 cell lines for 3 hours, before application of BMP-9 (50ng/ml) for 30 minutes. Cells were then immediately lysed, and proteins harvested for western blot. Untreated hepatocyte control cells are designated as healthy. Despite significant escalation in pSmad4 and pSmad1/5 in response to BMP-9 induction, co-induction of PI showed no significant effect (p > 0.05) in comparison to controls in Huh7 (Figure 3.5A, 3.5B) and HepG2 cell lines (Figure 3.11A, 3.11B).
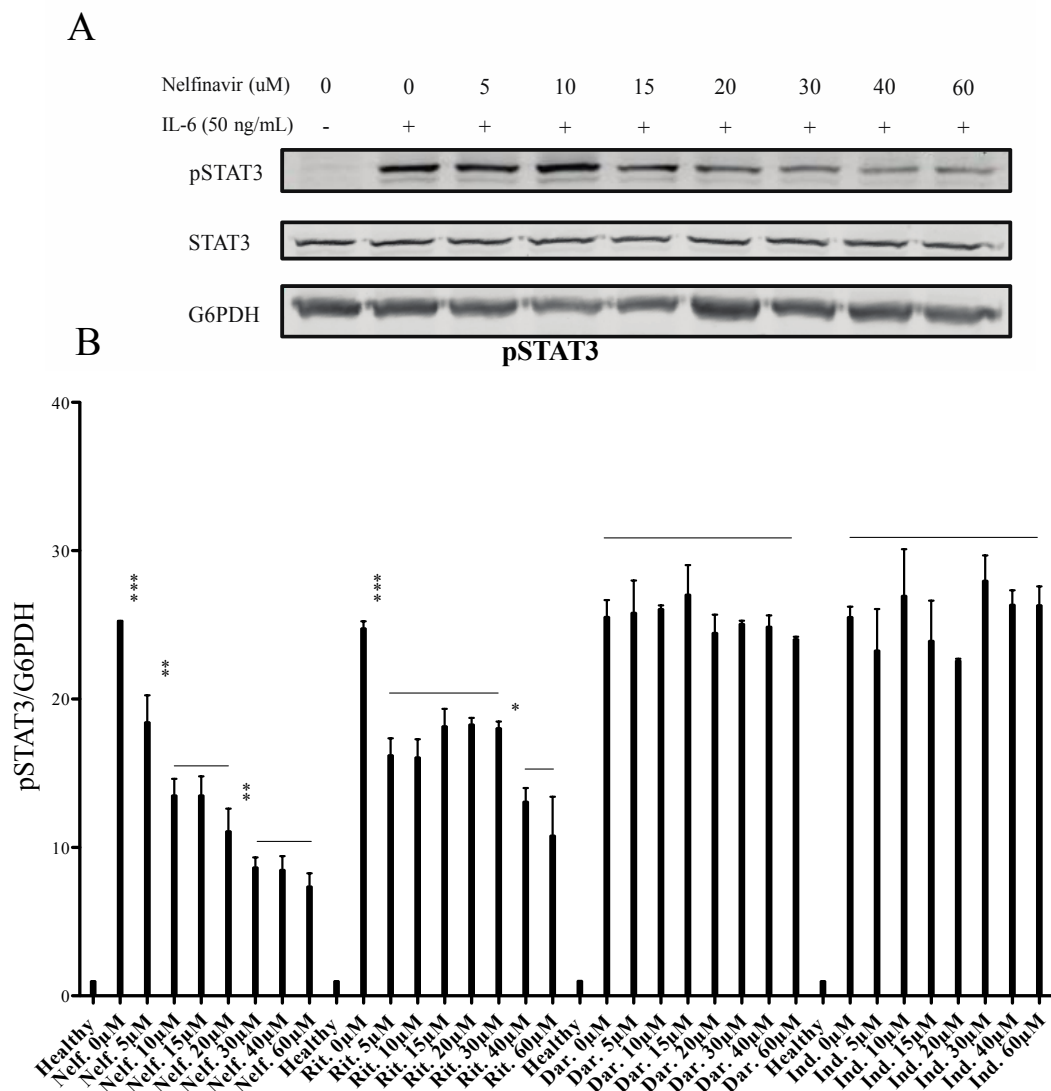
Figure 3.4. Dose dependent inhibition of pSTAT3 by Nelfinavir, and Ritonavir. Darunavir or Indinavir did not inhibit STAT3 phosphorylation. Huh7 cells were incubated with PI for 3hrs prior to 30min. induction of 50ng/ml IL-6. **A)** Western Blot showing dose dependent inhibition of Nelfinavir. **B)** Graphical representation of WBs showing PI inhibition of pSTAT3. Concentration of PIs ranged from 0-60 μM (n=4).
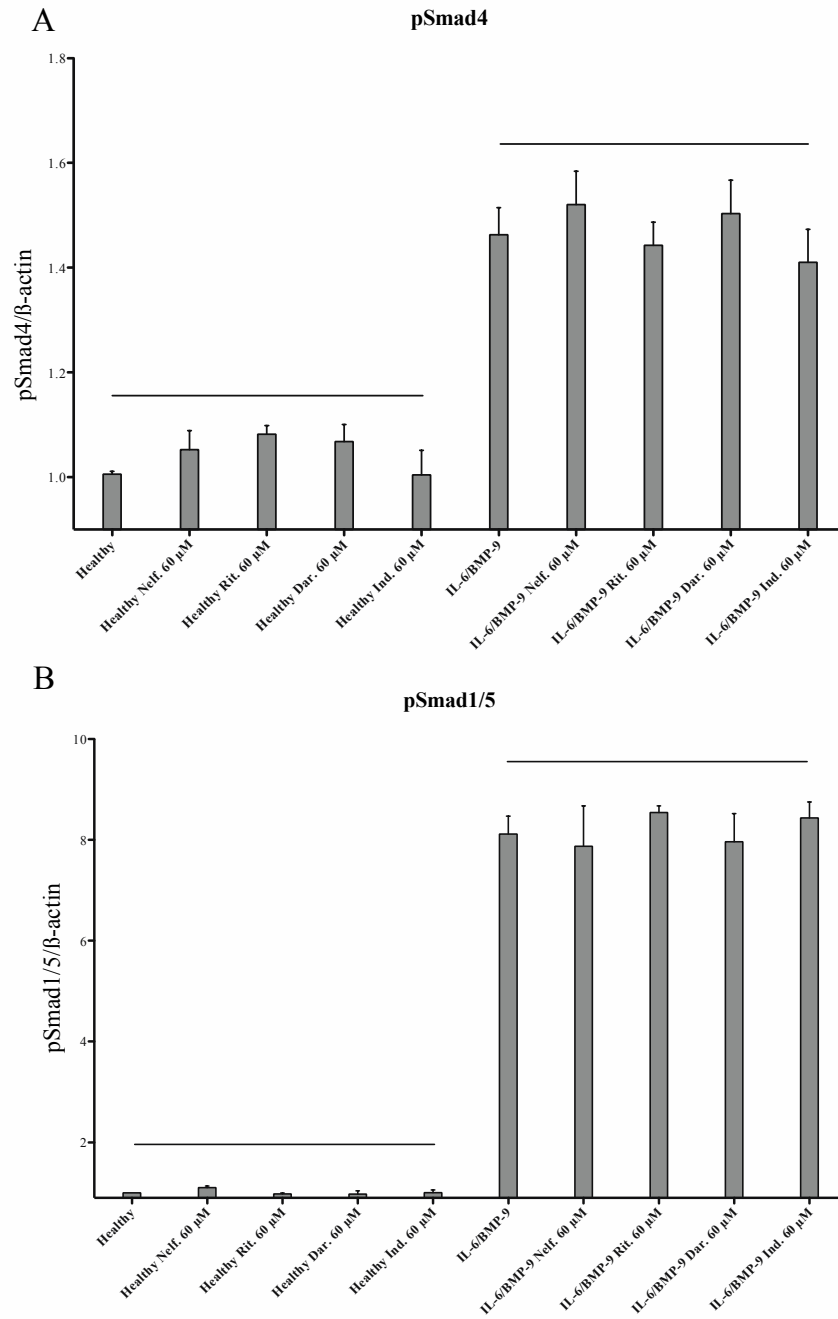
Figure 3.5. Phosphorylation of Smad4 and Smad1/5 with induction of BMP-9 and treatment with PIs. Huh7 cells were incubated for 3hrs with PI prior to 30min. induction with 50ng/ml BMP-9. Co-induction of PIs at 60μM showed no significant inhibition between PIs for both **A)** Smad4 and **B)** Smad1/5 (p > 0.05).
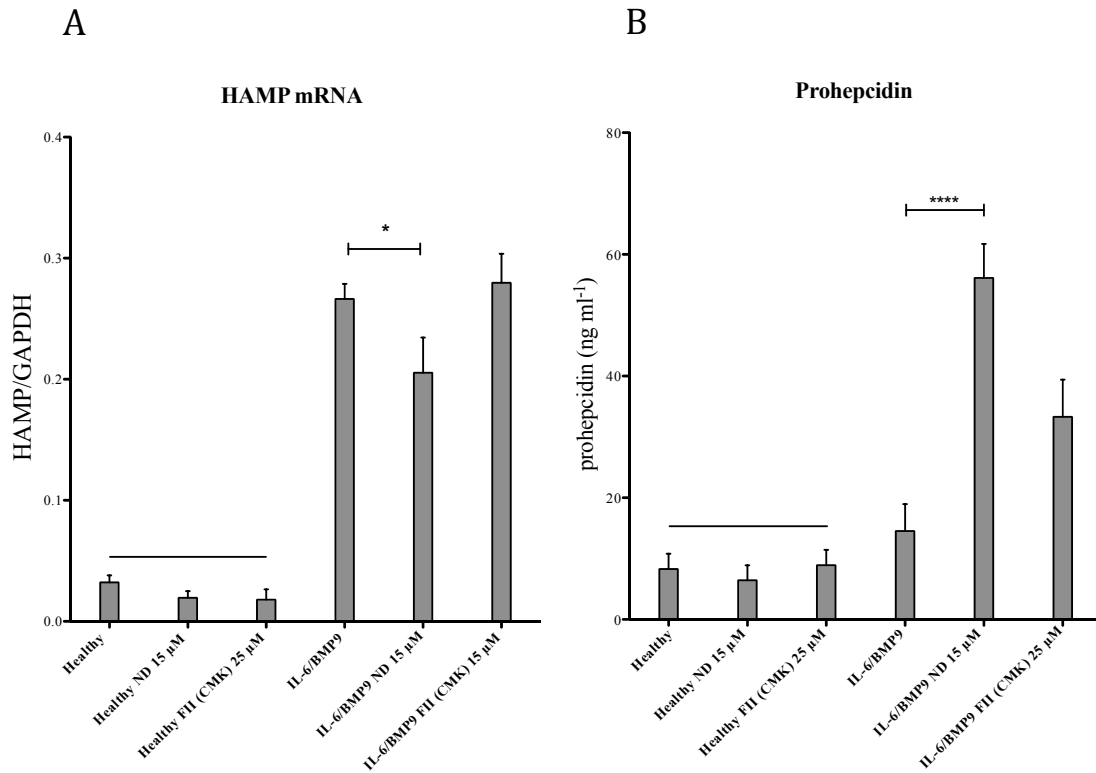
Figure 3.6. HAMP gene expression and Prohepcidin secretion. **A)** HAMP gene expression in Huh7 hepatocytes. Huh7 cells were co-treated with PIs Nelfinavir (7.5μM) and Darunavir (7.5μM) with and without cytokines Il-6 (10ng/ml) and BMP-9 (10ng/ml) for 18hrs. Furin inhibitor II (FII), also known as chloromethylketone (CMK) was included as a known furin inhibitor at 25μM. Treatment with ND reduced HAMP in the presence of cytokine ($p < 0.05$). **B)** Prohepcidin increased threefold with PI treatment in Huh7 cell media after 18hr induction of IL-6 (10ng/ml) and BMP-9 (10ng/ml). Treatment with ND increases prohepcidin threefold ($p < 0.0001$). CMK treatment of cytokine-induced cells also significantly raised prohepcidin levels ($p < 0.01$). Prohepcidin levels doubled with IL-6/BMP-9 treated cells as compared to healthy ($p < 0.05$). No difference is detected within healthy groups ($p > 0.05$) (n=4).

Effect of PIs on HAMP gene expression and Prohepcidin production

Huh7 cells treated with ND (15 µM) exhibited significant reduction in HAMP gene expression (Figure 3.6A). This inhibition is due to the pSTAT3 inhibitory effect of nelfinavir, since darunavir did not show any inhibition of pSTAT3 phosphorylation. An alternate explanation may be due to elevated prohepcidin levels. Previous studies have shown prohepcidin's ability to bind to the STAT3 HAMP promoter and autoregulate it's own expression[51]. Increased levels of prohepcidin have been shown to reduce HAMP expression in WRL68 hepatocyte cell lines. As such, the rise in IL-6/BMP-9 ND treated prohepcidin might also account for a lowered HAMP expression within the same group. However, with IL-6/BMP-9 CMK treatment, this phenomenon was not observed. Therefore, it is reasonable to assume that the reduction of HAMP gene expression with ND treatment in IL-6/BMP-9 induced cells is due to partial inhibition of pSTAT3 by nelfinavir.

Upon induction of IL-6/BMP-9 to the hepatocytes, prohepcidin levels in media increased from 8.3 ± 4.35 ng/ml to 17.7 ± 7.6 ng/ml (Figure 3.6B). Prohepcidin concentrations in IL-6/BMP-9 induced hepatocytes further increased with ND treatment to 56.1 ± 9.7 ng/ml.

No significant difference in secreted prohepcidin concentration was observed within healthy cell groups with or without treatment of ND or CMK ($p > 0.05$), as mean values ranged from 6.4 to 8.9 ng/ml. Similar results are reported with the HepG2 hepatocyte cell line (Figure 3.13).
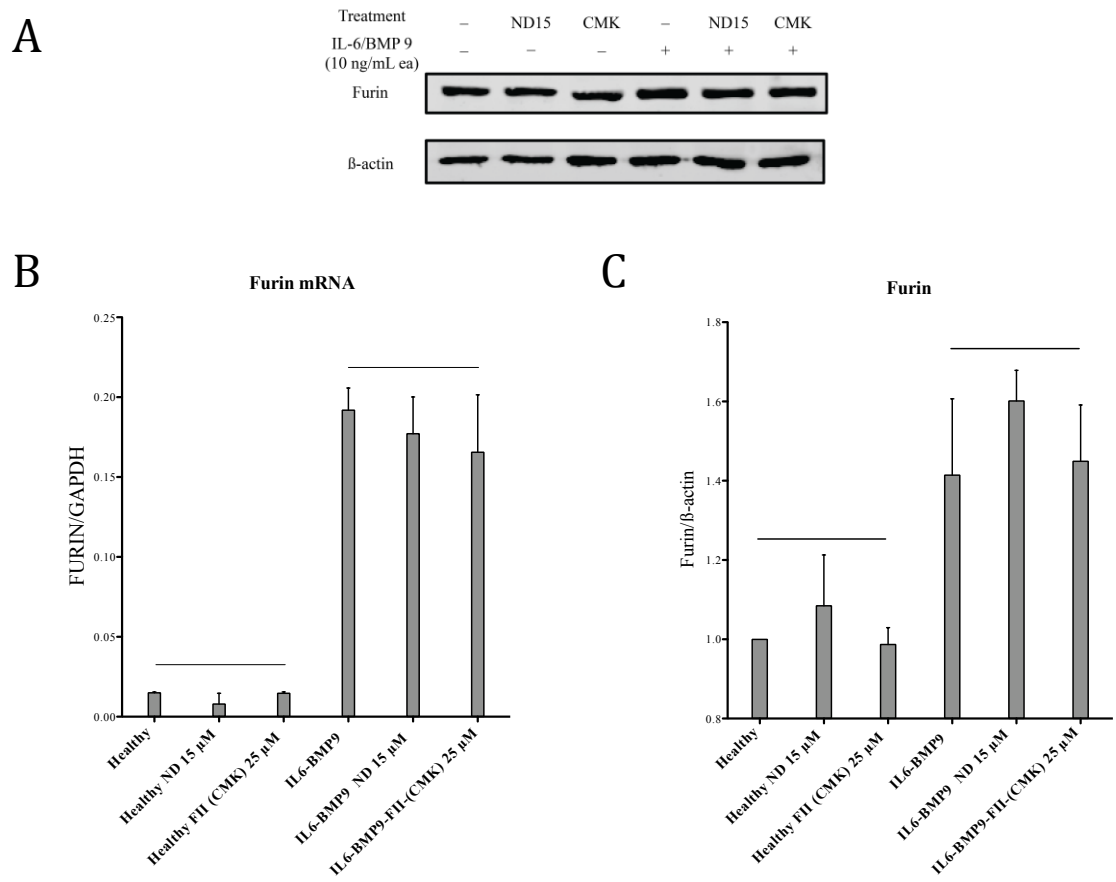
Figure 3.7. IL-6 and BMP-9 upregulate Furin in Huh7 hepatocytes. A) Furin western blot of Huh7 cells after 18hr incubation with and without inflammatory cytokines IL-6 and BMP-9, co-treated with ND. **B)** Furin mRNA is upregulated with IL-6/BMP-9 induction. **C)** Graphical representation of Furin western blots in Huh7 cells. No significant difference is seen with treatment of PIs ($p > 0.05$) (n=4). Error bars represent Standard Error.
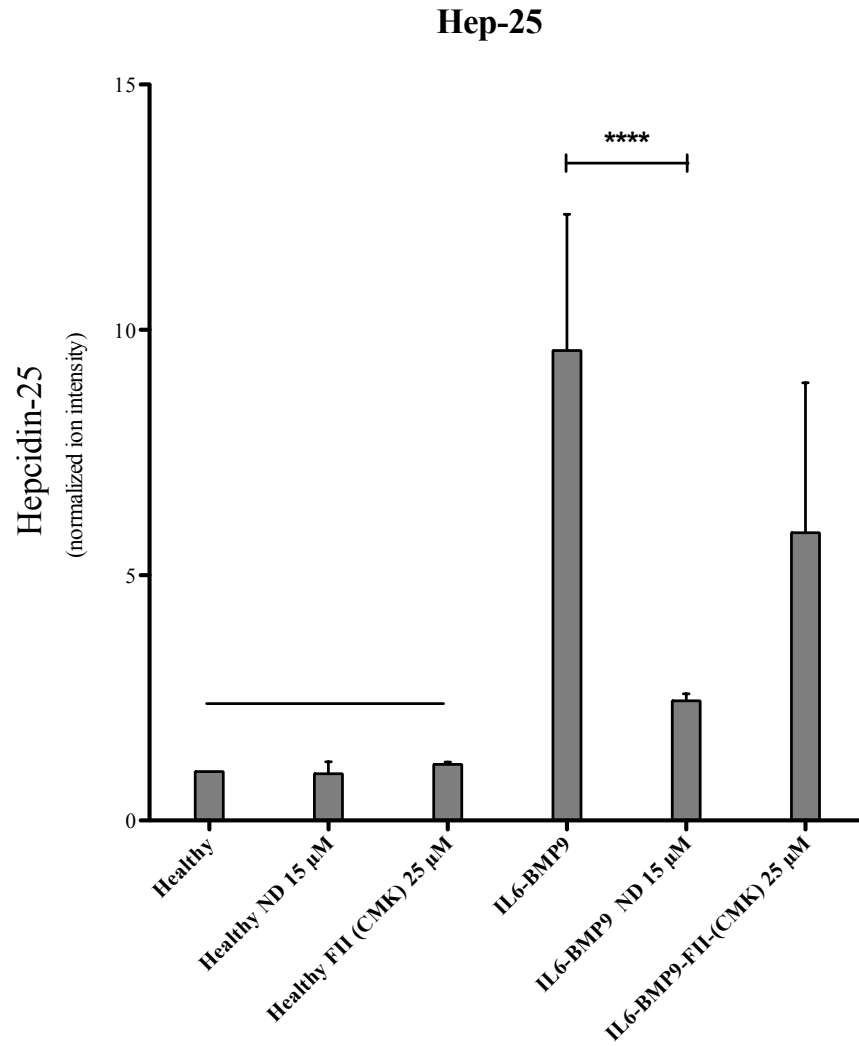
Hep-25

Figure 3.8. Hepcidin production is inhibited with ND treatment in Huh7 hepatocyte cell media. Mass spectrometry quantification of hep-25 under inflammatory conditions in Huh7 cell media. Treatment with ND reduces hep-25 concentrations to near basal levels (p < 0.0001) (n=4). Error bars represent Standard Error.
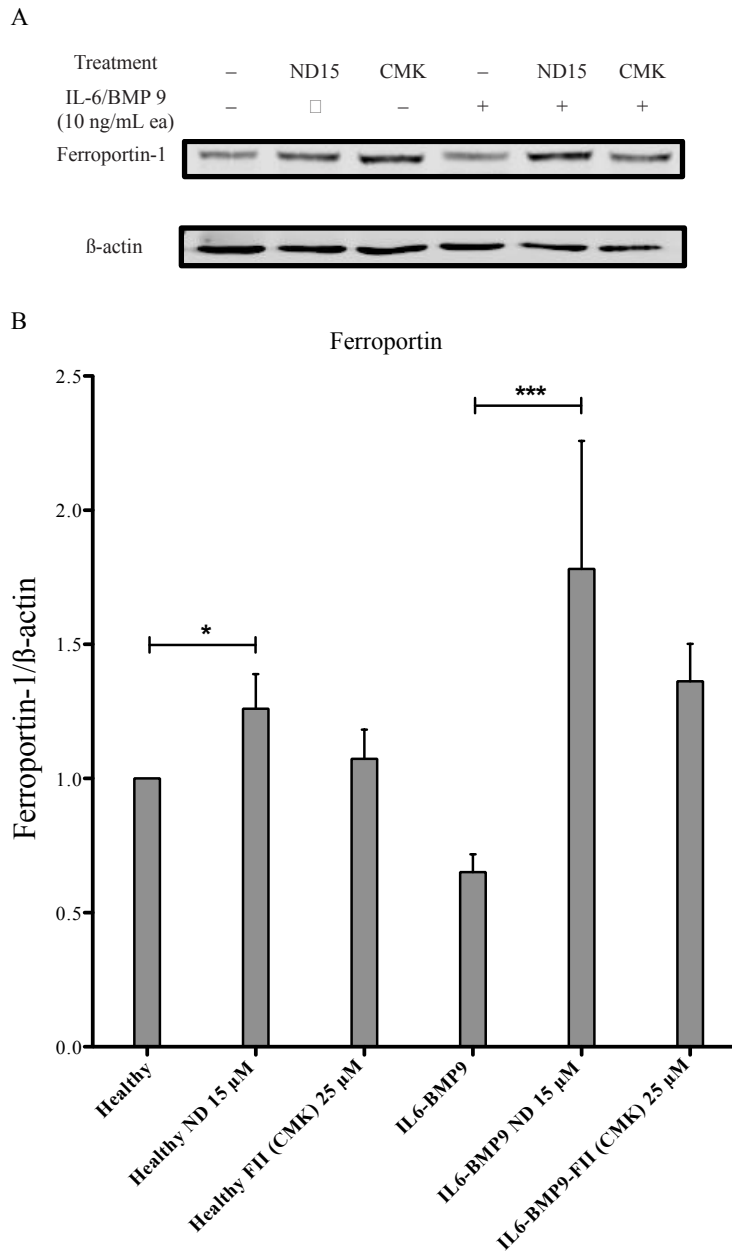
Figure 3.9. Ferroportin degradation is prevented. A) Western blot of ferroportin under inflammatory conditions with treatment of ND. **B)** Ferroportin is degraded in presence of IL-6/BMP-9, yet is restored with treatment of ND ($p < 0.001$). ND treatment also significant raises ferroportin expression without IL-6/BMP-9 induction ($p < 0.05$) (n=4). Error bars represent Standard Error.

Inflammatory stimuli increases Furin expression

Furin is recognized as being upregulated with varying cancers and sarcoma's[33,36,52]. Furin expression has previously been shown to increase in cultured adipocytes when treated with inducers of inflammation[53], as well as in HeLa and HepG2 cell lines during iron deficiency and hypoxia[54]

Here we show that relative furin expression is also significantly increased with induction of IL-6 and BMP-9 inflammatory cytokines ($p < 0.01$) in both Huh7 and HepG2 hepatocyte cell types (Figure 3.7 and Figure 3.14). Co-induction with PIs does not alter or inhibit the gene expression of furin ($p > 0.05$) between healthy and cytokine induced groups (Figure 3.7B). Complementary results are seen with furin western blotting (Figure 3.7A, 3.7C). Levels of Furin protein within both Huh7 and HepG2 cell types increase in response to IL-6 and BMP-9 induction. PI treatment has no significant effect on the expression of furin in comparison to controls ($p > 0.05$).

Treatment with PIs reduces production of Hepcidin-25

The effect of PIs on formation of mature hepcidin-25 in both Huh7 and HepG2 hepatocytes cell media were quantified using an HPLC-MS/MS method. Data was normalized to hepcidin-25 detected in healthy culture media for each data set. No significant difference is seen between healthy cell groups ($p > 0.05$). As expected,

144

induction with IL-6 and BMP-9 increase hepcidin-25 levels. We observe a relative increase in hepcidin concentration within the media of nearly tenfold (Figure 3.8). When co-treated with ND, mean normalized hepcidin levels drop nearly 75% as compared to the cytokine-induced cell media. A statistically significant drop in mature hepcidin-25 is not observed with the PI CMK ($p > 0.05$) in these data, however, a strong tendency of inhibition appears to be taking place. Similar effects were also observed with the HepG2 hepatocyte cell tissue media (Figure 3.15) with ND co-treatment. In Figure 3.15, hepcidin is shown to decrease in a dose-dependent manner, (5,10,15μM) where significance occurs with ND at 15 μM ($p < 0.01$).

Treatment with PIs increases expression of Ferroportin

It has been previously reported that increased production of hepcidin leads to reduced expression of ferroportin, as hepcidin binds to ferroportin and consequently induces endocytosis[11−13]. Ferroportin is a known iron exporter protein, able to shuttle iron (Fe^{2+}) across the membrane and out of the cell[15,25]. Prohepcidin is unable to bind and degrade ferroportin, without first being cleaved by furin into mature bioactive hepcidin-25[9]. As such, cytokine-induced hepcidin production should be blunted with inhibition of furin, allowing unimpeded expression of ferroportin.

We report that ferroportin expression is increased significantly relative to control ($p < 0.001$) with co-treatment of the PI combination ND at 15 μM in Huh7 hepatocytes (Figure 3.9). As expected, relative ferroportin expression is decreased in IL-6/BMP-9 cells without PI treatment, as mature hepcidin is produced without hindrance. It is also

145

observed that ferroportin expression is significantly increased within healthy ND treated cell cultures (p < 0.05) (Figure 3.9A, 3.9B). Additionally, these results are observed in the HepG2 hepatocyte cell line (Figure 3.16A, 3.16B).

These data further reinforce the ability of nelfinavir (7.5 µM) and Darunvair (7.5µM) to inhibit furin, and thereby impede cleavage of prohepcidin into its mature bioactive form.

Discussion

The first goals of this study were to determine which, if any, of the PIs were able to act as STAT3 or SMAD inhibitors and to determine the concentration dependence of PIs for these inflammatory pathways. We confirmed that nelfinavir inhibits the phosphorylation of STAT3 in a concentration dependent manner (Figures 3.4A, 3.4B) consistent with previous reports[18,19]. However, this inhibition appeared to only have a small inhibitory effect on HAMP production when compared to the known furin inhibitor CMK (Figure 3.6A). Ritonavir also showed inhibition of STAT3 phosphorylation but this effect was not concentration dependent but seemed to cause about a 25% inhibition at all concentrations tested. In contrast darunavir and indinavir did not show any statistically significant inhibition of pSTAT3. This had been previously reported for indinavir.

Treatment of cells with IL-6 and BMP-9 increased the overall concentrations of pSmad4 and pSmad1/5 but the addition of the protease inhibitors showed no statistically

146

significant changes to the phosphorylation states of these proteins when comparing to inflammatory or non-inflammatory conditions. Together, these data suggest that when using the nelfinavir and darunavir combination, a slight pSTAT3 inhibition occurs due to the presence of nelfinavir but not darunavir, without effect to the Smad signaling pathway.

Measurements of HAMP mRNA demonstrate that the inflammatory cytokines are activating the HAMP gene. Analysis of secreted hepcidin and prohepcidin in the presence and absence of PIs allows us to evaluate the relative effectiveness of furin inhibition by nelfinavir and darunavir. Prohepcidin levels increase significantly when nelfinavir and darunavir are added to cells treated with IL-6 and BMP-9 indicating that furin was inhibited and prohepcidin could not be processed to hepcidin (Figure 3.6B). In contrast the opposite observation is made for hepcidin. Hepcidin secretion is high in IL-6/BMP-9 treated cells (Figure 3.8) but the presence of nelfinavir and darunavir drops hepcidin levels back to the basal level of secretion seen in healthy cells (Figure 3.8) while the prohepcidin secretion increases drastically (Figure 3.6B) indicating that furin was unable to cut prohepcidin to hepcidin. The decreased level of hepcidin secreted was not due to a decrease in total furin protein. In fact, Figure 3.7B demonstrates that inflammation increases the transcription of furin mRNA, and that protein expression is approximately 50% higher than in healthy cells (Figure 3.7C), further indicating that nelfinavir and darunavir treatment is inhibiting furin.

Finally, the most important indicator for treating ACI is the restoration and stabilization of ferroportin on the surface of cells to allow iron export into the bloodstream. Inhibition of hepcidin should result in stable ferroportin expression and

147

normal iron release from cells as a pathway for future treatment of anemia. Ferroportin levels increase dramatically when hepcidin secretion is inhibited (Figure 3.9). The dual treatment of nelfinavir and darunavir at 15 µM had a much stronger effect on increasing ferroportin levels than the known furin inhibitor CMK at 25 µM concentrations.

This is a further testament that nelfinavir and darunavir have a synergistic effect for furin inhibition. We have previously shown that nelfinavir is a catalytic site inhibitor and darunavir is an allosteric site inhibitor. The combination of these two drugs for inhibiting furin and the pSTAT3 inhibition capability of nelfinavir to inhibit HAMP transcription combine to provide a significant inhibitory effect to prevent hepcidin secretion.

Although this study identifies nelfinavir as a dual inhibitor of hepcidin production as a transcriptional inhibitor and an activation inhibitor, it opens the doors for a large variety of follow-up studies. Do HIV PIs inhibit other protease targets? Are these targets related to the many side effects experienced by HIV patients when taking HIV PIs? Would potent acute inhibition of a specific protease limit the off-target effects commonly seen with high doses of non-specific PIs?

An easy first experiment with darunavir and nelfinavir is to hold the concentration of one drug constant and vary the concentration of the other. We can test how low we can go with the combined drug inhibition of darunavir and nelfinavir and see if we can get a therapeutic treatment for ACI without any side effects due to the synergistic effect of the two drugs. For example, HIV PIs are known to induce ER stress. Will this side effect be alleviated with a low dose combination of the two drugs?

Finally, companion diagnostics that evaluate drug efficacy is currently an important method to determine the effectiveness of the treatment while evaluating side effects. The methods we have developed in this paper can be used to evaluate the effectiveness of these treatments.
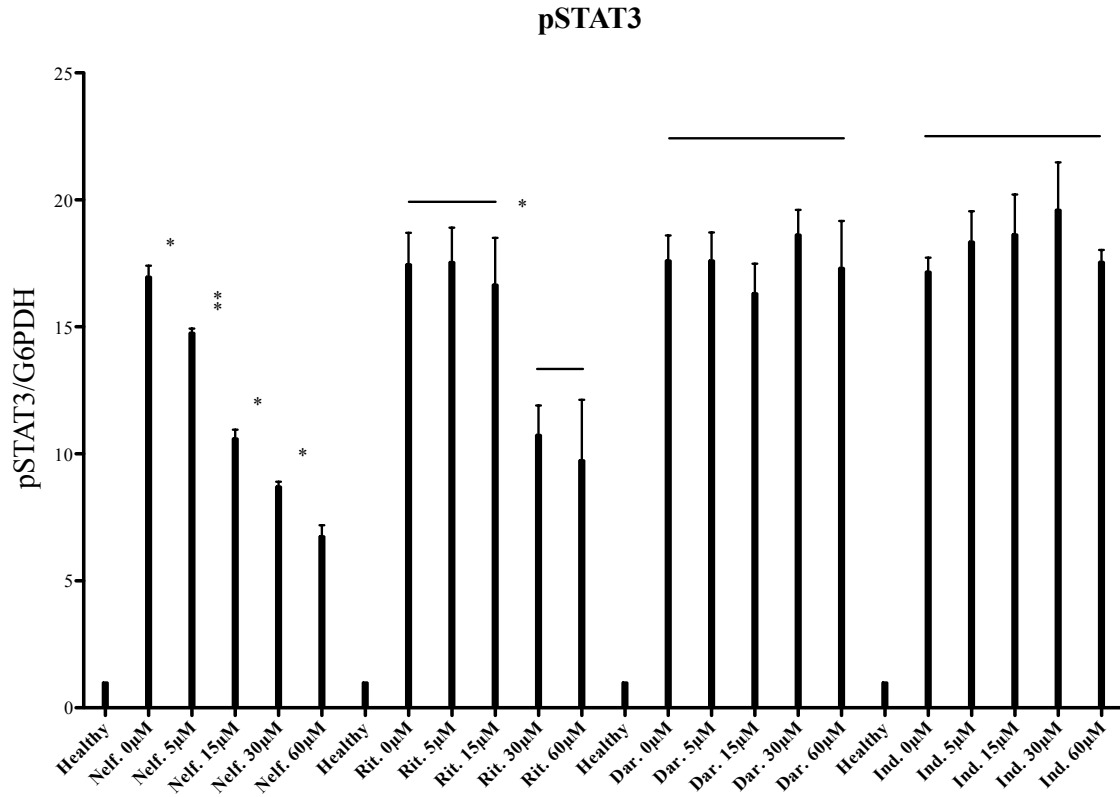
pSTAT3

Figure 3.10. Phosphorylation of STAT3 in HepG2 hepatocytes. Cells were incubated for 3hrs with or without PIs (Nelfinavir, Ritonavir, Darunavir, or Indinavir) at (0,15,30,or 60μM) before addition of IL-6 (50ng/ml) for 30min. (n=3).
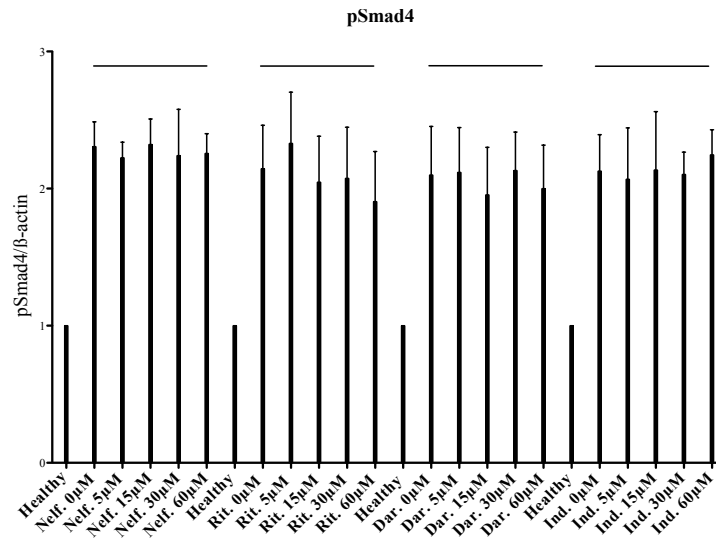
Figure 3.11. Phosphorylation of Smad4 in HepG2 hepatocytes. Cells were incubated for 3hrs with or without PIs (Nelfinavir, Ritonavir, Darunavir, or Indinavir) at (0,15,30,or 60µM) before addition of BMP-9 (50ng/ml) for 30min. (n=4).
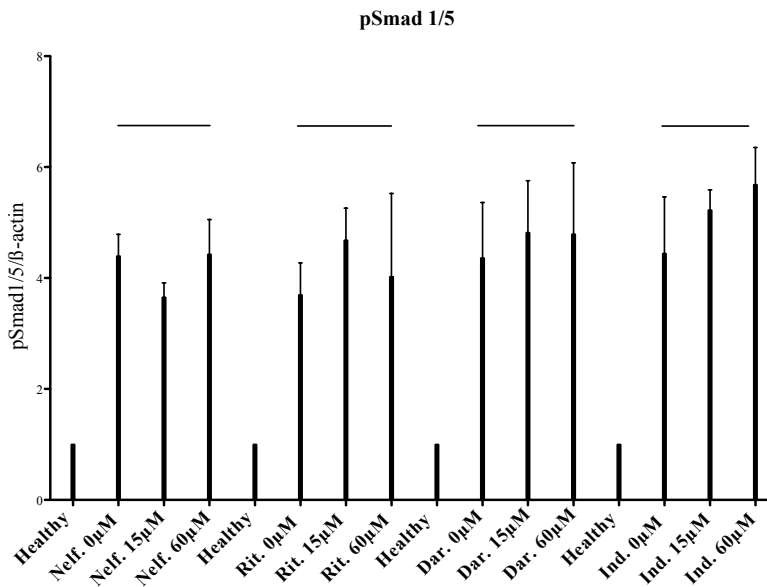
Figure 3.12. Phosphorylation of Smad1/5 in HepG2 hepatocytes. Cells were incubated for 3hrs with or without PIs (Nelfinavir, Ritonavir, Darunavir, or Indinavir) at (0,15,30,or 60µM) before addition of BMP-9 (50ng/ml) for 30min. (n=4).

HAMP mRNA
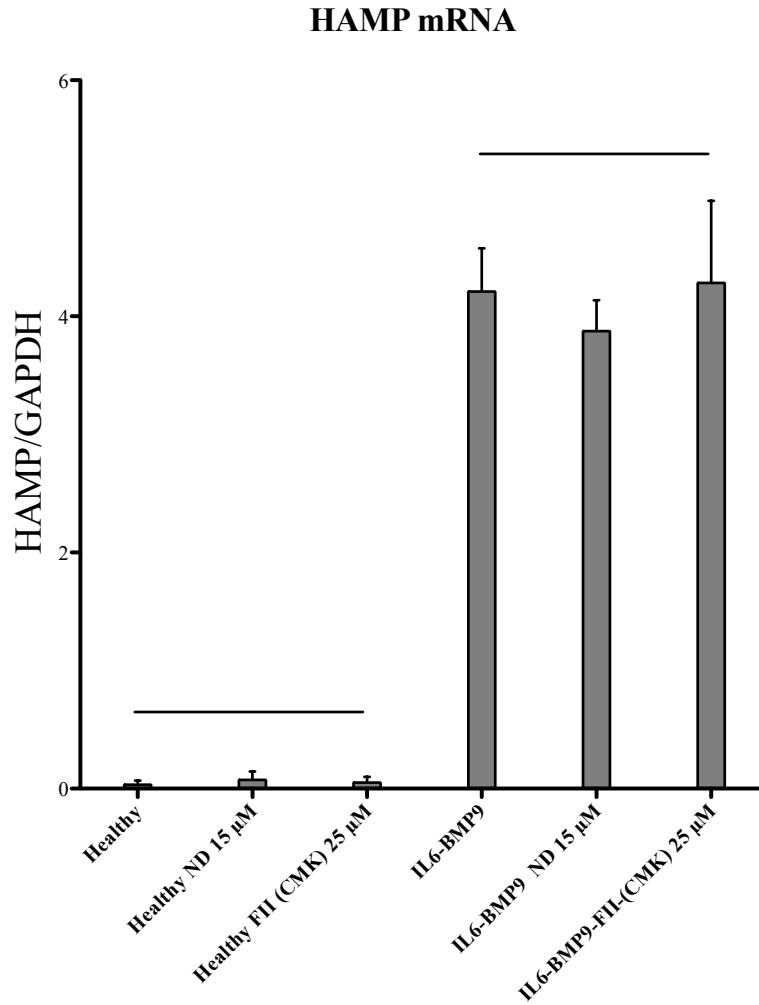
Figure 3.13. HAMP gene expression in HepG2 hepatocytes. HepG2 cells were co-treated with PIs Nelfinavir (7.5μM) and Darunavir (7.5μM) with and without cytokines Il-6 (10ng/ml) and BMP-9 (10ng/ml) for 18hrs. Furin inhibitor II (FII), also known as chloromethylketone (CMK) was included as a known furin inhibitor at 25μM. Treatment with ND did not reduce gene expression significantly ($p > 0.05$) (n=4).
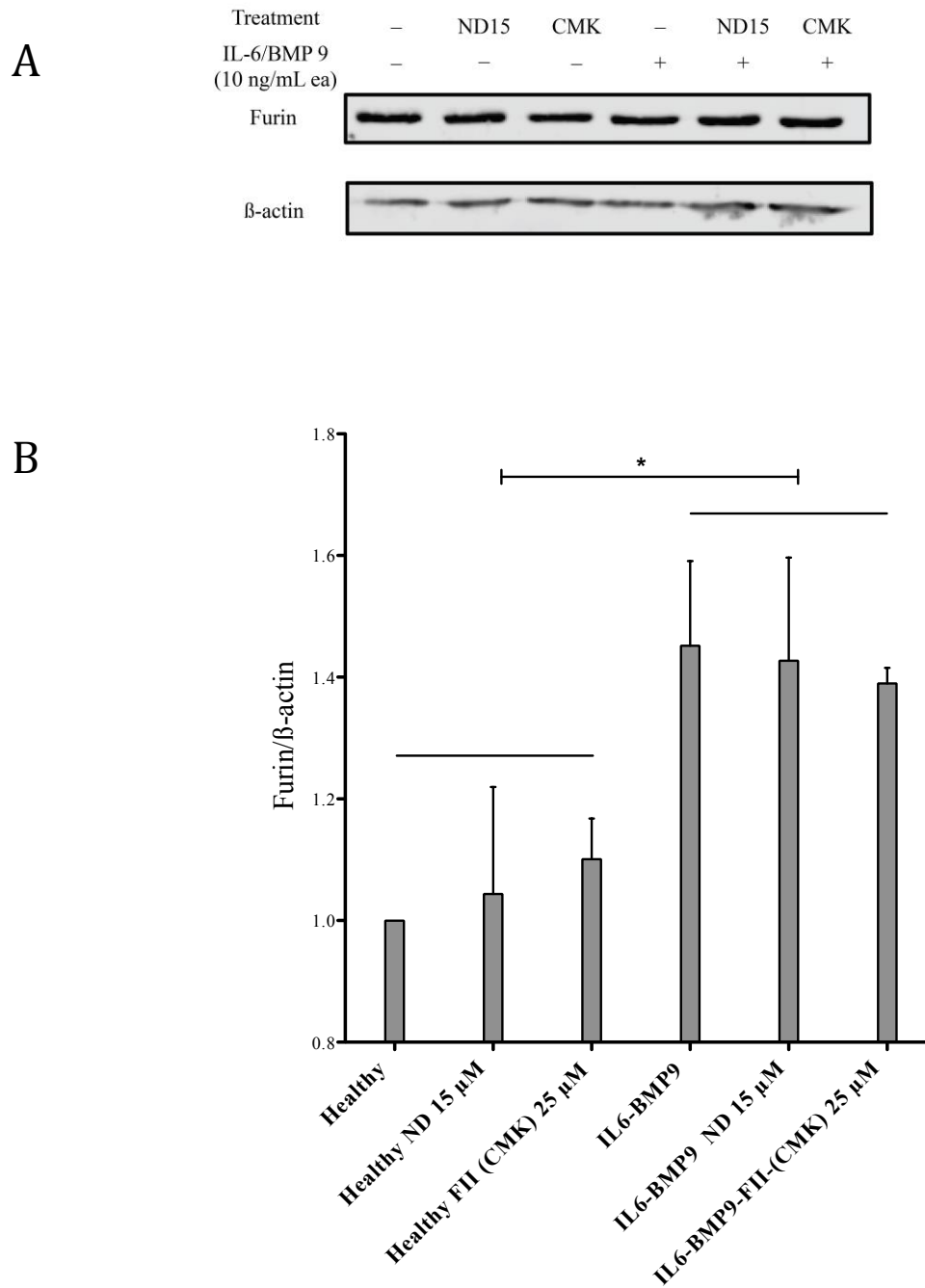
Figure 3.14. IL-6 and BMP-9 upregulate Furin in HepG2 hepatocytes. A) Furin western blot of HepG2 cells after 18hr incubation with and without inflammatory cytokines IL-6 and BMP-9, co-treated with ND and CMK. **B)** Graphical representation of Furin western blots in HepG2 cells. No significant difference is seen with treatment of PIs ($p > 0.05$), but significant difference exists between healthy and cytokine induced groups ($p < 0.05$) (n=4).
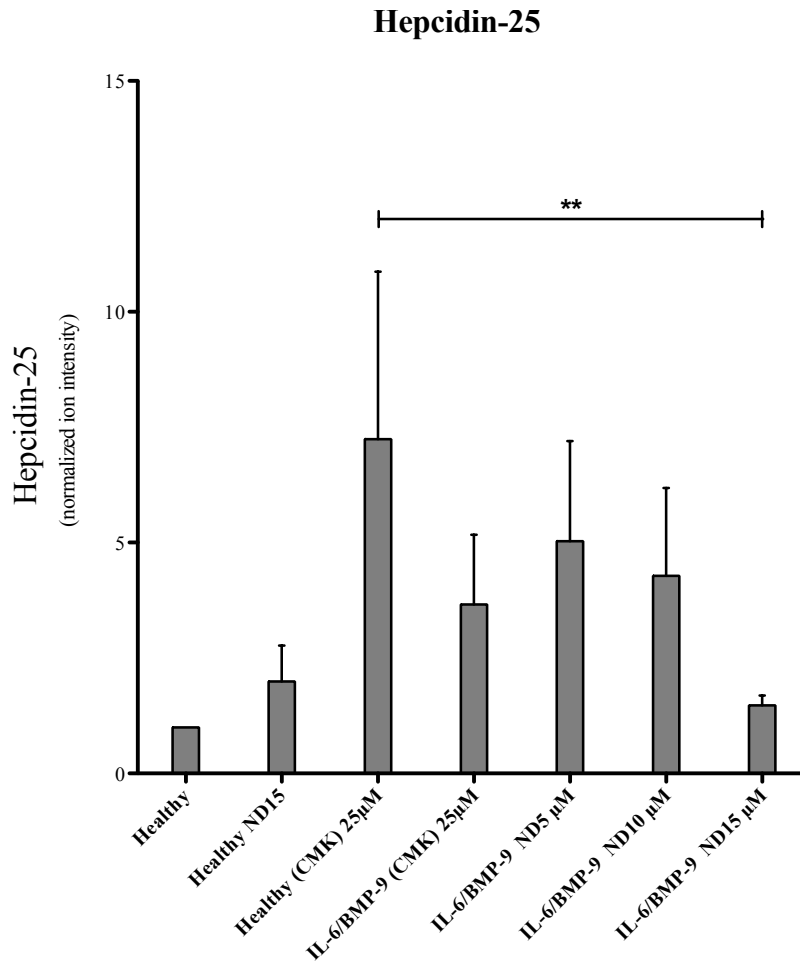
Hepcidin-25

Figure 3.15. Hepcidin production is inhibited with ND treatment in HepG2 hepatocytes. Mass spectrometry quantification of hep-25 under inflammatory conditions in HepG2 cell media. Treatment with ND reduces hep-25 concentrations to near basal levels ($p < 0.01$) (n=4).
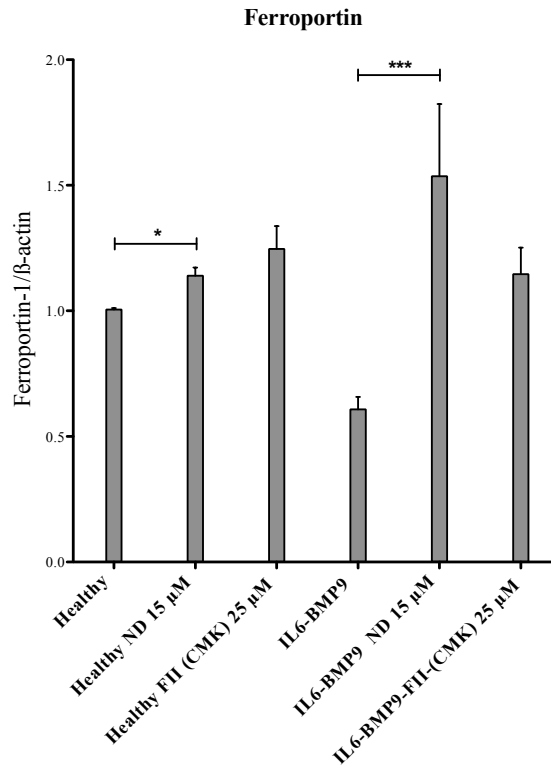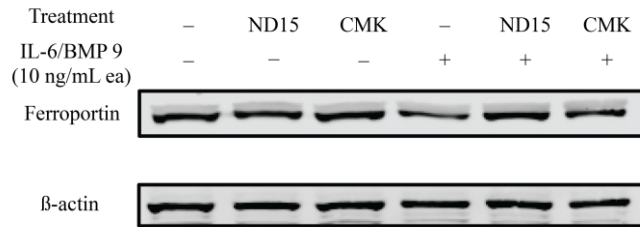
Figure 3.16. Ferroportin expression in HepG2 cells is elevated. A) Western blot of IL-6 (10ng/ml) and BMP-9 (10ng/ml) induced HepG2 cells, co-treated with PIs ND (15 μM), and CMK (25 μM). **B)** Graphical representation of WB data, showing significant increase in ferroportin expression in ND treated healthy cells ($p < 0.05$). Ferroportin expression in cells treated with CMK doubled (109%) when compared to IL-6/BMP-9 control ($p < 0.01$). Prominent expression of Ferroportin is most clearly observed with ND treated IL-6/BMP-9 induced cells, where expression increased 174% as compare to control ($p < 0.001$) (n=4).

References

1. Ganz, T. Hepcidin, a key regulator of iron metabolism and mediator of anemia of inflammation. *Blood* **102,** 783–788 (2003).

2. Casanovas, G., Banerji, A., d' Alessio, F., Muckenthaler, M. U. & Legewie, S. A Multi-Scale Model of Hepcidin Promoter Regulation Reveals Factors Controlling Systemic Iron Homeostasis. *PLoS Comput Biol* **10,** e1003421 (2014).

3. Andrews, N. C. Anemia of inflammation: the cytokine-hepcidin link. *J. Clin. Invest.* **113,** 1251–1253 (2004).

4. Cheng, P., Jiao, X., Wang, X., Lin, J. & Cai, Y. Hepcidin expression in anemia of chronic disease and concomitant iron-deficiency anemia. *Clin. Exp. Med.* **11,** 33–42 (2011).

5. Huang, H., Constante, M., Layoun, A. & Santos, M. M. Contribution of STAT3 and SMAD4 pathways to the regulation of hepcidin by opposing stimuli. *Blood* **113,** 3593–3599 (2009).

6. Falzacappa, M. V. V. *et al.* STAT3 mediates hepatic hepcidin expression and its inflammatory stimulation. *Blood* **109,** 353–358 (2007).

7. Valore, E. V. & Ganz, T. Posttranslational processing of hepcidin in human hepatocytes is mediated by the prohormone convertase furin. *Blood Cells. Mol. Dis.* **40,** 132–138 (2008).

8. Scamuffa, N. *et al.* Regulation of prohepcidin processing and activity by the subtilisin-like proprotein convertases Furin, PC5, PACE4 and PC7. *Gut* **57,** 1573–1582 (2008).

9. Gagliardo, B. *et al.* Pro-hepcidin is unable to degrade the iron exporter ferroportin unless matured by a furin-dependent process. *J. Hepatol.* **50,** 394–401 (2009).

10. Guillemot, J., Canuel, M., Essalmani, R., Prat, A. & Seidah, N. G. Implication of the proprotein convertases in iron homeostasis: Proprotein convertase 7 sheds human transferrin receptor 1 and furin activates hepcidin. *Hepatology* **57,** 2514–2524 (2013).

11. Nemeth, E. *et al.* Hepcidin Regulates Cellular Iron Efflux by Binding to Ferroportin and Inducing Its Internalization. *Science* **306,** 2090–2093 (2004).

12. Domenico, I. D. *et al.* The Molecular Mechanism of Hepcidin-mediated Ferroportin Down-Regulation. *Mol. Biol. Cell* **18,** 2569–2578 (2007).

13. Ramey, G. *et al.* Hepcidin targets ferroportin for degradation in hepatocytes. *Haematologica* **95,** 501–504 (2010).

14. Knutson, M. D., Oukka, M., Koss, L. M., Aydemir, F. & Wessling-Resnick, M. Iron release from macrophages after erythrophagocytosis is up-regulated by ferroportin 1 overexpression and down-regulated by hepcidin. *Proc. Natl. Acad. Sci. U. S. A.* **102,** 1324–1328 (2005).

15. Donovan, A. *et al.* The iron exporter ferroportin/Slc40a1 is essential for iron homeostasis. *Cell Metab.* **1,** 191–200 (2005).

16. Sun, C. C., Vaja, V., Babitt, J. L. & Lin, H. Y. Targeting the hepcidin–ferroportin axis to develop new treatment strategies for anemia of chronic disease and anemia of inflammation. *Am. J. Hematol.* **87,** 392–400 (2012).

17. Nemeth, E. Targeting the Hepcidin-Ferroportin Axis in the Diagnosis and Treatment of Anemias. *Adv. Hematol.* **2010,** e750643 (2009).

18. Aggarwal, B. B. *et al.* Signal Transducer and Activator of Transcription-3, Inflammation, and Cancer. *Ann. N. Y. Acad. Sci.* **1171,** 59–76 (2009).

19. Ikezoe, T. *et al.* HIV-1 protease inhibitor induces growth arrest and apoptosis of human multiple myeloma cells via inactivation of signal transducer and activator of transcription 3 and extracellular signal-regulated kinase 1/2. *Mol. Cancer Ther.* **3,** 473–479 (2004).

20. Gills, J. J. *et al.* Nelfinavir, A Lead HIV Protease Inhibitor, Is a Broad-Spectrum, Anticancer Agent that Induces Endoplasmic Reticulum Stress, Autophagy, and Apoptosis In vitro and In vivo. *Clin. Cancer Res.* **13,** 5183–5194 (2007).

21. Kartikasari, A. E. R. *et al.* Secretion of bioactive hepcidin-25 by liver cells correlates with its gene transcription and points towards synergism between iron and inflammation signaling pathways. *Biochim. Biophys. Acta BBA - Proteins Proteomics* **1784,** 2029–2037 (2008).

22. Nemeth, E. *et al.* Hepcidin, a putative mediator of anemia of inflammation, is a type II acute-phase protein. *Blood* **101,** 2461–2463 (2003).

23. Kemna, E., Pickkers, P., Nemeth, E., Hoeven, H. van der & Swinkels, D. Time-course analysis of hepcidin, serum iron, and plasma cytokine levels in humans injected with LPS. *Blood* **106,** 1864–1866 (2005).

24. Qiao, B. *et al.* Hepcidin-Induced Endocytosis of Ferroportin Is Dependent on Ferroportin Ubiquitination. *Cell Metab.* **15,** 918–924 (2012).

25. Ganz, T. Cellular iron: Ferroportin is the only way out. *Cell Metab.* **1,** 155–157 (2005).

26. Pigeon, C. *et al.* A New Mouse Liver-specific Gene, Encoding a Protein Homologous to Human Antimicrobial Peptide Hepcidin, Is Overexpressed during Iron Overload. *J. Biol. Chem.* **276,** 7811–7819 (2001).

27. Babitt, J. L. *et al.* Modulation of bone morphogenetic protein signaling in vivo regulates systemic iron balance. *J. Clin. Invest.* **117,** 1933–1939 (2007).

28. Truksa, J., Peng, H., Lee, P. & Beutler, E. Different regulatory elements are required for response of hepcidin to interleukin-6 and bone morphogenetic proteins 4 and 9. *Br. J. Haematol.* **139,** 138–147 (2007).

29. Rodriguez, R. *et al.* Hepcidin Induction by Pathogens and Pathogen-Derived Molecules Is Strongly Dependent on Interleukin-6. *Infect. Immun.* **82,** 745–752 (2014).

30. De Domenico, I., Ward, D. M. & Kaplan, J. Hepcidin regulation: ironing out the details. *J. Clin. Invest.* **117,** 1755–1758 (2007).

31. Pietrangelo, A. *et al.* STAT3 Is Required for IL-6-gp130–Dependent Activation of Hepcidin In Vivo. *Gastroenterology* **132,** 294–300 (2007).

32. Lane, D. J. R., Huang, M. L.‐H. & Richardson, D. R. Hepcidin, show some self-control! How the hormone of iron metabolism regulates its own expression. *Biochem. J.* **452,** e3–e5 (2013).

33. Thomas, G. Furin at the cutting edge: From protein traffic to embryogenesis and disease. *Nat. Rev. Mol. Cell Biol.* **3,** 753–766 (2002).

34. Bass, J., Turck, C., Rouard, M. & Steiner, D. F. Furin-mediated processing in the early secretory pathway: sequential cleavage and degradation of misfolded insulin receptors. *Proc. Natl. Acad. Sci.* **97,** 11905–11909 (2000).

35. Vey, M., Schäfer, W., Berghöfer, S., Klenk, H.-D. & Garten, W. Maturation of the trans-Golgi network protease furin: compartmentalization of propeptide removal, substrate cleavage, and COOH-terminal truncation. *J. Cell Biol.* **127,** 1829–1842 (1994).

36. Seidah, N. G. & Prat, A. The biology and therapeutic targeting of the proprotein convertases. *Nat. Rev. Drug Discov.* **11,** 367–383 (2012).

37. Vidricaire, G., Denault, J. B. & Leduc, R. Characterization of a Secreted Form of Human Furin Endoprotease. *Biochem. Biophys. Res. Commun.* **195,** 1011–1018 (1993).

38. Gardenghi, S. *et al.* Ineffective erythropoiesis in β-thalassemia is characterized by increased iron absorption mediated by down-regulation of hepcidin and up-regulation of ferroportin. *Blood* **109,** 5027–5035 (2007).

39. Tian, S., Huang, Q., Fang, Y. & Wu, J. FurinDB: A Database of 20-Residue Furin Cleavage Site Motifs, Substrates and Their Associated Drugs. *Int. J. Mol. Sci.* **12,** 1060–1065 (2011).

40. Pfaffl, M. W. A new mathematical model for relative quantification in real-time RT–PCR. *Nucleic Acids Res.* **29,** e45–e45 (2001).

41. Arikawa, E. *et al.* Cross-platform comparison of SYBR® Green real-time PCR with TaqMan PCR, microarrays and other gene expression measurement technologies evaluated in the MicroArray Quality Control (MAQC) study. *BMC Genomics* **9,** 328 (2008).

42. Aarnoutse, R. E. *et al.* Pharmacokinetics, food intake requirements and tolerability of once-daily combinations of nelfinavir and low-dose ritonavir in healthy volunteers. *Br. J. Clin. Pharmacol.* **55,** 115–125 (2003).

43. Malaty, L. I. & Kuper, J. J. Drug interactions of HIV protease inhibitors. *Drug Saf.* **20,** 147–169 (1999).

44. McCoy, C. Darunavir: A Nonpeptidic Antiretroviral Protease Inhibitor. *Clin. Ther.* **29,** 1559–1576 (2007).

45. Deeks SG, Smith M, Holodniy M & Kahn JO. Hiv-1 protease inhibitors: A review for clinicians. *JAMA* **277,** 145–153 (1997).

46. Danner, S. A. *et al.* A Short-Term Study of the Safety, Pharmacokinetics, and Efficacy of Ritonavir, an Inhibitor of HIV-1 Protease. *N. Engl. J. Med.* **333,** 1528–1534 (1995).

47. Barry, D. M., Gibbons, S., Back, D. & Mulcahy, F. Protease Inhibitors in Patients with HIV Disease. *Clin. Pharmacokinet.* **32,** 194–209 (1997).

48. Kaldor, S. W. *et al.* Viracept (nelfinavir mesylate, AG1343): a potent, orally bioavailable inhibitor of HIV-1 protease. *J. Med. Chem.* **40,** 3979–3985 (1997).

49. VIRACEPT®(nelfinavir mesylate)TABLETS and ORAL POWDER. at <http://dailymed.nlm.nih.gov/dailymed/archives/fdaDrugInfo.cfm?archiveid=5483>

50. Lagathu, C. *et al.* Antiretroviral drugs with adverse effects on adipocyte lipid metabolism and survival alter the expression and secretion of proinflammatory cytokines and adiponectin in vitro. *Antivir Ther* **9,** 911–20 (2004).

51. Pandur, E. *et al.* Prohepcidin binds to the *HAMP* promoter and autoregulates its own expression. *Biochem. J.* **451,** 301–311 (2013).

52. Yuasa, K., Suzue, K., Nagahama, M., Matsuda, Y. & Tsuji, A. Transcriptional regulation of subtilisin-like proprotein convertase PACE4 by E2F: Possible role of E2F-mediated upregulation of PACE4 in tumor progression. *Gene* **402,** 103–110 (2007).

53. Enomoto, T. *et al.* Regulation of adipolin/CTRP12 cleavage by obesity. *Biochem. Biophys. Res. Commun.* **428,** 155–159 (2012).

54. Silvestri, L., Pagani, A. & Camaschella, C. Furin-mediated release of soluble hemojuvelin: a new link between hypoxia and iron homeostasis. *Blood* **111,** 924–931 (2008).

CHAPTER 4: Inhibition of Furin Prevents Prohepcidin Cleavage and Restores Iron

Redistribution in an Animal Model of Anemia of Chronic Inflammation

Abstract

Context

Anemia of Chronic Inflammation (ACI) is characterized by macrophage and liver iron retention triggered by inflammatory cytokines that induce the expression of the master iron regulator hepcidin. Hepcidin is known to regulate iron efflux by binding to ferroportin and initiating endocytosis and degradation of ferroportin causing the iron retention of ACI. Hepcidin is cleaved into its active form by the serine protease known as furin.

Objective

We hypothesized the protease furin could be a drug target to prevent ACI. Using molecular modeling analysis and in vitro furin assays, we previously demonstrated that the protease inhibitor nelfinavir binds to and inhibits furin. The goal of this work was to verify that nelfinavir inhibited furin in animals. We propose that furin inhibition will prevent hepcidin activation, prevent ferroportin degradation and allow normal iron delivery to the bloodstream and bone marrow. We also recognize that more often than not, when drugs are involved, 'fu-rin' for a good time.

Design

We used an animal model of rheumatoid arthritis to induce anemia of chronic inflammation. Group A Streptococcal Peptidoglycan-Polysaccharide (PG-LPS) injection causes chronic activation of the immune system, increased production of cytokines, increased levels of hepcidin, and sustained anemia.

Results

At a therapeutic serum concentration, nelfinavir (4mg/L) inhibited mature hepcidin production by 47% while increasing prohepcidin 148%. Ferroportin expression increased 2.5 fold in animal liver, while iron in serum and bone marrow increased significantly ($p < 0.01$ and $p < 0.05$ respectively). However, anemia persisted, as hemoglobin and hematocrit did not significantly recover.

Conclusions

Nelfinavir treatment successfully inhibited hepcidin production and increased liver ferroportin allowing for restoration of iron in the serum and bone marrow.

Introduction

Anemia of chronic inflammation (ACI) is prevalent in kidney disease, cancer, autoimmune disorders, inflammatory disorders and infections[1−6]. Inflammatory cytokines trigger the production of an iron regulatory hormone called hepcidin that causes ACI[7−10]. Hepcidin binds to the iron export protein ferroportin and triggers its endocytosis and degradation[11,12]. Ferroportin exports iron from intestinal enterocytes into the bloodstream and also facilitates the export of iron stored in the liver and macrophages into serum. When iron exits ferroportin and enters the serum, it is bound by transferrin and delivered to cells that need iron such as the bone marrow that is synthesizing heme for red blood cells[13] (Figure 4.1). During ACI, anemia results because iron is trapped in iron storage cells or not absorbed from the diet and very little iron is available to be bound by transferrin for delivery to iron deficient cells. This results in iron-deficiency in the bone marrow and prevents the production of heme for red blood cell (RBC) synthesis[8,10].

In addition to iron-deficiency in the bone marrow, inflammatory cytokines decrease the production of erythropoietin (EPO), the hormone that triggers the proliferation of RBCs. The kidneys sense serum oxygen levels and when hypoxia is detected, the kidneys express and secrete EPO to stimulate RBC proliferation. However, inflammation inhibits EPO production and secretion into serum[14,15].

To treat ACI, patients are given synthetic erythropoiesis stimulating agents (ESAs) and iron supplements[16]. These treatments provide slight improvements to anemia but do not completely alleviate ACI for several critical reasons. First, iron supplements

do not efficiently transfer iron to transferrin; instead cells absorb the iron. Once the iron supplement enters the cells the iron is trapped because ferroportin is constantly being degraded by hepcidin. A second problem is called EPO resistance. ESAs signal for erythroblasts to differentiation into RBCs. In ACI, ESAs causes erythroblasts to differentiate but without sufficient iron in the bone marrow, the resulting RBCs lack iron in heme and are deficient in oxygen transport[17].

Therefore the successful treatment of ACI requires several coordinated steps. First, ferroportin must be stabilized so iron is properly exported from iron-rich cells or absorbed from the diet. Second, the iron must be properly loaded into transferrin. Third, transferrin must deliver iron to the bone marrow. Fourth, ESAs must be provided with the appropriate timing to stimulate erythroblast differentiation into RBCs when iron is present. To accomplish these goals requires the development of hepcidin inhibitors or methods to stabilize ferroportin on the cell surface.

Several studies have been performed to inhibit the production of hepcidin to treat ACI. The two most clearly identified pathways that trigger the expression of the HAMP gene that encodes for hepcidin, are the IL-6 initiated Jak/STAT pathway and the BMP-6 and BMP-9 stimulated Smad pathway. The understanding of these pathways has triggered a series of studies to inhibit the transcription of HAMP by inhibiting BMP receptors with dorsomorphin and its derivatives or inhibiting serum BMP levels using a soluble hemojuvelin domain fused with immunoglobulin Fc[18–20]. These methods have produced recovery of iron mobilization and redistribution by lowering serum hepcidin levels and increasing the stability of ferroportin on the exterior of iron rich cells. These studies successfully restored hemoglobin and hematocrit levels.

Sasu et al. targeted hepcidin in the serum with antibodies that eliminate hepcidin from serum as a method to increase ferroportin levels[21]. Anti-hepcidin antibodies decreased serum hepcidin levels and increased serum iron levels but did not allow the restoration of hemoglobin and hematocrit levels until the anti-hepcidin antibody was co-administered with ESAs. A related IL-6 targeting study by Song et al. targeted the IL-6 receptor with an antibody, tocilizumab, in Castleman disease[22]. In Castleman disease IL-6 is unregulated and overexpressed causing chronic inflammation. Blocking the inflammatory signal of IL-6 allowed the patients to recover from ACI.

In contrast to inhibiting BMP or IL-6 signaling or targeting hepcidin or IL-6 receptors with antibodies, we chose to target a different step in hepcidin production and activation. Hepcidin is synthesized in a precursor form called prohepcidin that must be cut by a protease called furin before it folds into its active conformation that binds to and degrades ferroportin[23,24]. Through the use of computational modeling and *in silico* molecular docking, along with *in vitro* fluorogenic assays, we demonstrated that inhibiting furin prevented the cleavage of prohepcidin to hepcidin. In this work, we demonstrate within an animal model that HIV protease inhibitors with high affinity to furin are able to stop the processing and activation step where prohepcidin is cleaved to produce hepcidin. This study provides proof of concept that furin is a valid target for restoring iron mobilization through ferroportin. We propose that protease inhibitors able to prevent furin from cleaving prohepcidin to hepcidin can be used to restore iron to the bone marrow, and suggest that in combination with ESAs, will provide a treatment for ACI.

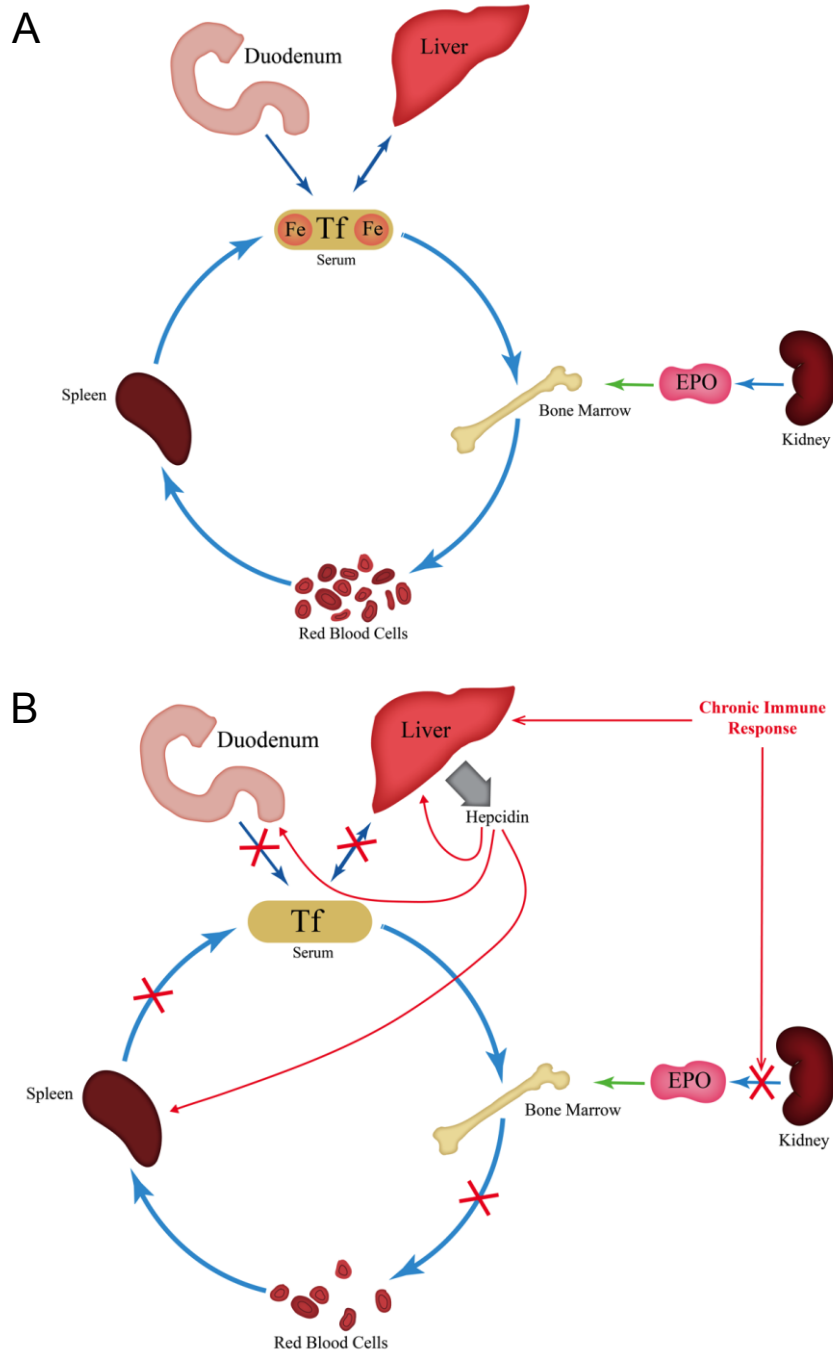**Figure 4.1. Iron cycling in mammals. A)** Normal or healthy iron cycling between tissues. **B)** During chronic immune activation, cytokines released into the serum activate hepcidin production. Hepcidin inhibits iron export from various tissues by triggering endocytosis of ferroportin within hepatocytes of the liver, macrophages in the speen, and enterocytes in the duodenum.

Materials and Methods

Animals

Female Lewis rats received at age 3-4 weeks and 75 g (Charles River Laboratories) were kept in a temperature-controlled (20°C ±1°C) and well-ventilated room with a 12:12-h light-dark cycle. Animals had free access to standard (Diet 8604, Harlan Teklad) rodent laboratory chow and water. Chow iron content was 300mg/kg. The Institutional Animal Care Committee of Brigham Young University approved all experimental procedures.

Female Lewis rats at seven weeks of age received a single intraperitoneal inoculation of Group A Streptococcal Peptidoglycan-Polysaccharide (PG-LPS; Lee Laboratories) suspended in a 0.85% saline. Total dose received was 12.5μg rhamnose/g body weight. Two weeks after PG-LPS injection, animals were tested for development of anemia, and randomized into groups with similar hemoglobin (Hb) and hematocrit (HCT) levels. Animals incurring a (>2g/dL hemoglobin drop from baseline range) were characterized as having anemia of chronic inflammation (ACI)[25].

Treated animals received a human equivalent dose of prescription Nelfinavir (Viracept) and Ritonavir (Norvir) via oral gavage. To utilize the potential of nelfinavir, ritonavir is co-administered to adequately promote nelfinavir serum concentrations. Ritonavir is known to inhibit cytochrome P450 enzymes 3A4, the enzyme primarily responsible for metabolizing nelfinavir within the liver[26,27]. By adding ritonavir

169

alongside nelfinavir, nelfinavir serum concentrations are sustained for longer periods of time[27–29]. HIV patients are commonly prescribed ritonavir along with nelfinavir as a therapeutic strategy for boosting PI serum concentrations[30].

The adjusted rat dose was calculated by the body surface area (BSA) normalization method as previously described[31], where the Human Equivalent dose (mg/kg) is equal to Animal dose (mg/kg) multiplied by (Animal K_m/Human K_m). Animal and Human K_m equal 37 and 6 respectively[32]. Drug treatment was administered every 12 hours via oral gavage.

Equal volumes of dimethyl sulfoxide (DMSO) and flax seed oil were used as vehicle. Protease inhibitors Nelfinavir and Ritonavir have high solubility properties in DMSO as compared to water[33,34]. The flax seed oil was used in combination to sustain serum concentrations for longer periods of time[29,30,34]. Both drugs were weighed and crushed together from tablet into powder form before being dissolved in DMSO, immediately prior to administration. One dose is represented as 1ml total volume.

Throughout the treatment period, ~0.5ml of blood was collected once a week from a small tail clip. Complete blood counts (CBC) were performed on a BeckmanCoulter HmX Hematology Analyzer. Serum iron analysis was performed via inductively coupled plasma mass spectrometry (ICP-MS). Animals were weighed daily and scored for pain and distress.

After 6 weeks of treatment (8 weeks after induction of ACI), all rats were euthanized with tissues being snap-frozen in liquid nitrogen and stored at −80°C for subsequent gene expression studies, iron analysis, and protein analysis.

Protein Extraction

Approximately 100 mg of liver frozen tissue was transferred to ice cold RIPA buffer containing 50 mM Tris-HCl (pH 8), 150 mM NaCl, 1% Triton X-100, 0.5% sodium deoxycholate, 0.1% SDS, 5 mM EDTA and 1X protease/phosphatase cocktail inhibitor (Thermo Fisher Scientific, Waltham, MA) and homogenized on ice with a glass pestle at 700 rpm. The homogenate was transferred to a pre-chilled, clean microfuge tube, subjected to three freeze-thaw cycles and centrifuged for 25 minutes at 12,000 rpm. The supernatant was collected and protein content was determined with a Lowry protein assay.

Western Blotting

Protein samples were prepared for electrophoresis and equal amounts of resulting protein were separated in 8% SDS–PAGE and then transferred to a Nitrocellulose membrane (Bio-Rad). After transfer, the membranes were blocked in Odyssey™ Blocking Buffer (927-40100, LI-COR Biosciences, Lincoln, NE) at room temperature, for 1 hour. Primary antibodies were diluted in blocking solution containing 0.2% Tween and incubated overnight at 4 °C with polyclonal antibody to ferroportin (rabbit, 1 : 1000

dilution; ab85370, Abcam, Cambridge, MA)) Blots were normalized by probing the membranes with β-actin (Cat. # 3700). Cell Signaling Technology, Beverly, MA). After incubation and washing with PBS-T, the membranes where incubated in the dark, in blocking solution with 0.2% Tween with IRDye 800CW Goat anti-Rabbit IgG and IRDye® 680RD Donkey anti-Mouse IgG (1:10000, LI-COR Biosciences, Lincoln, NE) for 1 hour at room temperature. The proteins were detected and visualized by fluorescence using the Licor Odyssey Classic Infrared Imaging system (LI-COR Biosciences, Lincoln, NE). Densitometry analysis of specific bands was performed with the Image Studio software provided by LI-COR Biosciences.

RNA preparation from tissue, reverse transcription and RT^2-qPCR

RNA was isolated by homogenizing frozen ground liver in Trizol reagent (Cat# 15596-018) from Invitrogen with an OMNI Tissue Master homogenizer, and then purified on RNeasy mini kit columns (Cat# 74104) from Qiagen. All samples were treated with DNase (Cat# 79254) from Qiagen. Two micrograms of RNA were used for reverse transcription and subsequent SYBR® Green ROX real time PCR for the genes of interest as previously described[35]. Reverse transcription kits (Cat #330401) and SYBR Green real-time PCR master mixes (Cat# 330523) were from Qiagen (Louisville, KY). The following primers and probes were used:

172

Rat hepcidin; HAMP (Cat# PPR43953A), Rat furin; FURIN (Cat# PPR43007A), Rat ferroportin; (Cat# PPR46085A), Rat glyceraldehyde 3-phosphate dehydrogenase; GAPDH (Cat# PPR 06557B).

Real time quantitative PCR was preformed on an Applied Biosciences Step One plus instrument and analyzed with StepOne software v2.3. The relative amounts of transcripts from each gene were normalized to reference gene glyceraldehyde 3-phoshpate dehydrogenase (GAPDH) and calculated as follows: $\Delta\Delta C_T$ = the average ΔC_T of sample B – the average ΔC_T of sample B, and their fold difference = $2^{-\Delta\Delta C_T}$ as previously described[36]. No statistical variance of reference gene expression was observed between tissue groups.

Enzyme-linked immunosorbent assays

The following commercially available ELISA kits were used to quantify protein concentrations in Lewis Rat serum.

Hepcidin-25 and Prohepcidin ELISA kits (Cat# EIA5258 and Cat# EIA4644 DRG International, Mountainside, NJ).

Interleukin-6 ELISA kits (Cat# 437107, BioLegend, San Diego CA).

Bone morphogenic protein-9 (BMP-9), also known as Growth Differentiation Factor-2 (GDF-2), protein ELISA kits (Cat# SEB728Ra, Cloud-Clone Corp., Houston TX).

Erythropoietin ELISA kits (Cat# MBS160249, MyBioSource, San Diego, CA).

Inductively coupled plasma mass spectrometry (ICP-MS) Fe analysis

Serum and tissue samples previously prepared and preserved in liquid nitrogen were weighed and dissolved in 1ml 70% OmniTrace® analytical grade nitric acid. Samples were then sonicated for 30 minutes, diluted to 3% nitric acid and heated to 95°C for 3 hours. Finally, they were centrifuged for 30 minutes at 15,000 g with supernatant collected for analysis. Trace iron Fe quantification was measured via a Perkin Elmer Elan 6000 Inductively coupled plasma mass spectrometer as previously described[37,38]. Multi-elemental standard solutions were used for calibration.

Data Analysis

Statistical analysis was carried out using GraphPad Prism 5.0 software. Calculations for statistical differences between various groups were evaluated using a one-way ANOVA or a two-way ANOVA where appropriate followed by a Bonferroni post hoc test. Statistical significance is defined as $p < 0.05$. Results are presented as means ± SE.

Results

Polysaccharide induced model of chronic inflammation

Chronic inflammation was induced in vivo using a well-established rat model of ACI. Streptococcal Peptidoglycan-Polysaccharide (PG-LPS) injections resulting in a chronic inflammatory state where anemia is sustained for many weeks[28,16]. Inflammatory cytokines known to induce HAMP gene expression, interleukin-6 (IL-6) and bone morphogenic protein-9 (BMP-9), were significantly elevated in the serum of PG-LPS treated animals (Figures 4.2A and 4.2B)[40]. Additionally, serum erythropoietin (EPO) showed no statistically significant differences between groups, consistent with other studies of ACI (Figure 4.2C)[15,41–44].

Protease inhibitors halt furin from cleaving prohepcidin into hepcidin.

The inflammatory cytokines IL-6 and BMP-9, which were present in the serum of PG-LPS treated animals (Figures 4.2A and 4.2B) are known to activate transcription of the HAMP gene and the expression of hepcidin[45] through STAT3 and Smad pathways respectively[46–50]. Since our proposal suggests that protease inhibitors block the proteolytic cleavage of prohepcidin to form hepcidin by inhibiting furin, we would not anticipate any inhibition of HAMP mRNA production.

Quantitative PCR (qPCR) of liver tissue was used to compare the expression of the HAMP gene between groups. HAMP expression remained low in the absence of chronic inflammation caused by PG-LPS treatment (Figure 4.3A), but PG-LPS treatment caused an approximate 6-fold increase in HAMP gene expression. Additionally, in PG-LPS treated animals, nelfinavir did not show any statistically significant changes in the transcription of HAMP mRNA indicating these drugs do not inhibit HAMP mRNA transcription.

As expected by the elevated HAMP mRNA levels in PG-LPS treated rats, the serum hepcidin levels increased in PG-LPS treated rats (Figure 4.3B). However, the serum hepcidin levels in PG-LPS and nelfinavir treated rats are approximately 2-fold lower than in PG-LPS rats indicating that nelfinavir inhibited furin from processing prohepcidin to hepcidin (Figure 4.3B). These results are further strengthened by a serum prohepcidin ELISA data, where serum prohepcidin is approximately 2.5-fold higher in PG-LPS treated rats treated with Nelfinavir (Figure 4.3C). Western Blot analysis of ferroportin from liver tissue shows that ferroportin is significantly higher in PG-LPS treated rats receiving Nelfinavir than PG-LPS treated rats without nelfinavir. These ferroportin results further confirm that lower serum hepcidin levels occur in nelfinavir treated rats, as hepcidin is known to bind and subsequently induce endocytosis and degradation of ferroportin[11,12] (Figures 4.3D, 4.3E).
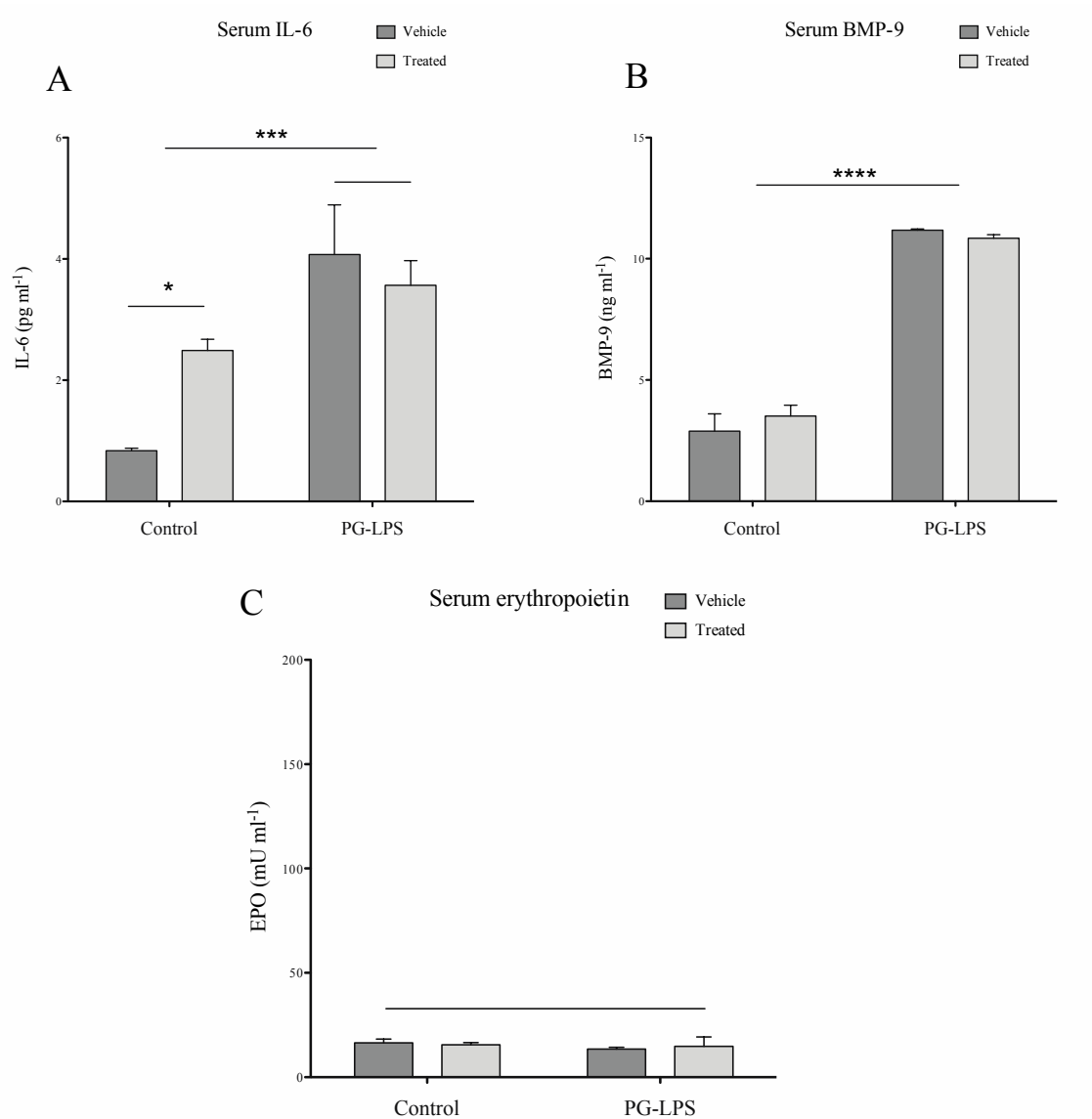
Figure 4.2. Cytokine and hormone levels present in serum 6 weeks post PG-LPS induction. A) Serum IL-6 concentrations are significantly higher in PG-LPS groups ($p < 0.0009$) but do not differ significantly between the PG-LPS control and treated ($p > 0.05$). **B)** Serum BMP-9 concentrations are significantly higher in PG=LPS groups ($p < 0.0001$) but do not differ significantly with treatment ($p > 0.05$). **C)** Serum EPO concentrations do not differ between groups ($p > 0.05$).
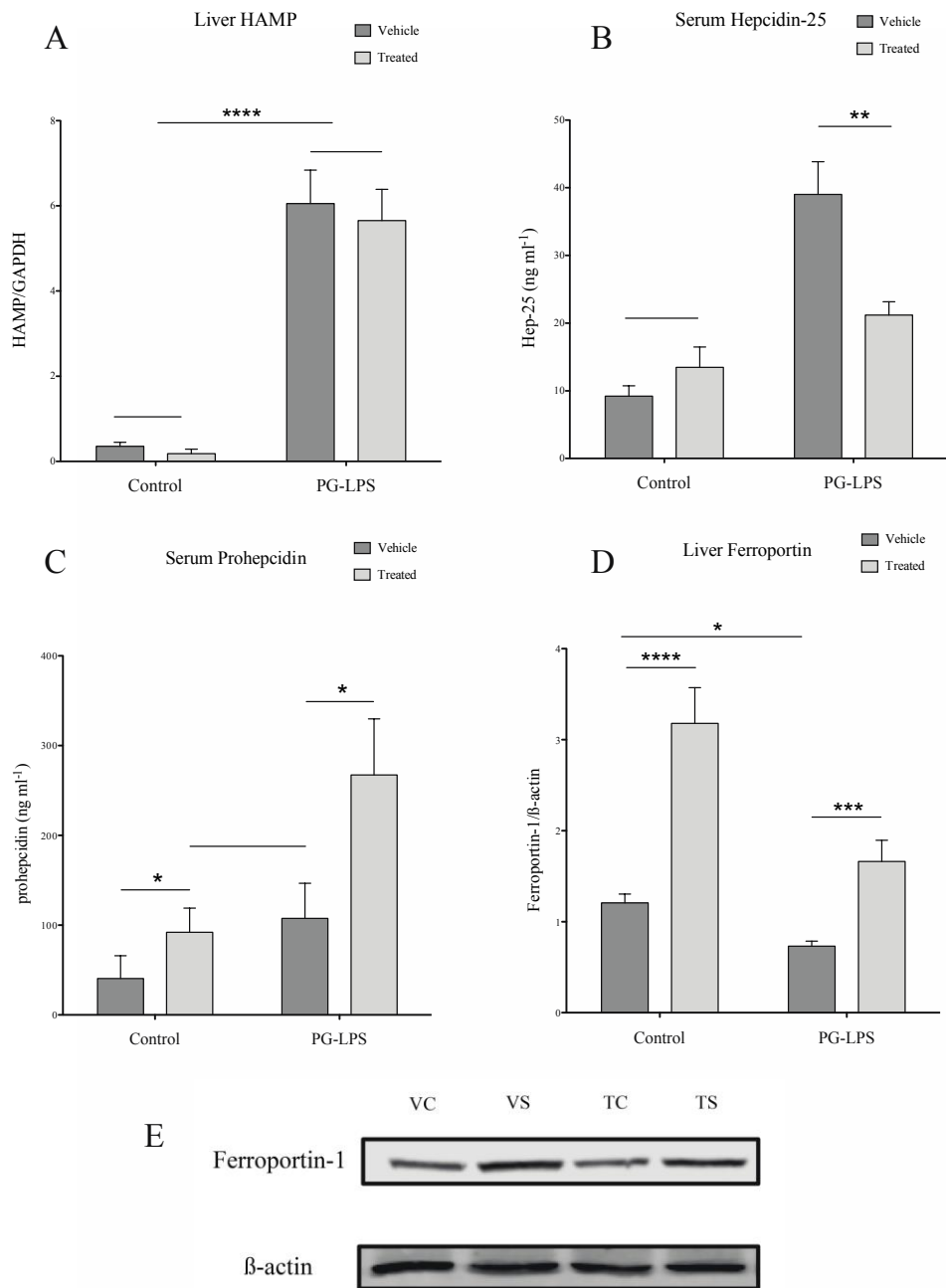
Figure 4.3. PIs block Hepcidin Secretion. A) HAMP mRNA is up-regulated by inflammation in the liver (p < 0.0001). **B)** Serum hepcidin is elevated with inflammation but inhibited by PIs (p < 0.01). **C)** Serum Prohepcidin increased slightly by inflammation but is significantly higher when PIs are used to

inhibit furin ($p < 0.05$). **D)**, **E)** Ferroportin is rapidly degraded in animals with inflammation ($p < 0.05$) but is stabilized with PIs in both control and PG-LPS animal groups ($p < 0.00001$) and ($p < 0.001$) respectively.

Nelfinavir treatment restores iron redistribution into serum and tissue.

The treatment of PG-LPS treated rats with Nelfinavir decreased serum hepcidin levels (Figure 4.3B) and increased ferroportin levels (Figure 4.3C). The increased level of ferroportin should allow the restoration of normal iron export from iron rich tissue and increase the iron content in the serum and bone marrow. The heart is another organ heavily dependent and sensitive to iron transport and metabolism[51–53]. Defective iron supply with blunted erythropoietin production due to chronic immune activation, has previously been shown to contribute to heart failure and myocardial infarction[14,16]. We predicted that nelfinavir treatment might also restore iron levels in heart tissue.

The data presented in Figure 4.4 confirm these predictions. Serum iron was not significantly different between healthy rats and healthy rats treated with nelfinavir (Figure 4.4A). In contrast, the serum iron content of PG-LPS treated rats dropped to approximately half the iron content of healthy rats. PG-LPS treated rats that also received nelfinavir had ~25% more serum iron than the PG-LPS treated rats which was a significant increase in serum iron concentrations (Figure 4.4A). This result is consistent with the lower hepcidin levels (Figure 4.3B) and the elevated ferroportin levels (Figures 4.3D, 4.3E).

Liver iron content dropped significantly in healthy nelfinavir treated group as compared to the healthy animals (Figure 4.4). This is easily explained by the

approximate 3-fold increase in ferroportin in these rats (Figure 4.3D). Although the hepcidin levels are slightly higher in healthy nelfinavir treated rats than healthy rats (Figure 4.3B), the prohepcidin levels are much higher than healthy rats (Figure 4.3C) suggesting the PIs are blocking the action of hepcidin by inhibiting furin.

Furin is recognized as being upregulated with varying cancers and sarcoma's[54,55]. Furin expression is also known to increase under conditions of chronic immune activation[56]. We report that with PG-LPS animals, furin is again characterized as being upregulated (Figure 4.6). Despite this occurrence, furin activity is still significantly reduced as mature hepcidin-25 serum levels are shown to decrease, while prohepcidin levels increase.

It is also interesting to note that the serum iron content in healthy and healthy nelfinavir treated animals is maintained at a similar value even though the liver iron content decreases drastically in the nelfinavir treated animals (Figure 4.3A). This likely represents optimal serum iron concentrations, as the highly elevated level of ferroportin is used to maintain serum iron concentrations in healthy nelfinavir treated animals (Figures 4.2D and 4.4A). The release of iron from the liver of healthy animals treated with nelfinavir suggests that nelfinavir might be a potential treatment for hemochromatosis that will allow the liver to export excess iron. Perhaps combined treatment of nelfinavir with the Fe^{3+} chelator desferal could facilitate iron export from iron loaded cells and allow complexation of the iron by desferal for iron excretion. The reason for why these animals are not absorbing iron from the diet is not currently understood and is the focus of current work in our lab.
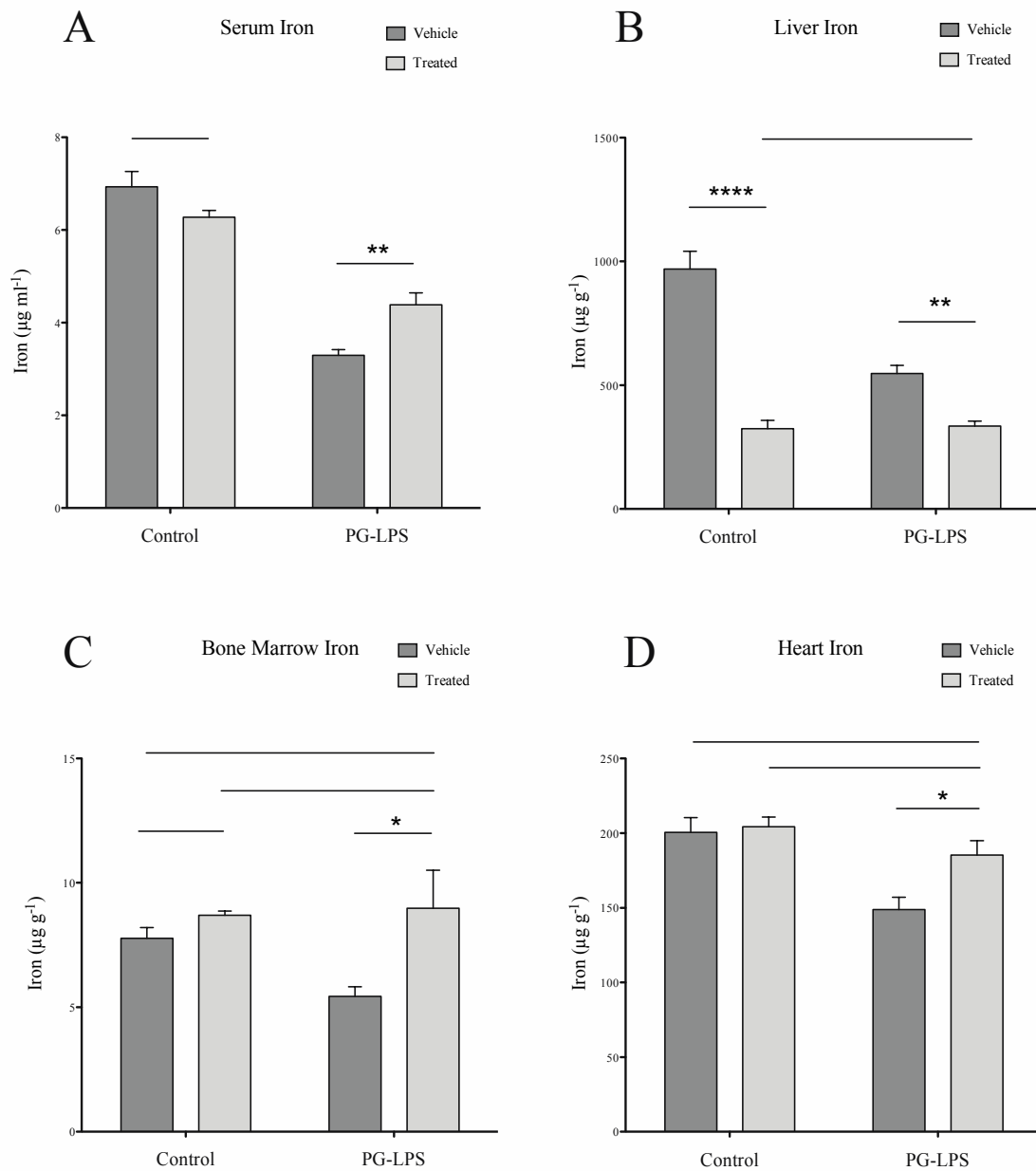
Figure 4.4. Iron Analysis. **A)** The total iron content in serum is significantly decreased in inflamed animals compared to healthy and PI treated healthy, but the presence of PIs causes a significant increase in total serum iron (p < 0.01). **B)** Liver iron content dropped in both the healthy PI treated and PG-LPS PI treated groups (p < 0.0001 and p < 0.01), consistent with elevated levels of ferroportin (Fig 3.2E). **C)** Bone marrow iron content is similar in healthy rats but lowest in inflamed rats. Treatment with protease

inhibitors produces an elevation in bone marrow iron similar to healthy rats (P < 0.05). **D)** Heart Iron content. Similar to Bone marrow, inflammation causes a decrease in heart iron but PI treatment restores normal iron redistribution and replenishes iron in the heart.

PG-LPS animals have lower liver iron content than healthy animals (Figure 4.4B). These results are likely due to the prolonged (6 weeks) inflammation incurred by the PG-LPS, as the average enterocyte life span ranges from only 4.7 to 10.2 days[57]. Dietary iron is not absorbed during inflammatory situations with hepcidin present. Because of this, iron availability in liver steadily diminishes, as was observed in this study.

The elevated serum iron levels caused by PI treatment replenished iron stores in the bone marrow, as bone marrow iron content reached concentrations similar to that found in healthy rats (Figure 4.4C). However, in the absence of nelfinavir, PG-LPS rats show the lowest bone marrow iron content (Figure 4.4C). These results provide the proof of concept that furin inhibition that prevents the cleavage of prohepcidin to hepcidin can be used to restore normal iron delivery to the bone marrow.
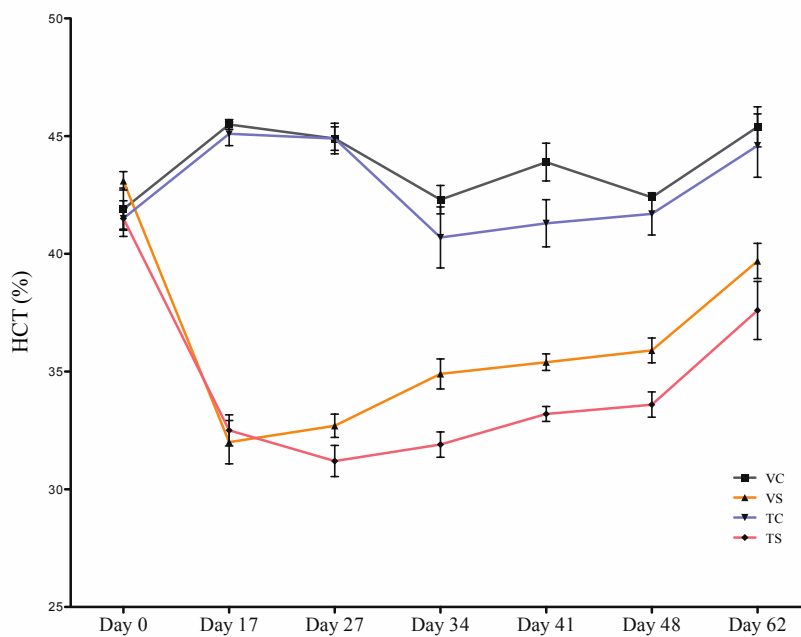
A
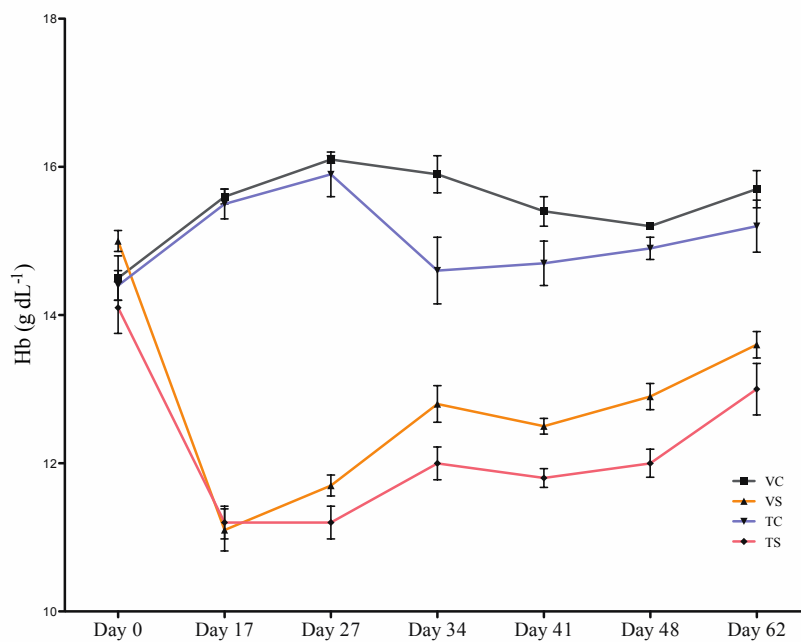
B

Figure 4.5. Hemoglobin and Hematocrit Time Course. Complete blood counts (CBCs) for **A)** Hemoglobin and **B)** Hematocrit over the course of the study.

Table 4.1. Summarized data of complete blood counts (CBCs).

Animal Group	Hb (g/dL)		HCT (%)		RDW (%)		MCV (fl)	
	Day 0	Day 62	Day 0	Day 62	Day 0	Day 62	Day 0	Day 62
Vehicle Control	14.5±0.6	15.7±0.5	41.9±1.8	45.4±1.7	12.6±0.1	13.2±0.3	55.7±1.1	53.3±0.9
Treated Control	14.4±0.4	15.2±0.2	41.5±0.9	44.6±2.7	12.6±0.1	37.2±0.7	55.3±0.7	49.7±0.5
Vehicle PG-LPS	15±0.4	13.6±0.5	43.1±1.1	39.7±2.1	12.5±0.3	42.3±2.1	55.7±0.8	47.6±0.6
Treated PG-LPS	14.1±1.1	13.0±1.1	41.5±2.4	37.6±3.9	13.6±2.5	42.8±1.2	55.8±1.5	46.7±0.6

* Values represent calculated mean of groups (Vehicle Control n=4, Treated Control n=4, Vehicle PG-LPS n=8, Treated PG-LPS (n=7).

Analysis of Blood markers associated with ACI and HIV protease inhibitor treatments.

PG-LPS animals showed significant signs of anemia within one week of induction. Mean Hb and Hematocrit levels fell from 15±0.4 and 14.1±1.1 g/dL to 13.6±0.5 13.0±1.1 g/dL with inoculation of PG-LPS. Hematocrit percentages also dropped from 43.1±1.1 and 41.5±2.4 to 39.7±2.1 and 37.6±3.9 within PG-LPS induced animals (Figure 4.4 and Table 4.1). These values illustrate the significant and prolonged anemia sustained within this model of ACI.

Interpretation of low MCV values traditionally indicate onset of microcytic anemia, a symptom common of iron deficiency anemia[58]. Here we observe low MCV in PG-LPS treated animal groups, along with a downtrend in treated controls (Figure 4.9B). MCV values for PG-LPS animals lowers 14 days after inoculation, and continues on a downtrend for the remainder of the study.

High levels RDW% is observed in PG-LPS animal groups, whereas the vehicle control group remains steady throughout the study (Figure 4.9A). High RDW is commonly associated with iron deficiency when MCV values are also low[59]. Treated control group RDW values increase over time to similar values. These data correlate with the loss in liver tissue iron with nelfinavir treated animals over time, concurrently representing a loss in tissue iron.

Deficiencies in vitamin B12 or folate often produce large or increased RDW values, but are diagnosed as such only with increasing MCV values. Here, we report high RDW values with PG-LPS inoculation, and within the PI treated control group.

185

These data likely represent the loss of iron available for sustained erythropoiesis within the animals, mimicking a clinical diagnosis of IDA.

PG-LPS induced models of inflammation are known to induce hepcidin and cause hyporferremia within hours[60,61]. The sustained length (62 days) of our study likely outlasted initial hypoferremia symptoms, resulting in consequent tissue iron loss over time. This may perhaps highlight a failure within this model to adequately provide sustained hypoferremia over long periods of time, as tissue iron stores are slowly depleted.

Discussion

ACI is the second most common form of anemia behind iron-deficiency anemia and the most prevalent cause of anemia in hospitalized patients[62]. As ACI becomes more severe in diseases the prognosis for patient health and survival drastically deteriorates[63]. The cause of ACI is directly linked to the iron regulatory hormone hepcidin. Inflammation induces the expression of HAMP through an IL-6/Jak/STAT pathways and BMP/Smad pathways[64]. HAMP mRNA is translated into preprohepcidin that is targeted to the ER/TGN for secretion. In the ER/TGN the targeting sequence is cleaved forming prohepcidin, which is further processed by furin to form hepcidin[23]. To inhibit hepcidin, researchers have targeted various steps in this process, from targeting cytokines and cytokine receptors to developing antibodies to target and eliminate hepcidin from serum.

The goal of this study was evaluate a different target, the proteolytic cleavage step in the production of hepcidin. We chose to inhibit furin, the protease that cleaves inactive prohepcidin into mature hepcidin, which causes ferroportin degradation resulting in ACI.

We used the same PG-LPS treatment used by Theurl et al. to induce inflammation and trigger chronic inflammation in Lewis rats[25]. We confirmed that IL-6 and BMP-9 were elevated and that EPO levels remained low in all animals consistent with previous models of ACI[15]. HAMP expression increased, and serum hepcidin levels were elevated approximately 4-fold in PG-LPS treated animals over untreated control animals. Additionally, serum iron decreased, and hematocrit and hemoglobin also decreased, all

187

consistent with the previously reported PG-LPS ACI model studies in animals[15,25]. Similar conditions of anemia were observed in murine models of ACI[21,65].

The transcription of the HAMP gene in PG-LPS treated animals was similar even with nelfinavir treatment indicating that nelfinavir did not provide significant inhibition of the IL-6/STAT3 or BMP/Smad pathways. Previous studies have shown that nelfinavir does have some potential to inhibit STAT3 phosphorylation but the concentration of nelfinavir used on those studies was up to 10 times higher than those used in this study[66,67]. Nelfinavir inhibition of HAMP transcription was not apparent in this study. This is most likely due to the fact that both IL-6 and BMP-9 were elevated in these animals. The BMP/SMAD pathway appears to be a more potent activator of HAMP and also influences the IL-6 activation of HAMP where the IL-6 pathway does not influence the BMP/SMAD pathway. Therefore the similar expression of HAMP even with nelfinavir treatment remains elevated.

As predicted by our hypothesis, nelfinavir treatment decreased serum hepcidin levels (~2-fold) and increased serum prohepcidin levels (~2.5 fold) in PG-LPS treated animals. This supports the hypothesis that nelfinavir inhibits furin and prevents prohepcidin cleavage. In addition, lower hepcidin levels allowed increased expression of ferroportin on the surface of liver tissue.

We evaluated the iron content of heart tissue as a second tissue to represent iron redistribution triggered by nelfinavir treatment during ACI conditions. Heart iron dropped significantly in PG-LPS treated rats, however PG-LPS treatment combined with nelfinavir treatment restored the iron content in heart tissue to normal iron levels (Figure

4.3D).   The data in heart tissue provides a second example of the restored iron redistribution associated with nelfinavir treatment in a model of ACI.

The decrease in hepcidin levels and increase in ferroportin levels allow iron export from iron-rich tissue. This was observed in PG-LPS nelfinavir treated animals with increased serum iron, bone marrow iron and heart iron. Similar serum iron concentrations were observed in our study and in other works indicating a similar response to the restoration of iron flow from trapped iron with hepcidin to recovery of iron redistribution after nelfinavir treatment.

In contrast to these studies, the nelfinavir treated PG-LPS treated animals did not demonstrate a recovery of hematocrit or hemoglobin levels, even with the recovery of serum iron and bone marrow iron[25,65]. Presumably the BMP concentrations that are inhibited by LDN-193198 and HJV-fc treatment are not affected by nelfinavir treatment. The BMP cytokines influence pathways related to inhibiting the proliferation and differentiation of erythroid progenitor cells and also impair EPO production and response to EPO[68,69]. Therefore, even though nelfinavir restores normal iron mobilization, the low levels of EPO in the PG-LPS model prevent erythropoiesis. Similar to the study by Sasu where anti-hepcidin antibodies were able to restore iron mobilization, the lack of EPO prevented the recovery of anemia until ESAs were co-administered with the anti-hepcidin antibody[21]. We propose that the use of ESAs with nelfinavir will allow the recovery of anemia in this model.

In summary, we have used the protease inhibitor nelfinavir to inhibit furin and prevent the processing of prohepcidin to hepcidin. This allows for the stable expression

189

of ferroportin on the surface of iron-rich cells during ACI and restores iron mobilization allowing normal iron levels in serum and bone marrow. We propose that nelfinavir can be used in combination with ESAs to treat ACI.
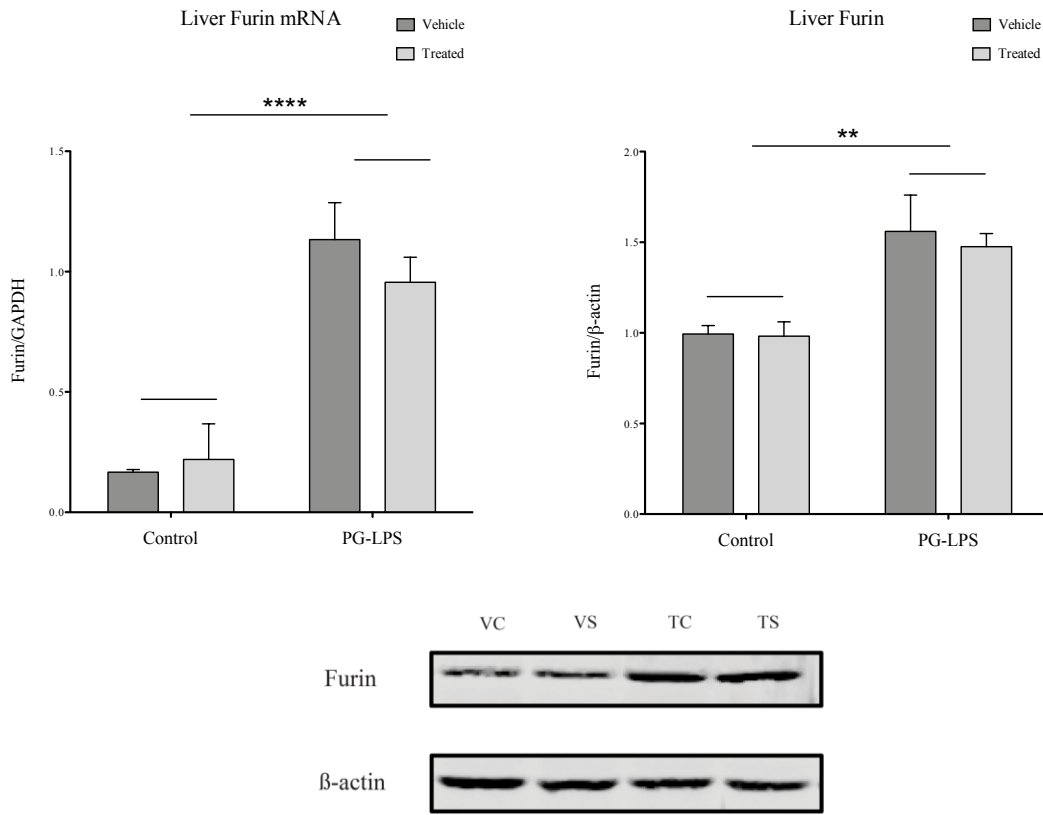
Figure 4.6. Furin from liver A) Furin mRNA from liver. **B)** Graphical representation of Furin liver expression. **C)** Western blot of furin liver expression between treatment groups. Treatment shows no significant interaction of PI treatment, whereas Furin is upregulated significantly between control and PG-LPS groups (p < 0.01).
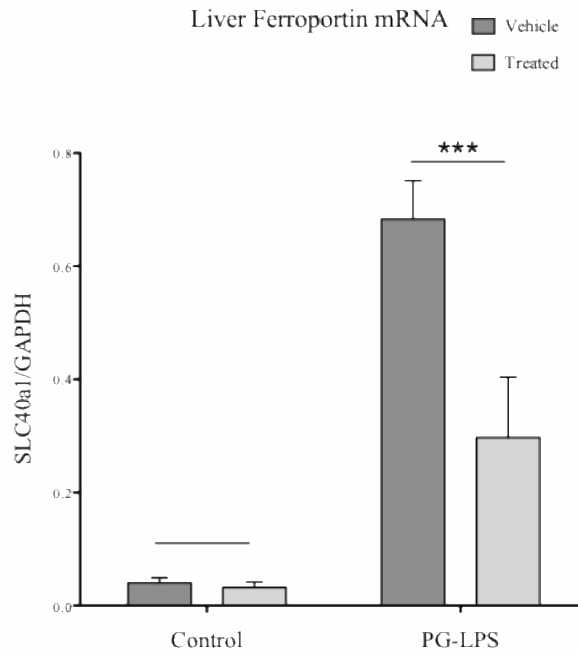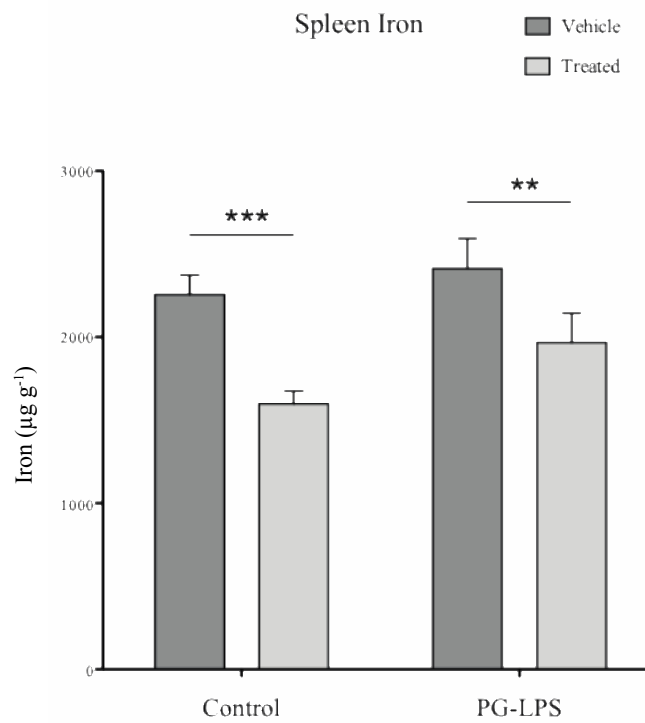
Figure 4.7. Liver Ferroportin mRNA (Slc40a).
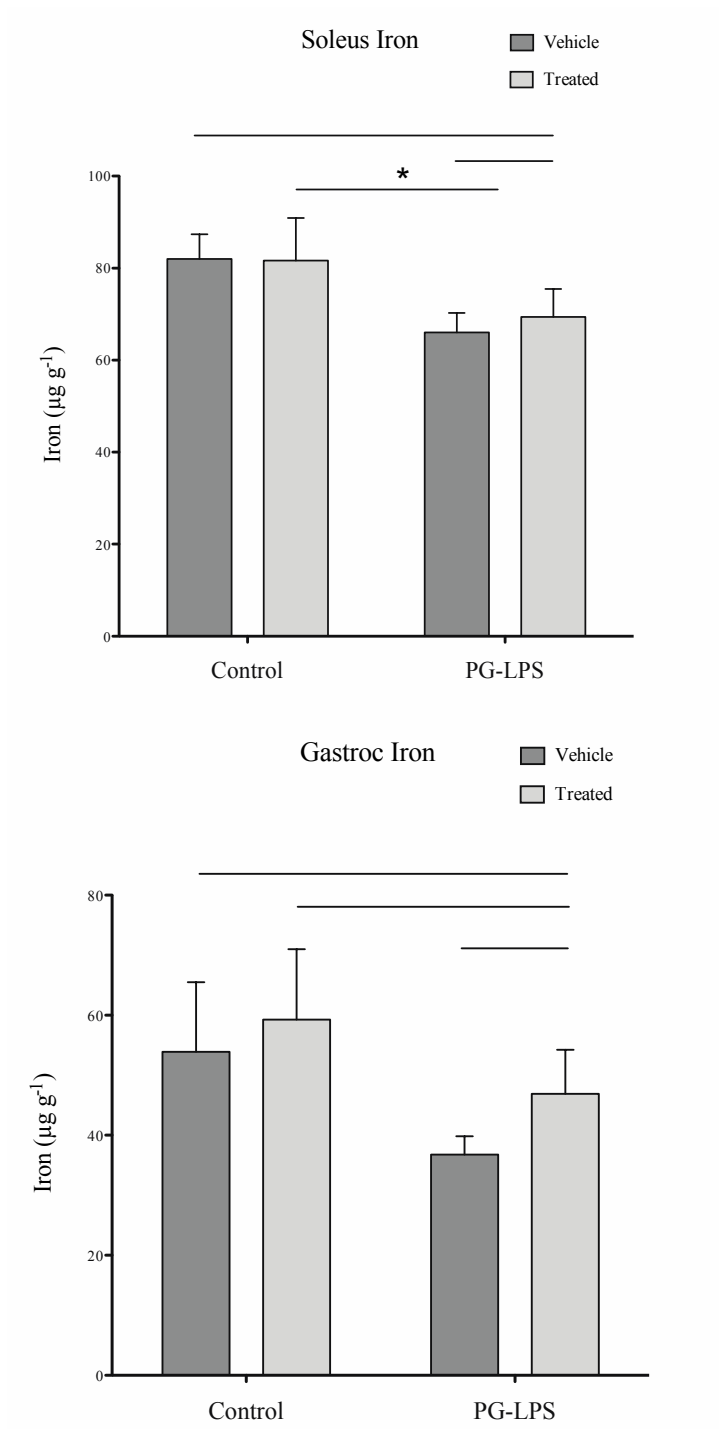

Figure 4.8. Spleen Iron.

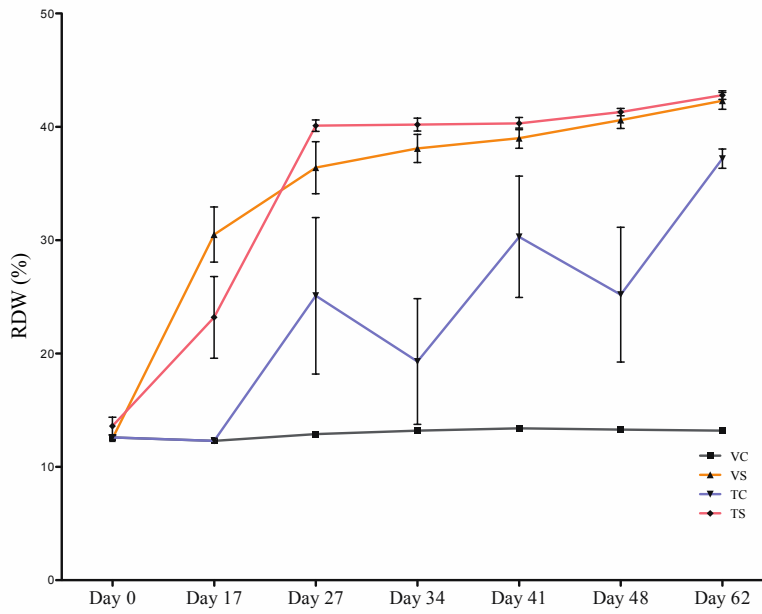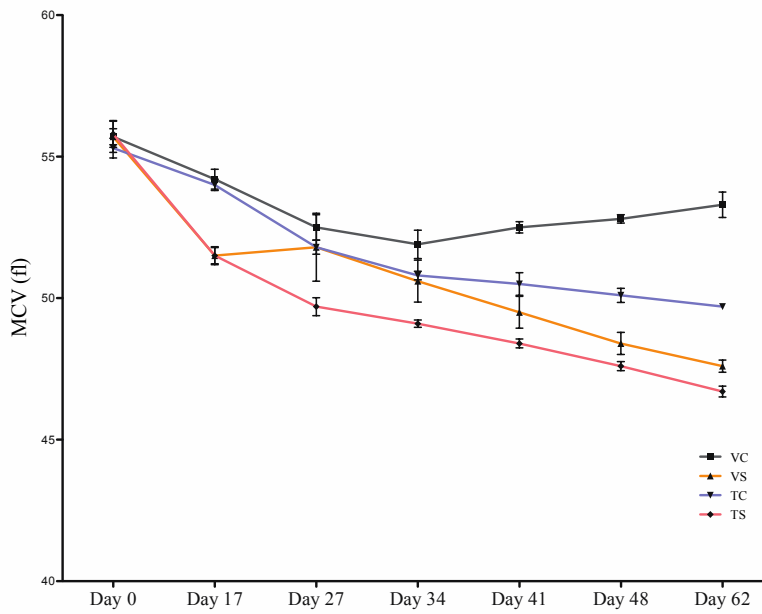**Figure 4.9. Muscle Iron. A)** Total iron in Soleus. **B)** Total iron in the Gastrocnemius.

Figure 4.10. Red blood cell indices. **A)** Red blood cell distribution width (RDW) and **B)** Mean corpuscular volume (MCV) of animals during the course of treatment after PG-LPS inoculation.
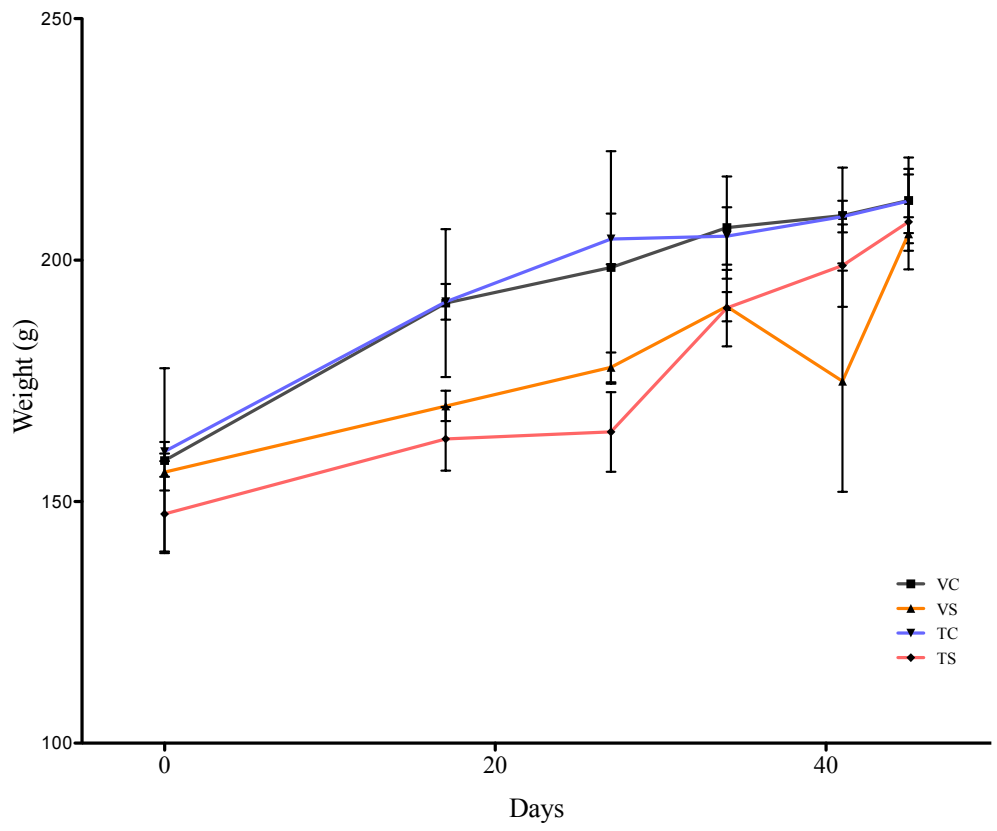
Figure 4.11. Animal Body Weights. Animal weights measured during the course of treatment after PG-LPS inoculation.

References

1. Agarwal, N. & Prchal, J. T. Anemia of Chronic Disease (Anemia of Inflammation). *Acta Haematol.* **122,** 103–108 (2009).

2. Cartwright, G. E. The anemia of chronic disorders. *Semin. Hematol.* **3,** 351–375 (1966).

3. Adamson, J. W. The Anemia of Inflammation/Malignancy: Mechanisms and Management. *ASH Educ. Program Book* **2008,** 159–165 (2008).

4. Kalantar-Zadeh, K., Kopple, J. D., Block, G. & Humphreys, M. H. A Malnutrition-Inflammation Score is correlated with morbidity and mortality in maintenance hemodialysis patients. *Am. J. Kidney Dis.* **38,** 1251–1263 (2001).

5. Denz, H. *et al.* Association between the activation of macrophages, changes of iron metabolism and the degree of anaemia in patients with malignant disorders. *Eur. J. Haematol.* **48,** 244–248 (1992).

6. McClellan, W. *et al.* The prevalence of anemia in patients with chronic kidney disease. *Curr. Med. Res. Opin.* **20,** 1501–1510 (2004).

7. Andrews, N. C. Anemia of inflammation: the cytokine-hepcidin link. *J. Clin. Invest.* **113,** 1251–1253 (2004).

8. Cheng, P., Jiao, X., Wang, X., Lin, J. & Cai, Y. Hepcidin expression in anemia of chronic disease and concomitant iron-deficiency anemia. *Clin. Exp. Med.* **11,** 33–42 (2011).

9. Ferrucci, L. *et al.* Proinflammatory state, hepcidin, and anemia in older persons. *Blood* **115,** 3810–3816 (2010).

10. Fleming, R. E. & Sly, W. S. Hepcidin: A putative iron-regulatory hormone relevant to hereditary hemochromatosis and the anemia of chronic disease. *Proc. Natl. Acad. Sci.* **98,** 8160–8162 (2001).

11. Domenico, I. D. *et al.* The Molecular Mechanism of Hepcidin-mediated Ferroportin Down-Regulation. *Mol. Biol. Cell* **18,** 2569–2578 (2007).

12. Nemeth, E. *et al.* Hepcidin Regulates Cellular Iron Efflux by Binding to Ferroportin and Inducing Its Internalization. *Science* **306,** 2090–2093 (2004).

13. Anderson, G. J., Darshan, D., Wilkins, S. J. & Frazer, D. M. Regulation of systemic iron homeostasis: how the body responds to changes in iron demand. *BioMetals* **20,** 665–674 (2007).

14. Opasich, C. *et al.* Blunted erythropoietin production and defective iron supply for erythropoiesis as major causes of anaemia in patients with chronic heart failure. *Eur. Heart J.* **26,** 2232–2237 (2005).

15. Theurl, I. *et al.* Regulation of iron homeostasis in anemia of chronic disease and iron deficiency anemia: diagnostic and therapeutic implications. *Blood* **113,** 5277–5286 (2009).

16. Silverberg, D. S. *et al.* The use of subcutaneous erythropoietin and intravenous iron for the treatment of the anemia of severe, resistant congestive heart failure improves cardiac and renal function and functional cardiac class, and markedly reduces hospitalizations. *J. Am. Coll. Cardiol.* **35,** 1737–1744 (2000).

17. Coccia, M. A. *et al.* Novel erythropoiesis stimulating protein (darbepoetin alfa) alleviates anemia associated with chronic inflammatory disease in a rodent model. *Exp. Hematol.* **29,** 1201–1209 (2001).

18. Babitt, J. L. *et al.* Bone morphogenetic protein signaling by hemojuvelin regulates hepcidin expression. *Nat. Genet.* **38,** 531–539 (2006).

19. Babitt, J. L. *et al.* Modulation of bone morphogenetic protein signaling in vivo regulates systemic iron balance. *J. Clin. Invest.* **117,** 1933–1939 (2007).

20. Yu, P. B. *et al.* Dorsomorphin inhibits BMP signals required for embryogenesis and iron metabolism. *Nat. Chem. Biol.* **4,** 33–41 (2008).

21. Sasu, B. J. *et al.* Antihepcidin antibody treatment modulates iron metabolism and is effective in a mouse model of inflammation-induced anemia. *Blood* **115,** 3616–3624 (2010).

22. Song, S.-N. J. *et al.* Down-regulation of hepcidin resulting from long-term treatment with an anti–IL-6 receptor antibody (tocilizumab) improves anemia of inflammation in multicentric Castleman disease. *Blood* **116,** 3627–3634 (2010).

23. Valore, E. V. & Ganz, T. Posttranslational processing of hepcidin in human hepatocytes is mediated by the prohormone convertase furin. *Blood Cells. Mol. Dis.* **40,** 132–138 (2008).

24. Gagliardo, B. *et al.* Pro-hepcidin is unable to degrade the iron exporter ferroportin unless matured by a furin-dependent process. *J. Hepatol.* **50,** 394–401 (2009).

25. Theurl, I. *et al.* Pharmacologic inhibition of hepcidin expression reverses anemia of chronic inflammation in rats. *Blood* **118,** 4977–4984 (2011).

26. Kumar, G. N., Rodrigues, A. D., Buko, A. M. & Denissen, J. F. Cytochrome P450-mediated metabolism of the HIV-1 protease inhibitor ritonavir (ABT-538) in human liver microsomes. *J. Pharmacol. Exp. Ther.* **277,** 423–431 (1996).

27. Eagling, V. A., Back, D. J. & Barry, M. G. Differential inhibition of cytochrome P450 isoforms by the protease inhibitors, ritonavir, saquinavir and indinavir. *Br. J. Clin. Pharmacol.* **44,** 190–194 (1997).

28. Kurowski, M., Kaeser, B., Sawyer, A., Popescu, M. & Mrozikiewicz, A. Low-dose ritonavir moderately enhances nelfinavir exposure. *Clin. Pharmacol. Ther.* **72,** 123–132 (2002).

29. Aarnoutse, R. E. *et al.* Pharmacokinetics, food intake requirements and tolerability of once-daily combinations of nelfinavir and low-dose ritonavir in healthy volunteers. *Br. J. Clin. Pharmacol.* **55,** 115–125 (2003).

30. Zeldin, R. K. & Petruschke, R. A. Pharmacological and therapeutic properties of ritonavir-boosted protease inhibitor therapy in HIV-infected patients. *J. Antimicrob. Chemother.* **53,** 4–9 (2004).

31. Ej, F., Ea, G., Dp, R., Lh, S. & He, S. Quantitative comparison of toxicity of anticancer agents in mouse, rat, hamster, dog, monkey, and man. *Cancer Chemother. Rep.* **50,** 219–244 (1966).

32. Reagan-Shaw, S., Nihal, M. & Ahmad, N. Dose translation from animal to human studies revisited. *FASEB J.* **22,** 659–661 (2008).

33. Nelfinavir. *DrugBank* (2013). at <http://www.drugbank.ca/drugs/DB00220>

34. Danner, S. A. *et al.* A Short-Term Study of the Safety, Pharmacokinetics, and Efficacy of Ritonavir, an Inhibitor of HIV-1 Protease. *N. Engl. J. Med.* **333,** 1528–1534 (1995).

35. Shanmugam, N. K. N. *et al.* Tumor Necrosis Factor α Inhibits Expression of the Iron Regulating Hormone Hepcidin in Murine Models of Innate Colitis. *PLoS ONE* **7,** e38136 (2012).

36. Arikawa, E. *et al.* Cross-platform comparison of SYBR® Green real-time PCR with TaqMan PCR, microarrays and other gene expression measurement technologies evaluated in the MicroArray Quality Control (MAQC) study. *BMC Genomics* **9,** 328 (2008).

37. Sariego Muiz, C., Marchante Gayn, J. M., Garcia Alonso, J. I. & Sanz Medel, A. Speciation of essential elements in human serum using anion exchange chromatography coupled to post column isotope dilution analysis with double focusing ICP-MS. *J. Anal. At. Spectrom.* **16,** 587–592 (2001).

38. Ciavardelli, D. *et al.* Phenotypic profile linked to inhibition of the major Zn influx system in Salmonella enterica: proteomics and ionomics investigations. *Mol. Biosyst.* **7,** 608 (2011).

39. Sartor, R. B. *et al.* Protracted anemia associated with chronic, relapsing systemic inflammation induced by arthropathic peptidoglycan-polysaccharide polymers in rats. *Infect. Immun.* **57,** 1177–1185 (1989).

40. Kemna, E., Pickkers, P., Nemeth, E., Hoeven, H. van der & Swinkels, D. Time-course analysis of hepcidin, serum iron, and plasma cytokine levels in humans injected with LPS. *Blood* **106,** 1864–1866 (2005).

41. Thomas, C. & Thomas, L. Anemia of Chronic Disease: Pathophysiology and Laboratory Diagnosis. *Lab. Hematol.* **11,** 14–23 (2005).

42. Jurado, R. L. Iron, Infections, and Anemia of Inflammation. *Clin. Infect. Dis.* **25,** 888–895 (1997).

43. Means, R. J. & Krantz, S. B. Progress in understanding the pathogenesis of the anemia of chronic disease [see comments]. *Blood* **80,** 1639–1647 (1992).

44. Means, R. T. *et al.* Treatment of the anemia of rheumatoid arthritis with recombinant human erythropoietin: Clinical and in vitro studies. *Arthritis Rheum.* **32,** 638–642 (1989).

45. Roetto, A. *et al.* Mutant antimicrobial peptide hepcidin is associated with severe juvenile hemochromatosis. *Nat. Genet.* **33,** 21 (2003).

46. Falzacappa, M. V. V. *et al.* STAT3 mediates hepatic hepcidin expression and its inflammatory stimulation. *Blood* **109,** 353–358 (2007).

47. Wrighting, D. M. & Andrews, N. C. Interleukin-6 induces hepcidin expression through STAT3. *Blood* **108,** 3204–3209 (2006).

48. Pietrangelo, A. *et al.* STAT3 Is Required for IL-6-gp130–Dependent Activation of Hepcidin In Vivo. *Gastroenterology* **132,** 294–300 (2007).

49. Huang, H., Constante, M., Layoun, A. & Santos, M. M. Contribution of STAT3 and SMAD4 pathways to the regulation of hepcidin by opposing stimuli. *Blood* **113,** 3593–3599 (2009).

50. Kautz, L. *et al.* Iron regulates phosphorylation of Smad1/5/8 and gene expression of Bmp6, Smad7, Id1, and Atoh8 in the mouse liver. *Blood* **112,** 1503–1509 (2008).

51. Muñoz, M., García-Erce, J. A. & Remacha, Á. F. Disorders of iron metabolism. Part II: iron deficiency and iron overload. *J. Clin. Pathol.* **64,** 287–296 (2011).

52. Jankowska, E. A. *et al.* Iron deficiency: an ominous sign in patients with systolic chronic heart failure. *Eur. Heart J.* **31,** 1872–1880 (2010).

53. Emans, M. E. *et al.* Red cell distribution width is associated with physical inactivity and heart failure, independent of established risk factors, inflammation or iron metabolism; the EPIC—Norfolk study. *Int. J. Cardiol.* **168,** 3550–3555 (2013).

54. Thomas, G. Furin at the cutting edge: From protein traffic to embryogenesis and disease. *Nat. Rev. Mol. Cell Biol.* **3,** 753–766 (2002).

55. Artenstein, A. W. & Opal, S. M. Proprotein Convertases in Health and Disease. *N. Engl. J. Med.* **365,** 2507–2518 (2011).

56. Enomoto, T. *et al.* Regulation of adipolin/CTRP12 cleavage by obesity. *Biochem. Biophys. Res. Commun.* **428,** 155–159 (2012).

57. Fan, M. Z., Stoll, B., Jiang, R. & Burrin, D. G. Enterocyte digestive enzyme activity along the crypt-villus and longitudinal axes in the neonatal pig small intestine. *J. Anim. Sci.* **79,** 371–381 (2001).

58. Iron Deficiency Anemia. (2013). at <http://emedicine.medscape.com/article/202333-overview>

59. Sarma, P. R. in *Clin. Methods Hist. Phys. Lab. Exam.* (eds. Walker, H. K., Hall, W. D. & Hurst, J. W.) (Butterworths, 1990). at <http://www.ncbi.nlm.nih.gov/books/NBK260/>

60. Kemna, E. H. J. M. *et al.* Regulation of hepcidin: Insights from biochemical analyses on human serum samples. *Blood Cells. Mol. Dis.* **40,** 339–346 (2008).

61. Montosi, G. *et al.* Kupffer cells and macrophages are not required for hepatic hepcidin activation during iron overload. *Hepatol. Baltim. Md* **41,** 545–552 (2005).

62. Patel, K. V. Epidemiology of Anemia in Older Adults. *Semin. Hematol.* **45,** 210–217 (2008).

63. Rachoin, J.-S., Cerceo, E., Milcarek, B., Hunter, K. & Gerber, D. R. Prevalence and impact of anemia in hospitalized patients. *South. Med. J.* **106,** 202–206 (2013).

64. Truksa, J., Lee, P. & Beutler, E. The role of STAT, AP-1, E-box and TIEG motifs in the regulation of hepcidin by IL-6 and BMP-9: Lessons from human HAMP and murine Hamp1 and Hamp2 gene promoters. *Blood Cells. Mol. Dis.* **39,** 255–262 (2007).

65. Steinbicker, A. U. *et al.* Inhibition of bone morphogenetic protein signaling attenuates anemia associated with inflammation. *Blood* **117,** 4915–4923 (2011).

66. Aggarwal, B. B. *et al.* Signal Transducer and Activator of Transcription-3, Inflammation, and Cancer. *Ann. N. Y. Acad. Sci.* **1171,** 59–76 (2009).

67. Ikezoe, T. *et al.* HIV-1 protease inhibitor induces growth arrest and apoptosis of human multiple myeloma cells via inactivation of signal transducer and activator of transcription 3 and extracellular signal-regulated kinase 1/2. *Mol. Cancer Ther.* **3,** 473–479 (2004).

68. Lichtenstein, A. Anemia in lymphoma: interleukin-6, hepcidin and erythropoietin. *Leuk. Lymphoma* **55,** 231–232 (2014).

69. JELKMANN, W. Proinflammatory Cytokines Lowering Erythropoietin Production. *J. Interferon Cytokine Res.* **18,** 555–559 (1998).